Novel ways to unravel the mechanism of kinesin

Verbrugge, S.

2009

document version
Publisher's PDF, also known as Version of record

Novel ways to unravel the mechanism of kinesin

Sander Verbrugge

PhD Thesis

July 22, 2009

This thesis was reviewed by:

prof.dr. Fred MacKintosh	Vrije Universiteit
dr.ir. Gijs Wuite	Vrije Universiteit
dr. Günther Woehlke	Technische Universität München
prof.dr. Hernando Sosa	Albert Einstein College of Medicine
prof.dr. Ton Visser	Vrije Universiteit and Wageningen UR

This work is part of the research programme of the 'Stichting voor Fundamenteel Onderzoek der Materie (FOM)', which is financially supported by the 'Nederlandse Organisatie voor Wetenschappelijk Onderzoek (NWO)'. The research was performed in the section 'Physics of Complex Systems' at the Vrije Universiteit.

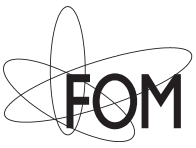

vrije Universiteit *amsterdam*

VRIJE UNIVERSITEIT

Novel ways to unravel the mechanism of kinesin

ACADEMISCH PROEFSCHRIFT

ter verkrijging van de graad Doctor aan
de Vrije Universiteit Amsterdam,
op gezag van de rector magnificus
prof.dr. L.M. Bouter,
in het openbaar te verdedigen
ten overstaan van de promotiecommissie
van de faculteit der Exacte Wetenschappen
op vrijdag 9 oktober 2009 om 10.45 uur
in de aula van de universiteit,
De Boelelaan 1105

door

Sander Verbrugge

geboren te Leiden

promotor: prof.dr. F.C. MacKintosh
copromotor: dr.ir. E.J.G. Peterman

Contents

Chapter 1

Introduction

This thesis describes four years of research on the motor protein Kinesin-1. During these four years we have constructed an approach that allows for high time-resolution (submilliseconds) fluorescence measurements on walking Kinesin-1 motors (chapter 2). With this approach we have found that Kinesin-1 has an intermediate state during stepping where only one motor domain is microtubule bound, that lasts several milliseconds (chapter 3). Moreover we have determined the binding time of (fluorescently-labeled) ATP in relation to the step-time (chapter 4). We have also developed two analysis approaches that can determine three fundamental motility parameters of Kinesin-1 using wide-field TIRF microscopy (chapter 5). To find out why one single protein deserves this much attention I will start this introduction with a broader view on the importance of motor proteins inside the cell and then give a short overview of the research that has already been performed on Kinesin-1. After that I will explain the experimental techniques that were used in this thesis and another technique that is often used to study Kinesin-1. I will finish the introduction with a summary of the four remaining chapters in this thesis.

1.1 Eukaryotic cells contain Kinesin-1

1.1.1 Eukaryotic cells

Cells are the fundamental unit of life, they are the building blocks for large organisms, such as animals (including humans) and plants, but single cells also occur as independent life forms, for instance bacteria and yeast [1]. Three different domains of life are distinguished in biology: *archeae*, *prokaryotes* and *eukaryotes*, all three with different cellular properties. This introduction will focus on the eukaryotic domain, because Kinesin-1 occurs in eukaryotic cells. Compared to the cells of the two other domains of life, eukaryotic cells have the most complex cell structure. They have special membrane enclosed compartments called organelles, all with a specific function inside the cell (e.g. Golgi apparatus, mitochondria). Moreover, there is one specific

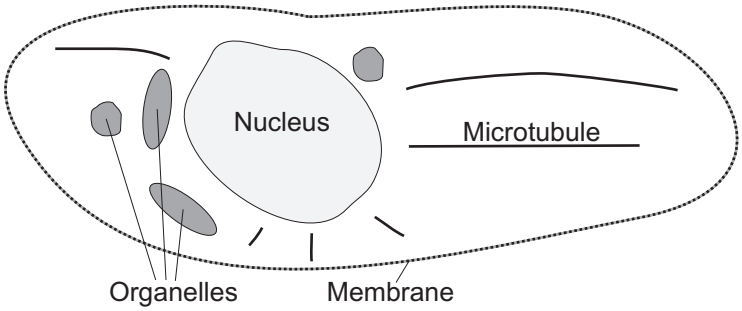

Figure 1.1 – Schematic representation of a eukaryotic cell

type of organelle called *the nucleus*, where genetic material is stored [1].

1.1.2 Kinesin-1 is important for active transport inside the cell

Each eukaryotic cell is a membrane-enclosed complex system that consists of many different parts and a wide variety of different proteins. To understand the role that Kinesin-1 plays inside the cell, there are two important elements of the cell that need to be discussed, the *nucleus* and the *cytoskeleton* (Figure 1.1). Genetic information is stored and maintained inside the nucleus and this information can be used to initiate the production of proteins that the cell needs to function. It is vital for the cell that these "freshly-produced" proteins are transported to all parts of the cell, and the same holds for many types of organelles. To achieve intracellular active directed transport, the cytoskeleton functions as a railroad network for motor proteins. The cytoskeleton is not just there to serve as a track for motor proteins, due to the abundance and strength of the filaments it also gives the cell structural integrity. It contains three different types of filaments; actin, intermediate filaments and microtubules. Microtubules are the filaments that Kinesins can bind to and walk on. They are hollow protein tubes that are build up of heterodimeric subunits, α- and β tubulin [3]. A microtubule has directionality due to its structure and in most non-dividing cells they are oriented such that the plus end points away from the nucleus towards the periphery.

Kinesin is the name of a superfamily of proteins that have two common properties, they can bind to microtubules and can hydrolyze ATP. The kinesin used in this thesis belongs to the Kinesin-1 family and is mainly involved in the transport of organelles and vesicles from the nucleus towards the periphery of the cell. Vesicles are small (micron-sized) membrane spheres that can contain important building blocks for the cell, like proteins and signaling molecules. Kinesin-1 was the first discovered family of kinesins [79] and the most important properties of Kinesin-1 (from now on also termed kinesin) are described in the following paragraphs.

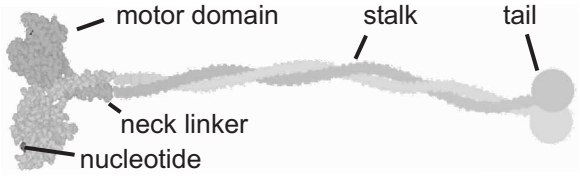

Figure 1.2 – Schematic representation of homodimeric kinesin

1.2 The structure and important motility parameters of Kinesin-1

1.2.1 Structure of Kinesin-1

It is important to have a clear view on the structure of kinesin to understand the details of its movement. The functional structure *in vivo* is a *tetramer* consisting of two identical heavy chains and two identical light chains that bind to the tail of kinesin and aid in cargo binding. However, I will focus on the functional structure for motility and that is a *homodimer* consisting of the two heavy chains that form two separate catalytic domains, and coil together to form one stalk and tail (Figure 1.2). The catalytic domain of kinesin has a microtubule binding site, a nucleotide binding site and a flexible linker, called the neck linker, that links the motor domain to the stalk [41]. From here on, the catalytic domain will be referred to as motor domain. Please note that in this thesis we only work with truncated kinesin constructs, this means that the tail and a part of the stalk of the protein are cut off. However, the remaining part of the dimeric construct is functional for motility and has the same motility parameters as the native construct [89].

1.2.2 Key motility parameters

Kinesin is a processive motor protein

Kinesin is able to make up to hundreds of steps along a microtubule (microtubule) before releasing from the microtubule. This property is called *processive movement* [36] and is very useful for the *in vivo* function of kinesin, because only a few kinesins need to be attached to a vesicle or organelle to maintain continuous microtubule attachment, and thus controlled transport over large distances [79]. The first experiments that clearly indicated that a single motor moves processively along a single microtubule, had kinesin stuck to a glass surface (gliding assays) [36] or to micron-sized beads (bead assays) [10,25] (Figure 1.3). In gliding assays the microtubules move in the direction of their minus end, because the surface-attached motors walk towards the plus-end of the microtubule (Figure 1.3b). At a high density of surface-attached motors there are continuously multiple motors bound to the microtubule, keeping the microtubule fixed to the surface at multiple points and hence the microtubule can not rotate and is guided in a fairly straight path of movement. At lower densities of

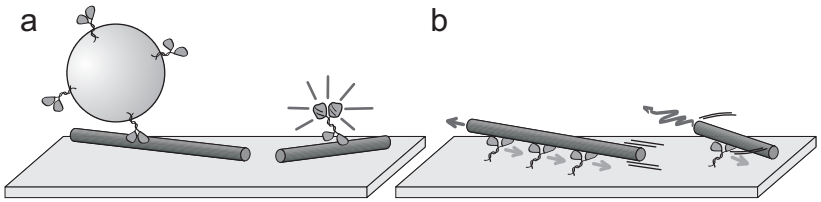

Figure 1.3 – Schematic representation of assays. a. Bead assay and a single-molecule walking assay, where microtubules are attached to the surface and kinesin can walk along it. **b.** In gliding assays microtubules are moved forward by surface-attached kinesin. Pictures are courtesy of Dr. Lukas Kapitein and is taken from [38]

surface-attached motors however, it is possible that a microtubule is moved forward by a single kinesin. When this occurs, the microtubule can rotate around the point where the kinesin is attached to the microtubule while still moving forward. This observation was first reported in 1989 [36] and it elegantly proves that a single motor can move on a microtubule while maintaining microtubule-attachment throughout the entire stepping-cycle, known as processive movement. In this report it is also observed that the velocity of the microtubules is not influenced by the density of surface-attached motors; that kinesin has a maximum velocity of $\sim$600 nm/s and kinesin obeys Michaelis-Menten kinetics with ATP as a substrate. ATP is a fuel molecule present in cells that consists of an adenosine with three attached-phosphates and it can be hydrolyzed into ADP (two attached phosphates) with an accompanied energy release of roughly 25 kT. Processivity, similar Michaelis-Menten and velocity behavior of kinesin were also observed with bead-assays (Figure 1.3a), where beads were moved forward by single motors [10, 25]. The beads were brought in proximity of the surface-attached microtubules using optical tweezers (see section 1.3.2).

Single-molecule fluorescence (see section 1.3.1) was the first technique that allowed for direct observation of single kinesin motors walking processively along a surface-bound microtubule, as depicted in Figure 1.3a) (in the first experiment it actually was a bundle of microtubules called an axoneme). Single-molecule fluorescence is a measurement technique that can visualize single-molecules termed fluorophores, by imaging the emitted fluorescence light onto a sensitive detector, in this case a camera. The fluorophores were fused to the motors and consecutive images were taken to visualize the position of the single motor in time [77]. The measurements yielded not only the average distance a motor travels along a microtubule, which is a measure for the processivity and is called the run length, but also yielded the velocity distribution of many single motors without external load applied to them.

Kinesin makes 8 nm steps and can move under backward loads up to 6 pN

An extension of the bead-assay approach is to use optical tweezers not only for positioning the bead (with kinesin attached) near the microtubule, but also to measure the displacement of the bead from the center of the trap. Moreover, if the trap is cali-

brated it can be used for force measurements (see section 1.3.2). The first report that measured the position of a bead attached to the tail of kinesin, showed that kinesin walks with eight nanometer steps, independent of load and ATP concentration [71]. An 8 nm step agrees very well with the size of an α-β tubulin dimer, the basic building block of microtubules [3], indicating that kinesin steps between consecutive dimers along the microtubule. It was also found that kinesin can withstand rearward loads up to 6 pN. At this force, called the stall-force, kinesin can make occasional backsteps without detaching from the microtubule [49]. Recently it was found that kinesin can walk backwards processivily, this occurs when the rearward load is quickly raised to forces up to 14 pN [14]. This 'moonwalking' [15] was found to be ATP dependent, and although *in vivo* relevance is debatable, it is a puzzling discovery that will require more research to be fully understood.

Kinesins hydrolyzes one ATP per 8 nm step

The mechanical work needed to make an 8 nm step forward against a load of 6 pN is roughly 48 pN nm ($\sim$12 kT) and it is obtained from the chemical energy that is released when ATP is hydrolyzed into ADP (releasing $\sim$25 kT). To find out how many ATP molecules are needed for kinesin to make one step forward, the stepping behavior of kinesin at low ATP concentrations was studied with optical tweezers. By studying the variance in the displacement over time of walking kinesin [70], it was found that there is a single rate-limiting step that determines the movement of kinesin at low ATP concentrations. This rate-limiting step must be binding of a single ATP and therefore it was concluded that one ATP binds per 8 nm step [63]. In a later study it was proven that this finding does not only hold at low ATP concentrations, but it holds for all ATP concentrations [17]. These findings clearly show that the chemical energy obtained from the hydrolysis of one ATP molecule into ADP is tightly coupled to a single 8-nm step forward by kinesin.

Kinesin moves via the alternating site mechanism

For a long time it was unknown how individual motor domains move in order to create an 8 nm displacement of kinesins tail. There were thought to be two options: a single motor domain displaces 16 nm and the motor domains alternate between being the forward and the rearward motor domain (alternating site mechanism or hand-over-hand movement), or both motor domains move 8 nm and the forward domain remains the leading one throughout an entire processive run (inchworm movement)(Figure 1.4). In the inchworm model there is one dominant catalytic site that controls the stepping. In the hand-over-hand mechanism, both motor domains go through exactly the same chemical cycle and the cycles are kept out of phase to ensure processive movement. It was known (from 1994 onwards) that kinesin releases its ADP upon microtubule binding in two distinct phases, and that was put forward as evidence that kinesin walks with the alternating site mechanism [31]. The measurements that unequivocally confirmed the hand-over-hand movement were reported within a short period of time at the end of 2003 by three different groups [4, 39, 92]. I will describe one of these experiments.

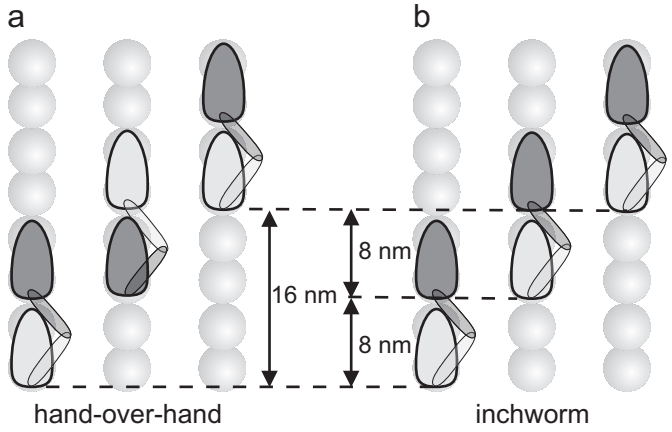

Figure 1.4 – Two different models for processive stepping. a. Hand-over-hand movement, where each motor domain alternates between leading and trailing motor domain. **b.** Inchworm model, where one motor domain remains leading throughout an entire processive run and one domain is the dominant catalytic site.

In single-molecule wide-field measurements the position of a fluorophore can be localized with sub-pixel resolution [62] and even with nanometer accuracy when enough photons are detected on the camera [43, 90]. This accurate, but video rate-limited (in this experiment one frame was acquired in 330 ms)), localization was used to determine the position of a fluorophore attached to the motor domain of dimeric kinesin walking at highly reduced velocities [92]. In these experiments the average displacement of the labeled motor domain was 17.3 ± 3.3 nm. Moreover, the dwell-time distribution of the steps showed that two rate-limiting steps occurred between two consecutive steps. One rate-limiting step was the result of the displacement of the labeled domain and the second rate-limiting step was concluded to be the 16 nm displacement of the unlabeled (and thus unobserved) motor domain. This experiment elegantly proved the hand-over-hand mechanism.

1.3 Single-molecule techniques to study Kinesin-1

1.3.1 Single-molecule fluorescence microscopy

In optical microscopy, light is used to visualize small objects or samples to study them. A dedicated apparatus, the microscope, is often used in combination with a camera that records images. In typical bright-field microscopy, light is transmitted through the sample onto the camera. This approach has a maximal resolution of roughly half the wavelength of the light used for imaging (typically 300 – 700 nm), where resolution can be defined as: 'how far apart do two entities have to be under the microscope to allow resolving them separately'. As a single kinesin motor is roughly

tens of nanometers long and a single motor domain is only 5 nm long, it is impossible to 'see' kinesin with bright field microscopy, let alone observe its motor domains. One of the techniques that does allow for visualization of kinesin (and microtubules) is single-molecule fluorescence.

Fluorescence is the light emitted by a fluorophore, which is a molecule that absorbs light and emits light with a longer wavelength (Figure 1.5). The difference in wavelength is used to visualize the single-fluorophores by separating the excitation and emission light and imaging just the emitted fluorescence. The fluorophores used in this thesis are typically a few nanometers in size and are covalently linked to the proteins. In this manner, a single kinesin that is labeled with a fluorophore can be observed in a single-molecule fluorescence microscope, under the restriction that there are no other fluorophores within a distance equal to the optical resolution of the microscope, because this will make the two separate fluorophores appear as one. A single fluorophore does not hinder the mechanical working of the molecule it is linked to, if it is attached to the right position. Unfortunately a fluorophore can break down under repetitive excitation, a process called photo bleaching, after which it will not emit measurable amounts of fluorescent light. In this thesis two single-molecule fluorescence techniques are used, total-internal-reflection fluorescence microscopy and confocal fluorescence.

Total-internal-reflection fluorescence microscopy

In total-internal-reflection fluorescence (TIRF) microscopy only a small region near the surface of the sample is illuminated. The incident excitation light is totally reflected on the glass-water interface and the sample is illuminated solely with an exponentially decaying wave, typically penetrating the sample for ∼100 nm [11]. The general layout of a TIRF microscope contains a light source, a 'defocusing' lens that focuses the beam onto the *back focal plane* of the objective, a high numerical aperture

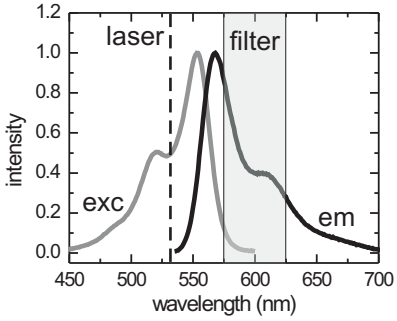

Figure 1.5 – Excitation(exc) and emission(em) spectrum of Alexa 555, a fluorophore used frequent in this thesis. The emission wavelength of the laser is depicted with a dashed line and the 'non-blocking' part of the filter is represented by a grey area.

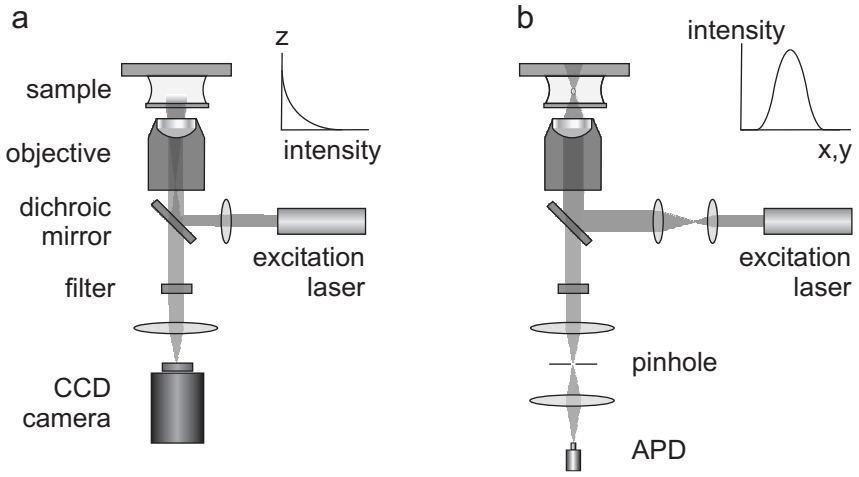

Figure 1.6 – Schematic representation of TIRF (a) and confocal (b) microscopy setups. The shape of the excitation intensity profile is indicated near the sample.

objective to create the evanescent wave, a dichroic mirror to separate the illumination/excitation light from the fluorescent light, a dedicated filter to reject all the remaining illumination light and a camera with single-molecule sensitivity (Figure 1.6).

A typical TIRF measurement is sensitive enough to detect single molecules and has a low background signal, because only a small part of the sample is illuminated. The optical resolution of the setup is half the wavelength of the fluorescent light whereas the temporal resolution is limited by the acquisition speed of the camera, which typically is ten milliseconds or more.

Confocal fluorescence microscopy

In confocal fluorescence microscopy, a diffraction limited spot (confocal spot) excites fluorophores in the sample and the backward emitted fluorescence is collected and detected by a point-detector (Figure 1.6). There are several specific elements in a confocal setup; the excitation beam is expanded to overfill the back aperture of the objective to obtain the best possible diffraction limited spot. Secondly, the fluorescent light is first focused onto a pin hole, to reduce axial background signal, before being imaged onto a point-detector [57].

A confocal fluorescence microscope can create three-dimensional images by collecting the fluorescence intensity from many single spots in the sample. The strength of confocal imaging is the possibility to image far from the sample surfaces (up to hundreds of microns) while excitation of fluorophores outside the confocal volume is limited and the detection of the fluorescent light emitted outside the spot is suppressed. The thus obtained signal to background ratio of confocal imaging is superior to that of common wide-field fluorescence imaging and the possibility to image in-depth of a sample is not possible in TIRF microscopy. The main drawback of confocal fluores-

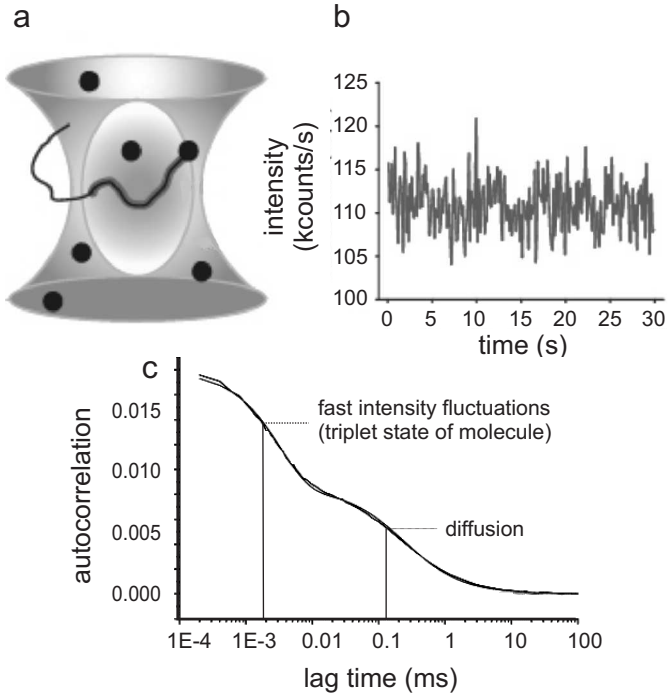

Figure 1.7 – Schematic representation of FCS. a. Fluorophores diffusing through a confocal spot. **b.** Fluorescence intensity trace. **c** Autocorrelation of the fluorescence intensity from diffusing molecules that also undergo microsecond intensity fluctuations (triplet state). (a) and (b) are from the W.W.Webb webpage (Cornell) and (c) is from Opitz et. al. [50].

cence imaging is the limited time-resolution in image acquisition, although commercial systems nowadays can image live cells with 3 ms time-resolution (spinning-disc confocal microscope).

In our custom-built confocal microscope, each detected photon is time-tagged using a counter board, limiting the temporal resolution of detecting a single-photon to the dead-time of the detector in combination with the detection limit of the counter board, in our case the first is ∼50 ns and the latter is 12.5 ns. The time resolution of imaging one diffraction limited spot in this setup is therefore 200,000 times better than is achieved with a camera with a maximum frame rate of 100 s^{-1}. In actual experiments however, the time-resolution is limited by the amount of photons per second that we can collect from the sample under given experimental conditions (i.e. background signal and photo-bleaching). The confocal-illumination and detection allow for single-molecule sensitivity and limited photo bleaching outside the confocal spot. However if we want to obtain images with our setup the sample needs to be displaced, and that produces images a lot slower than is possible with a camera.

Taken together, the strength of the confocal measurement approach to study ki-

nesin lies in the high time-resolution of measuring fluorescence intensities compared to TIRF microscopy. For a typical experiment we therefore positioned the confocal spot on a microtubule and detected the arrival times of fluorescence emitted by kinesins walking through the spot. This approach has similarities with fluorescence correlation spectroscopy (FCS), which will be discussed in the following paragraph.

Fluorescence correlation spectroscopy

A confocal setup can be used to measure the fluorescence emitted by diffusing labeled molecules. Fluorescence intensity fluctuations in the traces report on the diffusion of the molecules through the spot (typically milliseconds) but can also report on switching between different fluorescent states of molecules while they diffuse [65] (Figure 1.7). In most cases the fluorescence fluctuations are hidden in the average signal and correlation analysis is applied to obtain the characteristics of the fluctuations [46]. The autocorrelation of a fluorescence time trace at time lag τ is proportional to the conditional probability of detecting a photon at time $t + \tau$, after one has already been detected at t. In the calculation, the time intervals between the arrivals of all photons are taken into account, allowing discrimination of intensity fluctuations on a very short ($<$ ms) timescale (Figure 1.7). A major limitation of FCS on diffusing molecules is the fact that all molecules only reside in the confocal spot for a short time ($\sim$ms) and therefore it is not possible to study processes on a time-scale longer than a few milliseconds. Secondly, as the obtained autocorrelation is the result of the fluorescence taken from many diffusing molecules, it is intrinsically not a single-molecule approach but an ensemble average of many molecules.

1.3.2 Optical tweezers; micromanipulation and force detection

In this thesis we did not perform any optical tweezers measurements, however it has been and will remain to be a valuable technique to study kinesin and therefore a short description of the technique is given in this paragraph.

'Optical tweezers' is the common name for the measurement approach where a focused laser beam is able to trap small particles with a different refractive index than the medium they are submersed in. The main physical principle behind it is radiation pressure, the force that light exerts when colliding with matter. In every-day life, these forces are very small and we do not notice them, however for small objects ($<$ 100 μm) the forces can have a significant influence. This effect was first shown to occur with a focused laser beam with a power of 100-400 μW that could trap beads in the range from 10 μm down to $\sim$25 nm [7]. To explain why the particle is trapped in three dimensions near the focus of the laser beam a geometric-ray-optics approach is used (Figure 1.8). An optical trap is not only a manipulation tool, but also a sensitive position and force measurement device. Excellent reviews have been written on this topic (one of them being by Neumann and Block [48]) and I will not go into further detail here.

Optical tweezers are used to study kinesin by attaching a micron-sized bead to the tail of kinesin. The position of the bead is measured with high time-resolution (down to 50 μs) [8, 14] and high-spatial resolution ($\sim$nm) and effectively reports on the

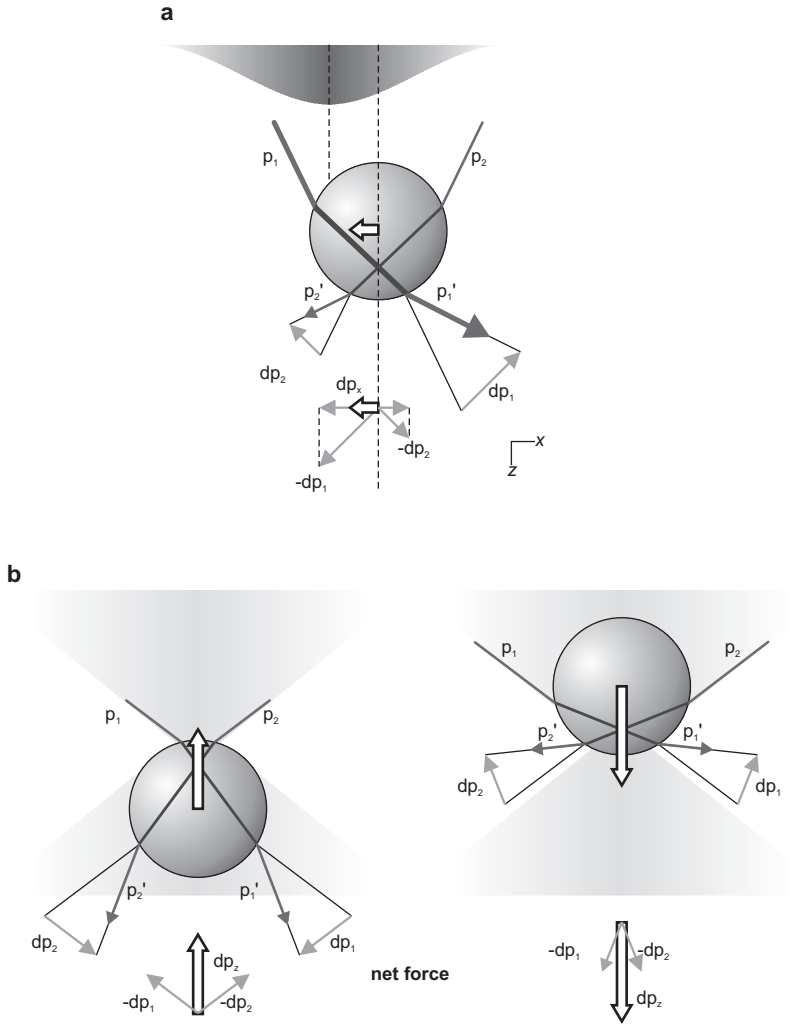

Figure 1.8 – Schematic representation of the light paths and the forces on a bead in an optical trap. a. The lateral force on the bead. **b and c.** The axial forces on the bead. The white arrows represent the restoring force. Pictures are a courtesy of Dr. Joost van Mameren-Schotvanger [81]

point of microtubule-attachment of kinesin. With optical tweezers experiments the force [14], ATP concentration [4,10,63,64,69,71,83] and substrate composition [29] can be varied and these experiments have led to many key findings about kinesin's motility.

1.4 Outline of this thesis

This section gives a brief summary of the contents per chapter in this thesis.

Chapter 2. Kinesin walking through the spotlight

In this chapter the confocal approach is described in detail, including the setup and data-analysis. The velocity distribution obtained with this approach is compared to the velocity distribution determined with classical wide-field fluorescence microscopy. We show that our confocal approach can determine the velocity of a single passing motor. Furthermore the photo-bleaching behavior of the attached fluorophores while traversing the confocal spot in combination with the increasing signal to noise ratio at increasing excitation intensities is discussed. The correlation technique for this type of data is introduced and via simulations its power in discriminating submillisecond intensity fluctuations in the fluorescence signal is investigated.

Chapter 3. Kinesin's step dissected with single-motor FRET

Four different homodimeric constructs of kinesin, each with a specific single-cysteine on each motor domain, are labeled with a donor and an acceptor fluorophore. Both the donor and acceptor fluorescence intensities are measured simultaneously and FRET between the two is observed for two constructs. These experiments show that an intermediate state exists ($\sim$3 ms) when kinesin steps at saturating ATP concentrations (step time is $\sim$12 ms). This intermediate state has one-motor domain bound to the microtubule while the other motor domain is not microtubule-bound, is rotated and close to the microtubule-bound domain. It is proposed that this state occurs directly after ATP binding and precedes ADP release of the microtubule-unbound motor domain.

Chapter 4. Alternating-site catalysis by Kinesin-1 confirmed with single-motor FRET using fluorescent ATP analogues

The binding and unbinding of single-fluorescently labeled ATP molecules was studied using single-labeled kinesin motors in our confocal setup. We observed kinesin moving processively in the presence of only fluorescently-labeled ATP and determined the Michaelis-Menten parameters. For fluorescently-labeled ATP $v_{\mathrm{max}} = 247 \pm 99$ nm/s and $K_{\mathrm{M}} = 32 \pm 22$ μM. For regular ATP $v_{\mathrm{max}} = 575 \pm 9$ nm/s and $K_{\mathrm{M}} = 13.4 \pm 0.6$ μM. After analyzing the autocorrelation of many single events in the presence of fluorescent ATP or mixtures of fluorescent ATP and regular ATP we found that the average fit parameters are well described by simulations of models that obey the alternating site mechanism, whereas single-site catalysis models all yielded poor fits to the obtained data.

Chapter 5. Novel ways to determine Kinesin-1's run length and randomness, using total-internal-reflection fluorescence microscopy

The goal of the research described in this chapter was to develop an experimental approach that can determine important motility parameters of kinesin with a measurement technique that is available to many research groups in the world. We used TIRF microscopy to obtain three key motility parameters of kinesin; the velocity, the number of rate-limiting steps in one single 8-nm step and the run length, all at different ATP concentrations. The average run length of hundreds of motors is obtained in a few minutes by analyzing the intensity profile over a microtubule that contains many labeled kinesins. Although single motors can not be discerned in this approach, the average run length can be obtained by analyzing the shape of the concentration profile. This approach is quick compared to other available techniques and does not require any correction for photo-bleaching due to the low excitation powers. We measure an average run length of 1220 $\pm$ 50 nm that is independent of the ATP concentration. The velocity is determined by analyzing the displacement-trajectories of many individually-tracked labeled kinesin motors. Analysis of the variance of the displacement trajectories allows us to determine the number of rate-limiting steps in one single 8-nm step, an analysis technique generally referred to as randomness analysis, and we verified that the randomness at saturating ATP lies between 0.33 and 0.5.

Chapter 2

Kinesin Moving through the Spotlight: Single-Motor Fluorescence Microscopy with Submillisecond Time Resolution

Abstract — Kinesin-1 is one of the motor proteins that drive intracellular transport in eukaryotes. This motor makes hundreds of 8 nm steps along a microtubule before releasing. Kinesin-1 can move at velocities of up to about 800 nm/s, which means that one turnover on average takes 10 ms. Important details, however, concerning the coordination between the two motor domains have not been determined due to limitations of the techniques used. In this study we present an approach that allows the observation of fluorescence intensity changes on individual kinesins with a time resolution far better than the duration of a single step. In our approach, the laser focus of a confocal fluorescence microscope is pointed at a microtubule and the photons emitted by fluorescently-labeled kinesin motors walking through the spot are detected with submicrosecond accuracy. We show that the autocorrelation of a fluorescence time trace of an individual kinesin motor contains information at time lags down to 0.1 ms. The quality and time resolution of the autocorrelation is primarily determined by the amount of signal photons used. By adding the autocorrelations of several tens of kinesins, fluorescence intensity changes can be observed at a time scale below 100 microseconds.

This paper has been published: *Sander Verbrugge*, Lukas C. Kapitein, Erwin J.G. Peterman, Biophysical Journal, 92(7):2536-2545, 2007

2.1 Introduction

Molecular motors of the kinesin superfamily are microtubule-binding proteins that hydrolyze ATP to drive motility. The most widely studied family is kinesin-1, which is one of the motors that drive intracellular vesicle transport [79]. Kinesin-1 consists of two identical motor domains and makes single steps of 8 nm along a microtubule [71] per ATP hydrolyzed [63]. Furthermore, it is able to make hundreds of such steps during one encounter with a microtubule, a property called processivity [15]. It is believed that release of the motor from the microtubule is prevented by keeping the chemical cycles of the two motor domains out of phase [83]. Consistent with this idea was the finding that each motor domain in turn steps 16 nm forward in a hand-over-hand fashion [4, 39, 92]. The molecular details of the coupling between the motor domains remains unclear, but mechanical interactions play a role [58, 78]. The enzymatic cycle of ATP hydrolysis by each motor domain consists of at least four distinct states, each coupled to the conformation of the neck linker and the affinity for the microtubule. The ATP-concentration dependence of kinesin's velocity follows Michaelis-Menten kinetics with a maximal velocity (v_{max}) of about 0.8 μm/s. Consequently, under saturating ATP-conditions, the average duration of a single catalytic cycle is about 10 ms [44, 56, 64]. In order to reveal the molecular details of the coupling between the chemical and mechanical cycles of the two motor domains of walking kinesin it is essential to use techniques that allow discrimination of the chemical states with submillisecond time resolution.

Our understanding of kinesin's mechanism has benefited a great deal from the application of single-molecule techniques. The key advantages of applying single-molecule methods to kinesin are that the properties (e.g. velocity, step size, generated force) of single kinesin motors can be determined directly and that synchronization of many motors is not needed (such as in stopped-flow kinetics experiments). Two single-molecule techniques that have been used extensively to clarify kinesin's mechanism are optical tweezers and wide-field single-molecule fluorescence microscopy. Using optical tweezers, the force exerted by a single motor as well as its centre-of-mass position can be measured with high time resolution (>5 kHz) and high force (< 1 pN) and spatial resolution (< 1 nm) [48]. In general, the properties of the motor are measured while it is subjected to an external load; measurements at low load are difficult. A limitation of this technique is that the mechanics of the kinesin as a whole are studied and that it does not allow for direct measurement on individual motor domains. Furthermore, information on the kinetics of transitions in kinesin's chemomechanical cycle can only be inferred from fitting kinetic models to the data [64], but cannot be observed directly. The other frequently used technique is wide-field single-molecule fluorescence microscopy, which allows direct observation of the motion of single, fluorescently labeled motors. By attaching the label to different parts of the molecule one can measure the motion of the centre of mass of the whole dimeric motor [77] or one of the motor domains [92]. Fluorescence microscopy has the advantage that also other parameters than location can be measured, such as relative distances using FRET (Förster Resonance Energy Transfer) [30], orientation using fluorescence polarization [68], and the presence of fluorescent substrate analogues [24]. In most applications of wide-field fluorescence microscopy to kinesin, CCD-cameras are used

for fluorescence detection [52]. These severely limit the time resolution of the technique, since they require integration of the emitted photons over 50-500 ms to obtain images with a high enough signal-to-noise ratio for accurate localization of the motor [92]. During such time intervals kinesin makes several steps, unless its velocity is lowered by limiting the ATP concentration. Both these techniques do not allow resolving the details of the coupling between the chemical and mechanical cycles of the two motor domains of walking kinesin. Wide-field single-molecule fluorescence microscopy does not have the time resolution required, whereas optical tweezers do not allow discrimination between the states of the individual motor domains.

In the present study we introduce another fluorescence-based approach, with a time resolution high enough to allow resolution of the transitions between kinesin's chemical states. Our approach is based on fluorescence detection of individual, labeled kinesin motors walking through the focus of a confocal fluorescence microscope, at saturating ATP-concentrations without applying an external load. This chapter is built up as follows. First, we describe the technical details of our method. Second, we test the properties of our kinesin construct and motility assay with traditional, wide-field single-molecule fluorescence microscopy. Then we show that our confocal fluorescence microscopy method is compatible with the wide-field results. Finally, we show by applying autocorrelation analysis that our method allows resolving fluorescence intensity fluctuations that take place on a time scale of 10 μs, a thousandth of kinesin's average turnover time at saturating ATP-concentrations.

2.2 Materials and Methods

2.2.1 Construction of a single-cystein kinesin construct.

We constructed a homodimeric kinesin with a single cys located in the tail (hK421C). We started with a human kinesin (KIF5B) construct of 560 amino-acids with a single cys at position 174 in a Pet23b vector [51] and changed the only cys present to ala. An upstream primer 5'-GCGCCACAGAGCGTTTTGTAGCAAGTCCAGATGAAGTTATGGATA3' and a downstream primer 5'-TATCCATAACTTCATCTGGACTTGCTACAAAACGCTCTGTGGCGC-3' were used to introduce the mutation and amplify the sequence with a site-directed mutagenesis kit (Quikchange II, Stratagene, La Jolla, CA). A cys was reintroduced at position 421 (cys in the wild-type sequence) using upstream primers 5'-GCTGAAAGAAGAAAGTGTGAAGAAGAAATTGCTAAATTATACAAACAGCTTGATG-3' and downstream primers 5'-CATCAAGCTGTTTGTATAATTTAGCAATTTCTTCTTCACACTTTCTTCTTTCAGC-3'. The plasmids were stored in XL1-blue *E.coli* cells.

For expression, the plasmid was introduced in *E.coli* Bl21(DE3) cells, grown to larger volumes (1 or 2l) and induced overnight at 22°C with isopropyl-beta-D-thiogalactopyranoside (AppliChem, Darmstadt, Germany). Bacteria were spun down and the pellet was lysed by adding lysosyme and applying three brief periods of sonification. The lysate was loaded on a NiNTA column and the motor, tagged with a 6x his repeat on the N-terminus, was eluted with 300 mM imidazole.

The motor was labeled with Alexa Fluor 555 maleimide (Invitrogen, Carlsbad, CA), by adding the dye (dissolved in dimethylformamide and diluted in demineralized

water) in a one-to-one fluorophore-to-kinesin monomer ratio and incubating for three hours at 4°C. Unreacted dye was separated from the labeled kinesin by microtubule affinity centrifugation [16].

2.2.2 Sample chamber preparation

Cover slips (#1.5, MenzelGlaser, Braunschweig, Germany) and slides (MenzelGlaser) were cleaned before use by sonification in 0.1 M KOH (1x, 10') and in demineralized water (3x, 10'). Cover slips were made positively charged by sonification in 0.1 % (V/V) N^1-[3-(Trimethoxysilyl)-propyl]diethylenetriamine (Sigma-Aldrich, St. Louis, MO) in water (1x, 10') and subsequent washing in water (3x, 10'). The cover slips were dried in an oven at 130°C and were stored dry. In contrast, the slides were cleaned each day and dried immediately before use. Sample chambers with three lanes (volume 5 µl) were made by gluing a cover slip to a slide using double-stick tape.

2.2.3 Sample lane preparation

Microtubule seeds were polymerized by mixing 7.5 µM unlabeled tubulin, 2.5 µM TMR-labeled tubulin and 1 mM GMPCPP (Guanosine-5'[(α,β)-methyleno]triphosphate (Jena bioscience, Jena, Germany)) for 15' at 36°C. Afterward they were stabilized with PEM80-taxol buffer (80 mM Pipes, 1 mM EGTA, 2 mM $MgCl_2$ pH 6.8 and 10 µM taxol) and were injected into the sample lanes. After 10' the lanes were rinsed three times with 10 µl PEM80-taxol buffer. Casein (sodium salt, from bovine milk, Sigma-Aldrich) at 0.4 mg/ml in PEM80-taxol buffer, was flushed into the lane and incubated for 10'. The lane was again rinsed three times with 10 µl PEM12-taxol buffer (equivalent to PEM80-taxol but with 12 mM Pipes). After these steps the mix with kinesin motors was flushed into the sample lane after which the sample was sealed with vacuum grease. In all experiments an oxygen scavenger system (20 µg/ml glucose-oxidase, 35 catalase µg/ml and 25 mM glucose), 4 mM dithiothreitol and 10 µM taxol were added. For samples at saturating ATP-concentrations, 2 mM ATP was added. In other experiments kinesin's velocity was decreased by instead adding 100 µM ATP and an ATP regeneration system (10 mM phosphocreatine and 50 µg/ml creatine kinase) [69].

2.2.4 Experimental setup

The attenuated, 532 nm beam of a Verdi V10 (Coherent, Santa Clara, CA) laser was circularly polarized with a quarter-lambda plate, expanded 6 times and coupled into an inverted microscope (TE-2000-U Nikon, Tokyo, Japan) with a 100x oil immersion objective (Nikon Plan Fluor, NA 1.3) (Figure 2.1). Fluorescence was collected through a dichroic mirror (Q545LP, Chroma, Rockingham, VT) and filtered with an emission filter (HQ575/50, Chroma). The fluorescence light was then imaged on a CCD camera (CoolsnapHQ, RoperScientific, Tucson, AZ) or focused onto a multimode optical fiber (100 µm core diameter), serving as a pinhole [35] and detected with

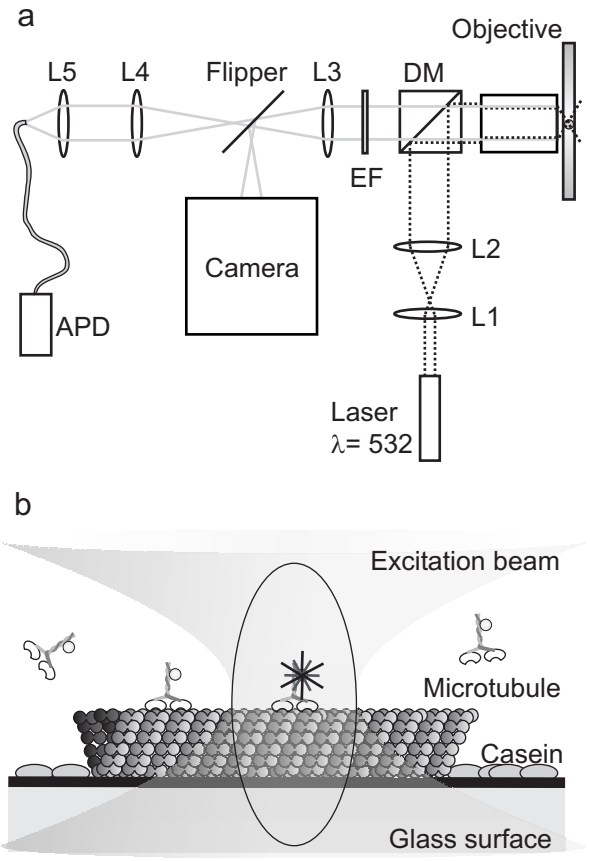

Figure 2.1 – Schematic representation of the experimental setup and the motility assay. a. Light paths of excitation (*dashed black*) and emission (*solid grey*) are indicated. The beam expander is represented by L1 and L2. DM is the dichroic mirror and EM is the emission filter. L3 is a lens located inside the microscope and L4 and L5 image the confocal spot onto the optical fiber. The dashed line represents the port selection of the microscope. **b.** Several kinesins in or near the confocal spot. The microtubule is attached to the glass via a positively charged (DETA) surface. Casein prevents non-specific sticking of the kinesin to the glass.

an avalanche photo diode (APD) (SPQM-AQR-14, PerkinElmer, Vaudreuil, Quebec, Canada). Photons detected by the APD were converted in TTL pulses, which were time-tagged with electronic counter board (6602, National Instruments, Austin, TX) with 12.5 ns time resolution. Arrival times of detected photons were stored on a computer using custom-built Labview software (Labview 7.1, National Instruments).

To accurately position the confocal spot and scan the sample we used a feed-backed controlled piezo translation stage (P-561, Physikalischer Instrumente, Karl-

sruhe, Germany) with a custom-built sample holder mounted on top of the scanner.

2.2.5 Positioning the confocal spot and acquiring high time-resolution data

Wide-field illumination and CCD-camera detection were used to locate the fluorescently labeled microtubules. The sample was translated to position the confocal spot within 1 micrometer of a microtubule. Then, a 1x1 μm area was scanned and the microtubule was positioned within 20 nm of the centre of the confocal spot. This positioning procedure was repeated every ten minutes to compensate for mechanical drift. Fluorophores on the microtubules were bleached, before measuring the fluorescence of kinesins moving through the confocal spot.

2.2.6 Determining the width of the confocal spot

The width of the confocal point spread function was obtained by fitting a two-dimensional Gaussian to a confocal image of fluorescent beads (40 nm diameter, excitation/emission = 565/580 nm, FluoSpheres, Invitrogen) stuck to the surface. The width (defined as σ of the Gaussian, i.e. the half width at $1/\sqrt{e}$) was corrected for the bead size by deconvolution and was determined to be 113 nm ± 5 nm (mean ± s.e.m.).

2.3 Results and Discussion

2.3.1 Characterization of the kinesin construct with conventional wide-field fluorescence microscopy

To test our kinesin construct (hK421C-Alexa 555) we measured run lengths and velocities of individual motors at saturating ATP concentrations with conventional wide-field fluorescence microscopy. In this assay, sparsely labeled microtubules (roughly one fluorophore per 1500 tubulin-dimers) were bound to a positively charged surface and kinesin was added. Movies were recorded and were analyzed using kymography [85] (not shown). Events were manually traced in the kymograph and the velocity and run length of each event was determined. To reduce tracing inaccuracy and to discard binding events of non-functioning motors only events longer than 0.6 seconds (two frames) were taken into account. Fitting a single Gaussian peak to the histogram of velocities of single motors (Figure 2.2a) yielded an average velocity of 886 ± 7 nm/s, similar to velocities published before [83]. The average of all the velocities (860 ± 5 nm/s, N = 657) is comparable to the value found by fitting.

The average run length was determined by fitting a single exponential to a plot of the fraction of kinesin still bound as a function of run length Figure 2.2b [66]. Using this method we found an average length of the runs of 1550 ± 30 nm. The amount of photo bleaching under our experimental conditions was determined by measuring the fluorescence intensity as a function of time for labeled kinesins fixed to microtubules with AMPPNP. A single- exponential decay fitted to these data yielded

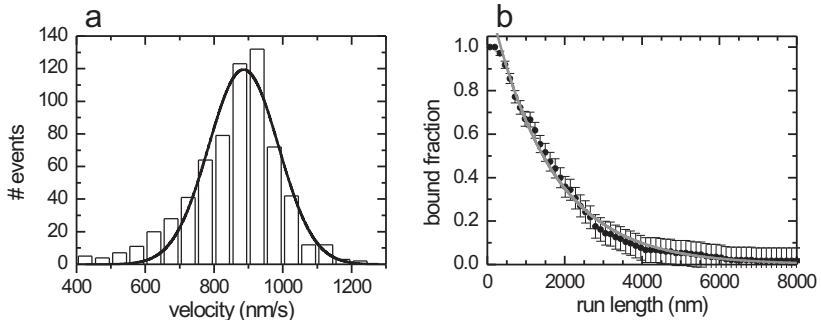

Figure 2.2 – Characterization of hK421C's motility on microtubules using single-molecule wide-field fluorescence microscopy assays. a. Histogram of the velocities of individual motors (N = 657). The solid line is a Gaussian fit to the distribution with its center position at 886 ± 7 nm/s (mean ± s.e.m.). **b.** Distribution of the probability of being bound after a given run length (N = 204). A single exponential fit (*solid grey line*) indicates that the average run length is 1550 ± 30 nm (not corrected for photo bleaching). The error bars are calculated from the square root of the absolute number of already detached motors and are normalized.

an average bleaching time of 27 ± 1 s (data not shown). The run length was corrected for photo bleaching with this value, yielding a corrected run length of 1680 nm. The run length is comparable to literature [66, 83]. Taken together, these results show that we have an active construct that functions in single-motor assays equivalent to native kinesin-1.

2.3.2 Typical events observed with confocal microscopy

We then switched from wide-field to confocal microscopy. When the laser was focused on a microtubule (Figure 2.1b), we observed fluorescence time traces as shown in Figure 2.3a. Labeled kinesins walking through the confocal spot show up as Gaussian peaks, which can be explained as follows. The kinesin-bound fluorophore senses a laser intensity that is determined by its location in the laser spot (which can be approximated by a Gaussian with width σ_{exc}). Consequently, under our experimental conditions (see below) the fluorophore emits with a rate proportional to this local excitation intensity. In a confocal microscope, the efficiency of detecting a photon emitted by a fluorophore also depends on its location as described by the collection efficiency profile (which can also be approximated by a Gaussian, with width σ_{CEF}), As a consequence, the total detected fluorescence intensity is proportional to the product of the excitation profile and the collection efficiency function. The product is also a Gaussian [93] and is called the confocal point spread function. Therefore, the fluorescence of a labeled kinesin moving at constant velocity through the confocal spot will appear as a Gaussian peak in a binned fluorescence time-trace. In Figure 2.3a, several Gaussian peaks can be discerned, all with nearly the same duration and am-

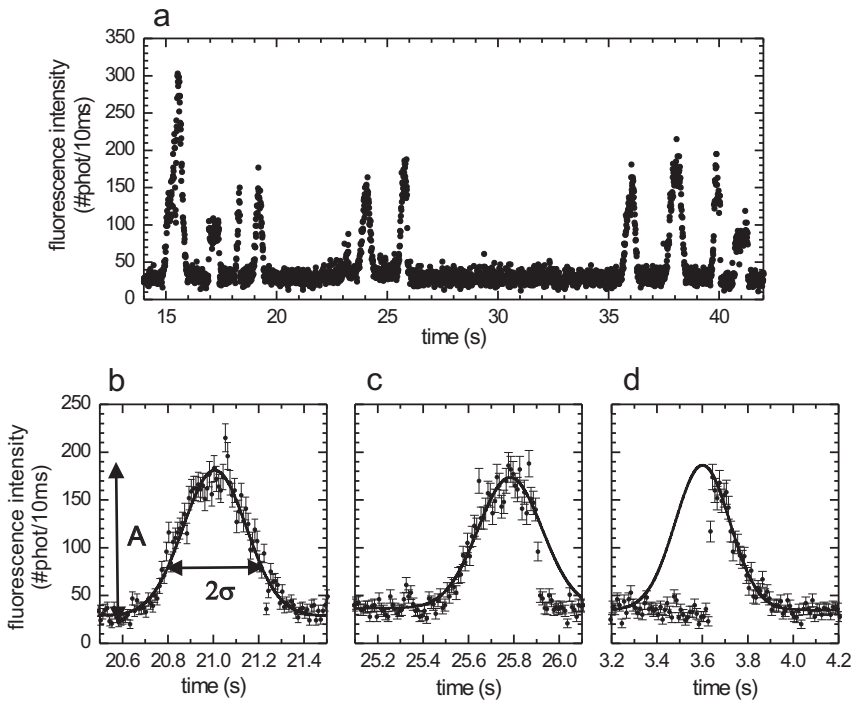

Figure 2.3 – Fluorescence intensity traces obtained when the confocal spot was positioned on a locally bleached microtubule. a. A time trace of 30 seconds shows several events, most with comparable amplitude. **b.** A *full* event, which is due to a motor landing before the confocal spot, walking in and through it and consequently showing a complete Gaussian profile. The solid line is a Gaussian fit to the trace. The amplitude (A) and width (σ) of the event are indicated for clarity. **c.** A *vanish* event, which is due to a kinesin walking into the confocal spot but abruptly photo bleaching or detaching somewhere in the spot and consequently showing only the leading flank of a Gaussian. **d.** A *landing* event, which is due to a kinesin landing on the microtubule somewhere in the spot and consequently showing only the trailing flank of a Gaussian. In (c) and (d) the Gaussian was fit to the points of the leading and the trailing flank respectively. Each error bar in graphs (b), (c) and (d) is the square-root of the corresponding intensity.

plitude, except for one, with an amplitude about twice as high. This latter signal is most probably due to a motor with two labels or two motors passing the focus at the same time. The time trace also shows two peaks with a constant, non-Gaussian fluorescence signal, which we attribute to fluorophores (loose or attached to kinesin) that get stuck somewhere in the confocal spot and detach or photo bleach after some time.

Closer examination of the apparent Gaussian peaks reveals that three types of

events can be discerned. (i) A large fraction of the events shows up like a complete Gaussian peak (Figure 2.3b). These events are due to labeled kinesins walking into and through the spot without detaching from the microtubule or photo bleaching. We call this type of events *full* events. (ii) The time traces of a second class of events show only the leading flank of a Gaussian (Figure 2.3c). We attribute such a signal to a kinesin walking into the spot, but abruptly photo bleaching or detaching somewhere in the spot. We call this type of events *vanish* events. (iii) In the third type of events only the trailing flank of a Gaussian can be seen (Figure 2.3d). We attribute such a signal to a kinesin landing from solution on the microtubule somewhere in the spot and walking through the remainder of the spot. This type is referred to as a *landing* event. Also shown in Figure 2.3b-d are Gaussian fits to the time traces, used to determine the amplitude (A) and the width (σ) of each event, which were used for further analyses.

2.3.3 Determination of the velocity of kinesins walking through the confocal spot

The Gaussian shape of the events indicates that the kinesin's velocity is constant during the passage through the confocal spot. Since the detected emission rate is proportional to the value of the confocal point spread function at the location of the motor, the motor's velocity equals the ratio of the spatial width of the point spread function and the temporal width of an event. A histogram of the temporal widths of all full events at a staturating ATP concentration of 2 mM is shown in Figure 2.4a. The distribution of the widths is Gaussian and peaks at 130.3 $\pm$ 1.7 ms (as determined with a Gaussian fit; the statistical average is 136.3 $\pm$ 1.5 ms). From this average temporal width an average velocity of 870 $\pm$ 40 nm/s can be calculated. The average value obtained in this way and the shape of the distribution compare very well to our wide-field fluorescence measurements, depicted in Figure 2.4C. To further validate our velocity determinations, confocal and wide-field measurements were also performed at 100 μM ATP, a concentration at which kinesin moves slower. The averaged temporal width of events at 100 μM ATP is larger (300 $\pm$ 20 ms) than at 2 mM. Furthermore, the distribution of the widths is wider as well (Figure 2.4b). Wide-field velocity determinations at the same ATP concentration show a similar average velocity (326 $\pm$ 9 nm/s) and distribution as the velocities calculated from the confocal measurements (344 $\pm$ 15 nm/s, Figure 2.4d).

2.3.4 Behavior of fluorophores at different excitation powers

Next, we determined the laser-power dependence of the emission time traces of labeled kinesins walking through the confocal spot. One would expect that high excitation powers lead to a higher rate of photon detection (improving photon statistics), but at the same time increase the probability of photo bleaching (decreasing the number of *full* events). First, we determined the average amplitude as a function of laser power. Figure 2.5a shows that the amplitude depends linearly on the excitation power, as expected for the intensities used in our assay [20]. Second, we determined

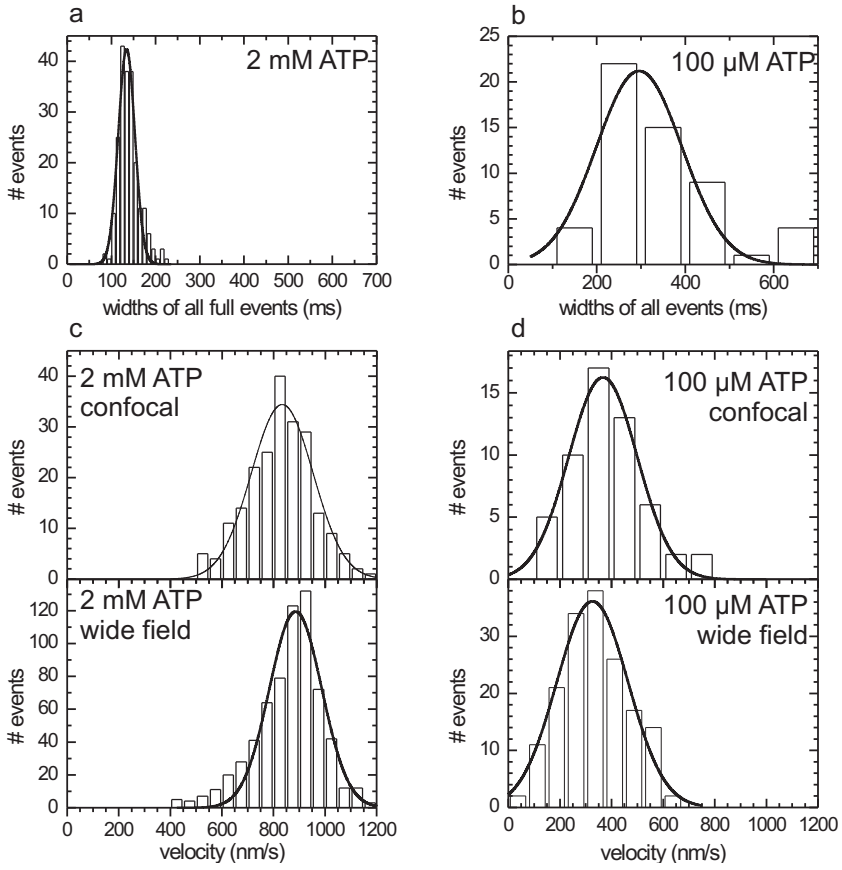

Figure 2.4 – Wide-field and confocal velocity measurements at two different ATP concentrations. a and b. Histogram of the widths of full events at 2 mM ATP and 100 µM ATP (N = 213 for 2mM and N = 55 for 100 µM, events at different excitation powers were pooled). The calculated velocities from these widths are plotted together with the velocities obtained from wide-field measurements for both 2 mM ATP **c.** and 100 µM ATP **d.** The solid lines represent Gaussian fits to the data.

that the width (of *full* events, i.e. kinesin's velocity) does not depend on the laser power (Figure 2.5b), as expected. Also the landing ratio, which we define as the number of *landing* events divided by the number of *vanish* and *full* events, does not depend on laser power (Figure 2.5c). In contrast, the *vanish* ratio, which we define as the ratio between *vanish* events and the sum of *vanish* and *full* events, depends in a nonlinear way on the excitation power (Figure 2.5c). This data can be described by exponential relaxation with an asymptote at a probability of one and an offset at zero power. The offset is caused by motor detachment due to the finite run length. The exponential relaxation can be explained by the exponential dependence of the

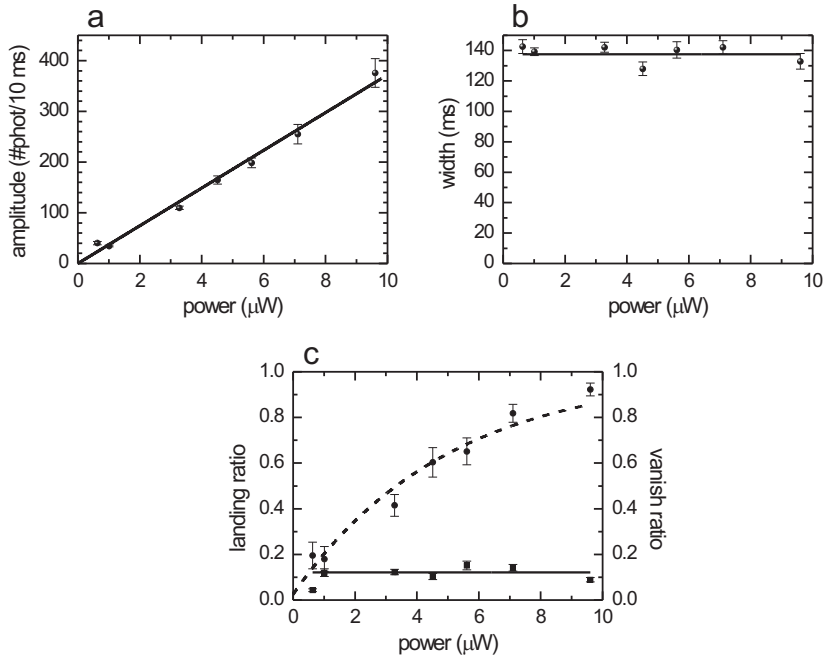

Figure 2.5 – **a.** The average amplitude of all full events as a function of excitation power. The solid line represents a linear fit (without offset) with a slope of 3700 ± 80 photons/(s*μW). **b.** The average width of all full events as a function of excitation power. The solid line represents a fit of a constant value (137 ± 2 ms). **c.** *Landing* ratio (*squares*) and *vanish* ratio (*solid spheres*) (see text) as a function of excitation power. The solid line represents a fit of a constant to the landing ratio data points (0.12 ± 0.01). The dashed curve represents a fit to an exponential decay, (y = 1 - a*exp(-x / t1), where a = 0.97 ± 0.05 and t1 = 5 ± 0.5 μW).

probability of a fluorophore not having photo bleached after emitting a given number of photons. The number of photons emitted during a full event is linearly proportional to the excitation power. Therefore, the probability of a kinesin completing a *full* event decays exponentially with excitation power. We chose to not perform a more quantitative analysis on these data, since that would strongly depend on an accurate estimation of the effective distance over which beginning or ending of an event can be discriminated from back ground, which is problematic. In the following we will present a quantitative analysis of autocorrelated fluorescence time traces, which do not suffer from this problem.

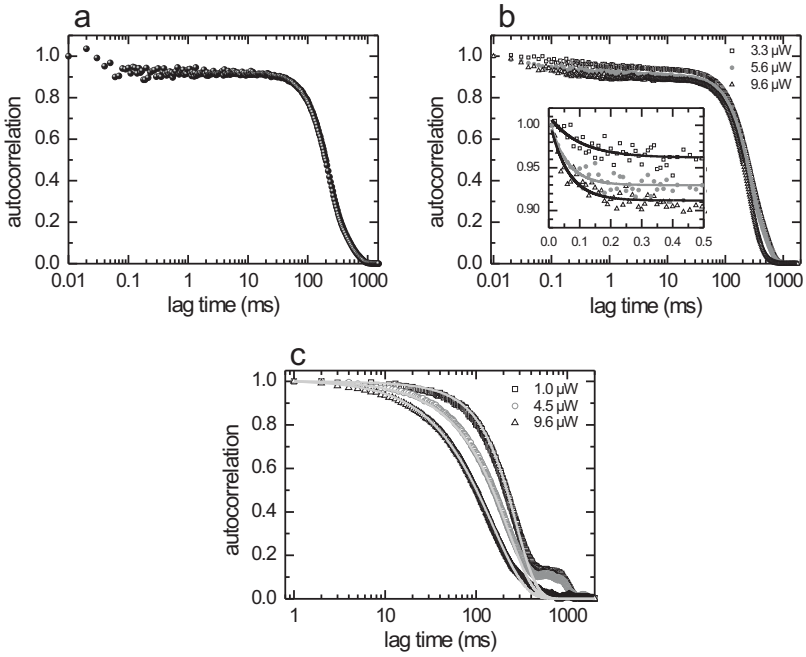

Figure 2.6 – Autocorrelation analysis of the time traces obtained with single-kinesin confocal microscopy. a. Normalized autocorrelation of a single *full* event at an excitation power of 9.6 μW. **b.** Normalized summed autocorrelation for three different excitation powers of *only full* events (time binned with 10 μs). Inset shows the exponential decay with their fits at the submillisecond timescale, probably due to triplet blinking of the fluorophore; the amplitudes increase with excitation power (0.049 ± 0.006, 0.079 ± 0.009 and 0.097 ± 0.008 respectively) whereas time constants of the fits are similar (0.10 ± 0.04 ms, 0.056 ± 0.011 ms and 0.058 ± 0.010 ms respectively). **c.** Normalized summed autocorrelations at three different excitation powers of *vanish* and *full* events (time binned with 1 ms). The small shoulders observed around 900 ms are due to small errors in the background correction and the finite time interval of the correlated trace (2000 ms in all graphs shown here). The grey lines represent a simulation for the three different powers, see text for details of simulation.

2.3.5 Autocorrelation of fluorescence time traces

So far we have used 10-ms time binning of the photon-arrival-times in our data analysis. To determine the effective time resolution of our method, we performed autocorrelation analyses to fluorescence time traces with smaller bin widths [22]. It should be noted that we do not expect the fluorescence intensity of the kinesin construct used for these experiments to change due to switches from one mechanical or chemical state to another, because it is labeled in the tail.

Events due to individual kinesin dimers walking through the confocal spot were selected after visual inspection of the fluorescence time traces. The centre point and background levels were determined for each event by fitting a Gaussian to 10-ms binned time traces. The autocorrelation was calculated from 2 s long, background-subtracted binned time traces containing an event with its centre point in the middle. The time traces were binned with bin sizes of 1 ms or 10 μs depending on the time-scale of interest (the calculations at small time bins require substantial computation time). For the autocorrelations with 10 μs bins we applied a coarse-grain step afterwards to improve the signal-to-noise ratio on the longer time-scales: the correlation times were chosen to increase logarithmically with time [84]. The correlation values within a bin were averaged.

The normalized autocorrelation of the fluorescence trace of a single motor passing through the confocal spot (Figure 2.6a) is roughly Gaussian with a larger width than that of the time trace it was calculated from (as expected since the autocorrelation of a Gaussian is a Gaussian with a $\sqrt{2}$ larger width). The time-symmetric autocorrelation is only shown for positive lag times, on a logarithmic time scale to more clearly represent the curve over 5 decades of time,

Even with a limited number of photons (11,000 in this event) the autocorrelation function of a single event still contains information at 0.1 milliseconds. The signal-to-noise ratio depends both on the distribution of times between consecutively detected photons and the total number of detected photons. The former can be improved by using higher fluorescence intensities. This leads however to an unwanted increase of the photo bleaching. The number of photons detected and in that way the time resolution of the autocorrelation can be increased by summing the autocorrelations of multiple events, as shown for all full events at three different powers (Figure 2.6b). In this way, we obtain curves with relatively low noise down to 10 μs, showing that with our approach fluorescence fluctuations down to the 10 μs time scale can be observed. The traces show an exponential decay at lag times up to 0.1 ms (inset Figure 2.6b), which is probably due to the triplet state of Alexa555, since its amplitude increases with excitation intensity and its decay time hardly changes for the relatively small range of changes in amplitude [86]. The three curves measured with different excitation intensity have the same width of about 200 ms (only full events were used and kinesin's velocity does not depend on the excitation intensity (Figure 2.5). When *vanish* events are also included in the summation, (Figure 2.6c) the higher power curves turn out to be narrower than the lower power ones, which is indicative of increased photo bleaching, leading to more and narrower *vanish* events.

2.3.6 Simulations of the autocorrelated fluorescence time traces

To fully understand the effects of photo bleaching and detachment of the motor, we focused further analysis on the 1-1000 ms time scale of summed autocorrelations of all *full* and *vanish* events (Figure 2.6c) and simulated the autocorrelated fluorescence time traces. Simulations were performed as follows. The emission rate of a labeled motor moving with constant velocity (v) depends on its position in the Gaussian excitation profile with width σ_{exc}. The detection efficiency depends on the location of the motor in the collection efficiency profile, which we assume Gaussian with a width of

σ_{CEF}. The number of detected photons (N_{det}) between time interval t and $t+\Delta t$, due to such motor can be calculated using:

$$N_{\mathrm{det}}(t) = \Delta t P \alpha \exp\left(\frac{-(vt)^2}{2\sigma_{exc}^2}\right) \eta \exp\left(\frac{-(vt)^2}{2\sigma_{CEF}^2}\right) \tag{2.1}$$

Where P is the power of the excitation laser, α is the setup- and fluorophore-dependent factor that relates the excitation power to the rate of emitted photons and η is the maximum collection efficiency. Here we assume that at t=0 the motor passes the coinciding maxima of the excitation and collection profile.

Next, for each event photo bleaching was introduced, by assuming a constant probability of bleaching for each emitted photon (the reciprocal of the bleach constant b). The probability of bleaching, $p_{\mathrm{bleaching}}$, during an interval between t and $t+\Delta t$ can be expressed as:

$$p_{bleaching}(t) = \frac{\Delta t}{b} \alpha P \exp\left(\frac{-(vt)^2}{2\sigma_{exc}^2}\right) \tag{2.2}$$

Note that the probability of bleaching as a function of time only depends on the location of the fluorophore in the excitation spot and is not influenced by the location in the collection efficiency profile. For each step, this probability was compared to a randomly-generated number (between 0 and 1), to decide whether photo bleaching had occurred. In case of photo bleaching, the signal was set to zero for the rest of the event.

In a similar way the finite length of kinesin runs was introduced. During each time interval the motor has a constant probability of detaching from the microtubule (p_{detach}), independent of its location:

$$p_{detach} = \exp\left(\frac{-v\Delta t}{l}\right) \tag{2.3}$$

Where l is the average run length.

In this way, fluorescence time traces of 15,000 events were generated for different excitation powers using varying values for the other parameters. Subsequently, these traces were autocorrelated and summed. The measured autocorrelation curves, can be simulated very well with a value for the run length (l) of 1700 nm, for the velocity (v) of 870 nm/s, for the width of the collection efficiency function (σ_{CEF}) of 220 nm, for the width of the excitation spot (σ_{exc}) of 150 nm, for the maximum collection efficiency (η) of 0.1, and for a bleach parameter (b) of 55,000 photons. Varying the value for the run length in the simulations (from 800 to 2000 nm) hardly altered the simulated correlation traces (data not shown), since the length scale of observing motion in our instrument ($4\sigma_{\mathrm{PSF}} \approx 500$ nm) is several times smaller than the run length. The overall good correspondence of the model to the data indicates that the behavior of labeled motor proteins walking through the confocal spot is sufficiently understood. The small shoulder around 900 ms lag time in the autocorrelation curve of 1.0 μW is due to small inaccuracies in the background correction of the events.

2.3.7 Simulation of a construct whose fluorescence fluctuates due to stepping

The ultimate goal of our approach is to observe transitions between the chemomechanical states of walking kinesin. For this, labeled kinesin constructs are needed with at least two states in the cycle with differing fluorescence intensities. To examine the potential of our approach to yield new information on kinesin's mechanochemistry we have simulated time traces and intensity autocorrelations of a kinesin construct capable of Förster Resonance Energy Transfer (FRET) between its two motor domains. We assume a construct with a donor fluorophore on one motor domain and an acceptor fluorophore at the same position on the other motor domain. The stepwise behavior of the motor is taken into account and each step is assumed to consist of two distinct fluorescent states. We assume that the FRET transfer-efficiency between donor and acceptor is 0.16 when the two motor domains are attached to consecutive binding sites on the microtubule (8 nm apart). During a step, we assume that the two motor domains are closer and that the transfer efficiency equals 0.8. The proximity could be due to a sub-step but can also be due to the overtaking of the forward head by the rearward one. It is known that kinesin's stepping takes less than 1 ms [64].

Focusing on the intensity of the fluorescence emitted by the acceptor we assume that a single step consists of a short-lived high-fluorescent state and a longer lasting low-fluorescent state. We mimic the Poisson-like behavior of the motor by randomly selecting the occupation times of both states from an exponential distribution. In a first simulation we use an average occupation time of the high fluorescence state of 0.5 ms and of the low fluorescent state of 9.5 ms. The maximum emission rate of the acceptor is 20 photons/ms (as expected for the typical excitation powers used in our experiments) and the background signal is 1 photon/ms. The photon arrival times are generated from an exponential distribution with a decay time that depends on the fluorescent state and the position in the confocal spot.

In the simulated, binned fluorescence intensity traces the short-lived high-fluorescent state is hidden in the amplitude fluctuations of the Gaussian envelope (Figure 2.7a, black curve). The autocorrelation of this single event shows a decay around 0.5 ms, a signature of short bursts of fluorescence with on average this duration (Figure 2.7b, black curve). Averaging the autocorrelations of 20 simulated full events (Figure 2.7c, black curve) yields a smooth curve with an even more clear decay at 0.5 ms. In a next set of simulations we decreased the time the molecule spends in the high state to on average 0.1 ms, while the low-fluorescent state lasts 9.9 ms. Comparison of the binned fluorescence traces for the two different sets of simulations shows no clear differences (Figure 2.7a, black and grey curve). Moreover, in the autocorrelation of a single event, clear features on the 0.1 ms time scale cannot be discerned (Figure 2.7b, grey curve). If we however average 20 events with these setting we observe a clear decay around 0.1 ms (Figure 2.7c, grey curve), demonstrating that our approach can yield insight in chemomechanical transitions taking place in less than 0.1 ms. In the simulations conservative estimates of the parameters are used. A further improvement of the detectable time scale could be obtained by averaging even more events.

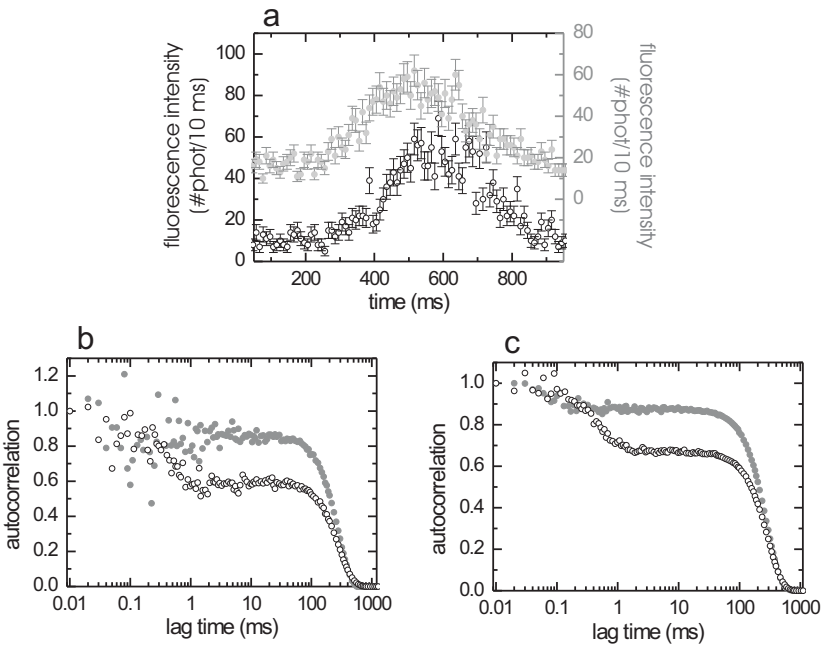

Figure 2.7 – **a.** Simulated fluorescence intensity traces of kinesin stepping through a Gaussian excitation profile switching between high and low FRET states. The graph with solid grey circles is shifted upwards for clarity; it's axis is on the right-hand side of the graph. Each error bar is the square-root of the intensity. **b.** Intensity autocorrelations of the events shown in figure (a). **c.** Summing the autocorrelation of 20 separately simulated events improves the signal to noise ratio, in particular on the short timescales. See text for details of the simulations. For all three graphs: the solid grey circles circles represent a simulation with the low FRET state (emitting 4 photons/ms in the acceptor channel) lasting on average 9.9 ms and the high FRET state (20 photons/ms) lasting 0.1 ms. Black open circles represent a simulation with the low FRET state lasting 9.5 ms and the high FRET state lasting 0.5 ms.

2.4 Conclusions

We have presented a new approach to study the motion of fluorescently labeled kinesin with submillisecond time resolution. In our approach labeled kinesins walk through the excitation spot of a confocal microscope and the emitted photons are detected with nanosecond resolution. Fluorescence time traces measured in this way have an approximately Gaussian profile, the width of which is a signature of the motor's velocity. We find an average velocity of 870 ± 40 nm/s. Summed autocorrelations of the fluorescence time traces from individual motors allow discrimination of fluorescence intensity fluctuations on a timescale down to 10 μs. The autocorrelations

and their excitation intensity dependence can be well described using a simple model taking into account the profiles of the excitation intensity and collection efficiency, the velocity of the motor, photo bleaching and detachment from the microtubule track.

Our approach is related to fluorescence correlation spectroscopy [46]. Fluorescence correlation spectroscopy is often used to study freely diffusing labeled molecules, but it has also been applied to study flow inside cells [40] and microfluidic devices [28] In these studies, diffusion of the labeled biomolecules could be discriminated from drift with the solvent flow and flow velocities could be determined. Our approach is different in the key aspect that it is a truly single-molecule approach. We detect the trajectories of individual biomolecules walking through the confocal spot. This allows us to restrict our analysis to events with properties we expect for functional, singly-labeled kinesin. We can select on properties such as width (a signature of velocity) and intensity (a signature of the amount of motors and labels).

For the labeled kinesin construct studied here, fluorescence fluctuations due to kinesin's mechanochemistry were neither expected nor observed. We have shown however that our approach allows for the observation of fluctuations on a time scale down to 10 μs, i.e. a thousand times faster than kinesin's stepping time. The confocal fluorescence approach shown here, paves the way to study kinesin's mechanochemistry on the single-motor level, provided labeled kinesin constructs are used that report on chemical and conformational changes. One could for example think of fluorescence polarization as a reporter of conformational changes [68] or fluorescent ATP-analogues to directly observe substrate binding and release [24]. Another example would be a kinesin with a donor fluorophore on one motor domain and an acceptor on the other as a FRET (Förster resonance energy transfer) reporter of the distance between the motor domains. We have performed a simulation with such a construct and show that fluorescence intensity changes can be observed at time scales below 0.1 ms.

2.5 Acknowledgments

We thank J. Van Mameren for programming the kymograph software, I. Schaap for purifying microtubules, H. Sosa (Albert Einstein College of Medicine, Bronx, NY) for his generous gift of the kinesin plasmid and J. Enderlein (Forschungszentrum Jülich, Germany) for generously sharing his fast correlation computing algorithm.

This research was supported by a *VIDI* fellowship from the Research council for Earth and Life Sciences (ALW) and by a *Projectruimte* grant from the Dutch Foundation for Fundamental Research on Matter (FOM).

Chapter 3

Kinesins step dissected with single-motor FRET

Abstract — The motor protein Kinesin-1 drives intracellular transport along microtubules, with each of its two motor domains taking 16 nm steps in a hand-over-hand fashion. The way in which a single motor domain moves during a step is unknown. Here we use Förster resonance energy transfer (FRET) between fluorescent labels on both motor domains of a single kinesin. This allows us to resolve the relative distance between the motor domains and their relative orientation, on the sub-millisecond timescale, during processive stepping. We observe transitions between high and low FRET values for certain kinesin constructs, depending on the location of the labels. These results reveal that, during a step, a kinesin motor domain dwells in a well-defined intermediate position for about 3 ms.

This paper is under review. *Sander Verbrugge*, Zdenek Lansky and Erwin J.G. Peterman

3.1 Introduction

Conventional kinesin, Kinesin-1, drives intracellular transport of vesicles and organelles along microtubules (MT) [79]. As a result of the concerted action of its two identical motor domains, kinesin moves in 8 nm steps, hydrolyzing one ATP per step [58, 83]. The velocitiy of the motor is ATP dependent, following Michaelis-Menten kinetics, and is 600-800 nm/s at saturating ATP-concentrations, which corresponds to ∼10 ms per step. The motor domains step in a "hand-over-hand" manner, each moving in turn 16 nm [4, 39, 92]. Kinesin is a processive motor, making hundreds of steps before detaching from the MT. It is thought that processivity is achieved by keeping the ATP-hydrolysis cycles of both motor domains out-of-phase, by a gating mechanism, operated via tension on the linkage between the two motor domains [26, 91]. It is not fully understood whether gating prevents ATP binding to the leading motor domain, ADP release from the trailing one, or both [26, 29]. Tension might also be required to release the trailing, ADP-bound motor domain from the MT [26, 91].

Stepping occurs between configurations with both motor domains strongly bound to the MT and 8 nm apart, the "two-head-bound" state, which has been observed in single-motor FRET [47] and fluorescence polarization studies [5]. It is not very well understood what happens during a step between two subsequent "two-head-bound" states and what fraction of the time the motor domains spend in such configuration. At high ATP concentrations, optical trapping experiments with a time resolution of 50 μs, showed that a bead attached to kinesin's tail makes instantaneous steps and no intermediates could be resolved [14]. On the other hand, substeps have been predicted on the basis of models for kinesin's mechanism [64]. At low ATP concentrations, kinesin spends substantial time in the "ATP-waiting state", before making a step. In this state, one motor domain is MT-bound and "waiting" for ATP, while the position of the other motor domain, containing ADP, is currently under debate. Some studies have indicated that this latter motor domain is MT-bound, similar to the "two-head-bound" state [5, 33, 92]. In contrast, more recently, it was proposed on basis of electron microscopy data that the ADP-bound motor domain is docked on the nucleotide-free one and positioned slightly in front [2]. In another study, using single-molecule FRET, the ADP-bound motor domain was also proposed to be not attached to the MT, but behind the nucleotide-free one [47]. In this latter study, which had a time resolution of 10 ms, such a "one-head-bound" state was not detected at physiological, saturating ATP concentrations. So far, experiments that can directly resolve the motion of individual motor domains on the sub-millisecond time scale during processive motion have been lacking. Here, we apply a single-motor motility assay combining confocal fluorescence microscopy [82] with FRET to achieve this.

3.2 Results

3.2.1 Fluorescent labelling approach

In order to sense distance changes between kinesin's motor domains using FRET, we generated four homodimeric kinesin constructs with single cysteine residues in differ-

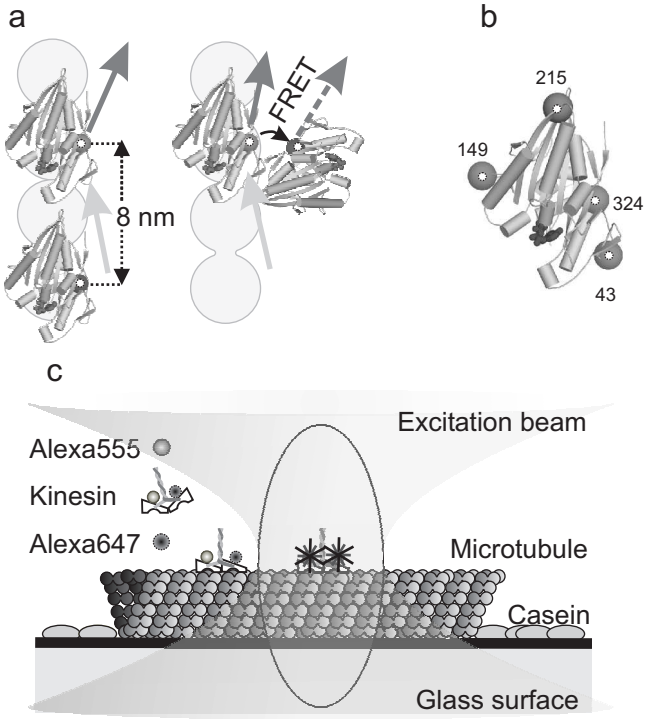

Figure 3.1 – Schematic representation of the kinesin constructs and the single-motor confocal fluorescence microscopy assay a. Two kinesin motor domains (PDB code 2kin) in a two motor domains MT bound state, too far apart for FRET, and a potential intermediate with motor domains close enough for FRET. The grey circles represent a single MT protofilament, plus-end pointing upwards. Light grey, dark grey, dashed and black arrows represent excitation light, donor emission, acceptor emission and FRET, respectively. **b.** The four positions where cysteines were introduced for specific labelling (grey spheres with white dots). **c.** Experimental assay with fluorescently-labelled kinesin landing on a MT and walking through the confocal volume (dark grey ellipse), where it senses a Gaussian-shaped excitation intensity profile. Drawing not to scale; FWHM of the profile is ∼250 nm, corresponding to ∼30 kinesin steps.

ent positions on both motor domains (Figure 3.1b). To these cysteines we attached Alexa Fluor 555 as donor and Alexa Fluor 647 as acceptor fluorophore. This FRET pair has a Förster distance of 5.1 nm (Molecular Probes). We anticipated that FRET would not occur for donor-acceptor labelled kinesins when both motor domains are bound to subsequent binding sites 8 nm apart. FRET would, however, occur in a potential intermediate with only one domain MT-bound and the other closer (Figure 3.1a). We chose constructs with cysteines on position 324, 215, 43, or 149 (Figure 3.1b), since it had been reported that these constructs are functional [73], which we confirmed

by their unaltered velocity and processivity. FRET had been measured before, using a similar 324 construct [47].

3.2.2 FRET measured on single, walking motors using confocal microscopy

To detect short-lived stepping intermediates, a single-motor fluorescence assay with sub-millisecond time resolution is required, since kinesin's stepping cycle takes on average ∼12 ms at saturating ATP concentrations [71]. To overcome the limited time resolution of wide-field fluorescence approaches [52], we have developed a confocal fluorescence microscopy assay allowing measurement of fluorescence intensity fluctuations on walking kinesins on time scales down to 100 µs [82]. Here, we use this assay to measure variations in FRET efficiency by positioning the focussed laser beam on a MT and collecting photons emitted by a single labelled motor walking through (Figure 3.1c). Photons are separated by wavelength into two channels, detected and time tagged with 12.5 ns accuracy. Due to the motor's constant velocity and the Gaussian excitation profile, its fluorescence intensity time trace has a Gaussian shape (Figure 3.2a&d) [82]. The width of this Gaussian is a direct measure of kinesin's velocity. The donor and acceptor fluorescence intensities directly reflect the labelling stoichiometries. We have restricted our analysis to events arising from kinesins labelled with one donor and one acceptor. In time traces of A215C and S149C obtained at a saturating ATP concentration (2 mM), only small fluctuations (∼20% of the signal) can be observed in donor and acceptor channel, while the fluctuations for T324C and S43C are much larger (∼50%) and seem anti-correlated (Figure 3.2a, Supplementary Figure 3.6a). To investigate whether this is due to FRET occurring only in the latter constructs, we calculated the apparent FRET-efficiency (acceptor intensity divided by sum of donor and acceptor intensities). The efficiency of T324C and S43C shows two populations (Figure 3.2b, Supplementary Figure 3.6b). In contrast, for A215C and S149C only one population can be distinguished (Figure 3.2e, Supplementary Figure 3.6d), similar in efficiency to the low-FRET population of T324C and S43C. In the occasional events where the acceptor photo-bleached, the instantaneous drop of acceptor signal was accompanied by a rise of the donor signal for T324C and S43C, but not for A215C (Figure 3.2c&f, Supplementary Figure 3.7). Taken together, these results indicate that during processive movement, the T324C and S43C kinesins switch between low and high-FRET states. In contrast, no high-FRET state is observed for the A215C and S149C constructs.

3.2.3 Auto- and cross-correlation analysis

To further confirm this and determine the timescale of FRET fluctuations, we analysed the fluorescence time traces using correlation techniques [82], similar to fluorescence correlation spectroscopy [46]. The fluorescence intensity autocorrelation at time lag τ is proportional to the probability of detecting a photon at time $t+\tau$, after one has already been detected at t. The autocorrelation calculated from a donor fluorescence time trace of a single T324C event, ranging from 0.1 to 1000 ms, (Figure 3.3a) has

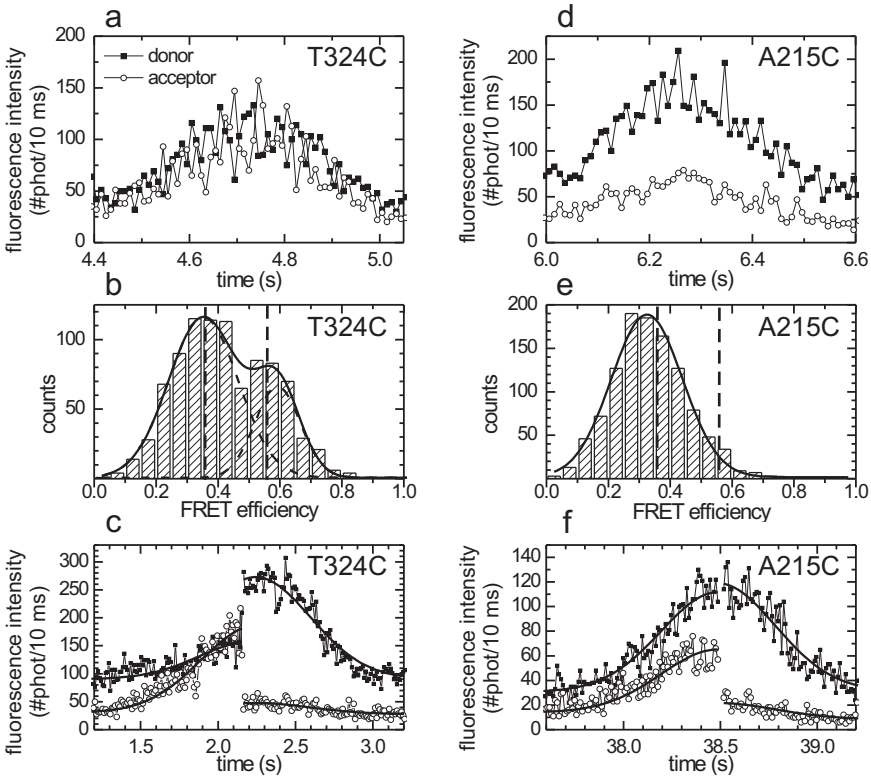

Figure 3.2 – FRET is observed for donor-acceptor labelled T324C kinesin and not for A215C. **a.** T324C fluorescence intensity time trace binned over 10 ms showing large fluctuations. Black squares: donor fluorescence intensity, open circles: acceptor fluorescence intensity. **b.** Apparent-FRET-efficiency histogram of T324C ($I_A/(I_A+I_D)$, binned over 2 ms, central 200 ms of 6 events) showing two peaks (at FRET efficiencies of 0.353 ± 0.009 and 0.59 ± 0.01, obtained from double Gaussian fit). **c.** Intensity time trace of a single T324C event. The black lines represent global fits with two Gaussians (one for the donor (solid squares) and one for the acceptor channel (open circles)) with a common width, offset and centre position and with an amplitude step at the moment of acceptor photo-bleaching. The fitted amplitudes show that after acceptor photo bleaching (at $\sim$ 2.2s) the donor intensity increased by a factor of 2.6 ± 0.2. ATP concentration: 20 μM. **d.** A215C fluorescence intensity time trace. The intensity fluctuations appear lower than in (a). **e.** Apparent-FRET-efficiency histogram of A215C (5 events). Only one peak, corresponding to the low FRET one in (b) is observed (FRET efficiency $= 0.325 \pm 0.003$). **f.** Intensity time trace of a single A215C event. After acceptor photo bleaching (at $\sim$38.5 s), the donor intensity is hardly affected (increase of a factor 1.07 ± 0.05). ATP concentration: 50 μM.

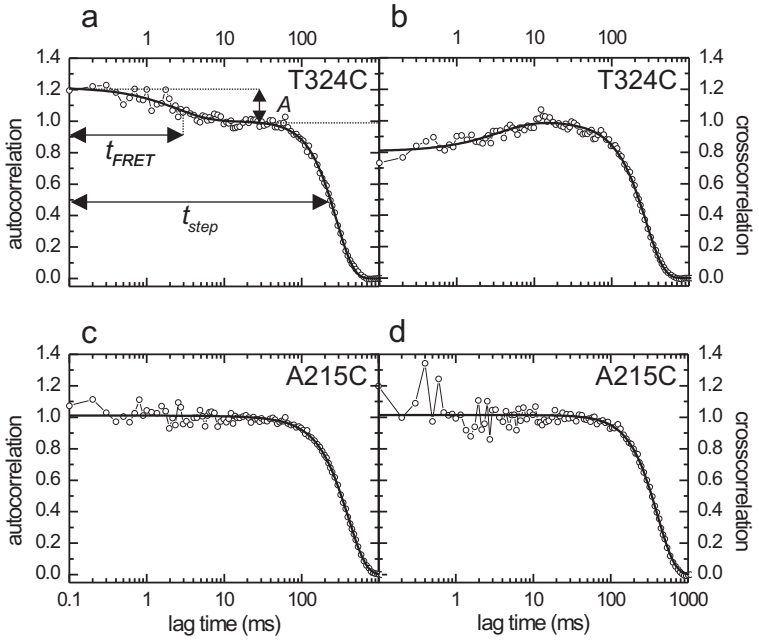

Figure 3.3 – Millisecond intensity fluctuations due to FRET are observed for T324C and not for A215C. a. Autocorrelation of the donor fluorescence intensity time trace of Figure 3.2a (T324C). Shown is a fit (black curve) of the data with Equation 3.2, consisting of a Gaussian (transit through confocal spot) and an exponential (FRET) component. The FRET component has an amplitude, A, of 0.22 ± 0.01 and a decay time, T_{FRET}, of 2.5 ± 0.3 ms. **b.** Cross-correlation of donor and acceptor intensity time traces of the same T324C event. The FRET-related correlation decay has an amplitude of -0.20 ± 0.01 and a decay time of 3.6 ± 0.6 ms. **c.** Autocorrelation of the fluorescence intensity time trace of the A215C event of Figure 3.2d. No decay of the autocorrelation on the ∼ms timescale can be discerned. **d.** Cross-correlation of donor and acceptor intensity time traces of the same A215C event. No decay of the correlation is observed on the ∼ms timescale, indicating that no fluctuations occur due to changes in FRET.

two contributions [82]: a Gaussian with half width ∼250 ms, reflecting the transit time through the confocal spot, and an exponential decay on the millisecond scale. To test whether this fast component is due to FRET, we calculated the cross-correlation between donor and acceptor signals. The cross-correlation (Figure 3.3b) shows the same two contributions, the fast one having, however, negative amplitude. This indicates that the fast fluctuations are anti-correlated in donor and acceptor signal, a clear sign of FRET [75]. A similar, ∼ms FRET component was observed in the cross- and autocorrelations of S43C, but not of A215C and S149C (Figure 3.3, Supplementary Figure 3.8).

For further quantitative analysis, we focus on donor autocorrelations only, since

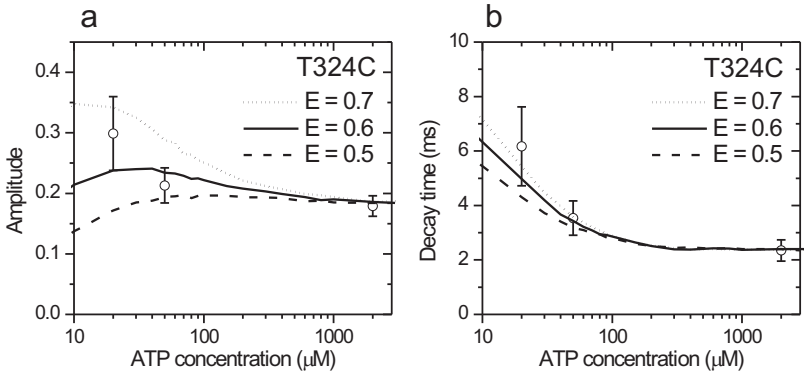

Figure 3.4 – A three-state model describes the ATP dependence of the FRET signals of kinesin T324C. a and b. Amplitudes and decay times of the FRET autocorrelation decay. Symbols represent the values obtained from the autocorrelations of the measured time traces (mean ± s.e.m.). The lines represent Monte-Carlo simulations with three different values for the FRET efficiency of the ATP-waiting state. All other parameters were kept fixed.

donor-signal fluctuations are a direct measure of the FRET efficiency, not affected by cross talk between donor and acceptor [30]. Fitting the T324C autocorrelations (N = 16, in total ∼500 steps) with Equation 3.2 yielded an amplitude of 0.18 ± 0.02 (average ± s.e.m.) and a decay time of 2.4 ± 0.4 ms for the exponential FRET contribution. The average step time was 15 ± 2 ms, as obtained from a Gaussian fit to the time traces. For S43C (N = 19) we found an amplitude of 0.17 ± 0.02, a decay time of 2.5 ± 0.3 ms, and a step time of 11.6 ± 0.6 ms. The decay time of the FRET contribution is substantially shorter than the step time, indicating that switching between different FRET states occurs within one step. A kinetic model is required to convert the amplitudes and decay times into FRET efficiencies and lifetimes of distinct states. In the simplest, two-state model, kinesin switches from a no-FRET state with both motor domains MT-bound, to a FRET state and back, completing an 8 nm step. Using this model (Equations 3.3, 3.4 and 3.5), we calculate, that kinesin T324C (S43C) switches between a no-FRET state with lifetime 12 ± 2 ms (7.9 ± 0.8 ms), and a FRET state with lifetime 3 ± 0.9 ms (3.7 ± 0.6 ms) and FRET efficiency 0.88 ± 0.12 (0.69 ± 0.06). These values indicate that, kinesin's stepping cycle includes a so far unresolved intermediate state with both motor domains in close proximity, lasting ∼3 ms at saturating ATP concentration.

Next, we determined how the FRET signals of kinesin S43C and T324C depend on ATP concentration. From intensity time traces, we calculated apparent FRET efficiencies and observed these to increase with decreasing ATP concentration for both constructs (Supplementary Figure 3.9, Table 3.1), in agreement with earlier results on a similar 324 construct [47]. We calculated autocorrelations of the donor signals, fitted them and calculated lifetimes and FRET efficiencies using the two-state model. The lifetimes of both FRET and no-FRET state changed with ATP concen-

tration (Supplementary Figure 3.10, Table 3.2). ATP-binding is rate limiting at low concentrations [63] and in our model, this should have resulted in the lifetime of only one state being ATP dependent, indicating that a more complex model is needed. Our data is intrinsically noisy due to the limited number of photons detected. More elaborate models create several challenges: their autocorrelations are in many cases more complex than single exponential [53] and additional free parameters are required. In order to circumvent these challenges, we considered a constrained three-state cyclic model (see Methods), with two states identical to the two-state model used above: a no-FRET state, with both motor domains MT-bound and a FRET state, the intermediate. The third state has an ATP-dependent lifetime, calculated using Michaelis-Menten kinetics (Equation 3.6). This is the "ATP-waiting" state characterized before [2, 47]. At 2 mM ATP, its lifetime is negligible and the model reduces to two states. Only the FRET efficiency of this state was a free parameter. Lifetimes and FRET efficiencies of the other two states were taken from the two-state modelling (at saturating ATP) and kept constant. Autocorrelations were calculated from time traces generated using Monte-Carlo simulations and compared to the experimental ones. A good description of the experimentally obtained parameters was achieved using FRET efficiencies of 0.6 ± 0.1 (0.4 ± 0.15) for the ATP waiting state of T324C (S43C) (Figure 3.4, Supplementary Figure 3.11). Taken together, our data and analysis indicate that kinesin's stepping at different ATP concentrations can be described with a 3-state model, with (1) a no-FRET state with ∼10 ms lifetime, (2) a medium-FRET state with ATP-dependent lifetime, and (3) a high-FRET state with ∼3 ms lifetime.

3.3 Discussion

How do the three states fit in kinesin's chemomechanical cycle? Autocorrelation analysis is invariant to the order of the states. We believe, however, that the ∼3 ms, high-FRET intermediate state follows ATP binding to the leading motor domain and precedes ADP release from the trailing motor domain, since its lifetime corresponds to that of ADP release after an ATP chase (3.3 ms) [32]. In addition, it is widely accepted that ATP binding is followed by a fast change to a "closed" conformation enabling hydrolysis [19, 61], which might correspond to the high-FRET intermediate we have observed. This intermediate state ((3) in Figure 3.5), is followed by forward displacement and attachment of the unbound motor domain to the MT, releasing ADP. In the resulting state (1), with both motor domains MT-bound, lasting ∼10 ms, ATP is hydrolyzed and phosphate released from the leading motor domain. Next, the motor goes in the "ATP-waiting" state (2), with a medium FRET efficiency, which indicates that only one motor domain is tightly bound to the MT, consistent with some earlier studies [2, 47]. In addition, it suggests that the ADP-bound motor domain alternates between configuration (1) and (3), or that it is tethered and can freely move within several nanometers. In this state, the flexibility of the ADP-bound motor domain is relatively large, since both neck linkers, which together form the link between the motor domains, are most likely undocked [6, 56]. Next, upon ATP binding, the neck linker of the tightly MT-bound motor domain docks, pulling the ADP-bound motor domain closer, returning to the high-FRET state (3). We have only observed FRET

using kinesin labelled on the 324 and 43 positions, and not 149 and 215. This suggests that, in the high-FRET state (3), only one motor domain is MT-bound and the other one is oriented and translated in such a way, that the 324-324 and 43-43 distances are shorter than ∼4.5 nm, while the 149-149 and 215-215 distances are larger than ∼6 nm (Supplementary Methods, section 3.6.10). These distance constraints are fulfilled by configurations with both neck-linker bases relatively close together and motor-domain fronts pointing apart (Supplementary Figure 3.12). The FRET efficiency in state (3) is higher than in the "ATP-waiting" state (2), indicating that on average the motor domains are closer together. This is in agreement with the neck linker of the ATP-bound motor domain being in the docked conformation, shortening the tether between both motor domains.

In wide-field single-molecule fluorescence studies employing FRET [47] and nanometer localization [92], the ∼3 ms high-FRET state we report has not been resolved, most likely due to limited time resolution. Furthermore, no sub-steps have been observed in optical trapping experiments, measuring the displacement of a microsphere attached to kinesin's tail with 50 μs time resolution [8, 14]. This indicates that transitions in the location of the motor domains do not lead in all cases to motion of the motor's tail. Our data does not allow to conclude when the 8 nm step of kinesin's tail occurs in the cycle: after ADP release (from (3) to (1)) or immediately after ATP binding (from (2) to (3)). However, experimental evidence seems to favor the latter picture [8, 29, 56]. To conclude, single-motor FRET experiments based on confocal fluorescence microscopy, have provided us the observable parameter and time resolution to discern an up-till-now hidden intermediate in Kinesin-1's stepping cycle. This intermediate configuration might play a key role in directing the stepping motor domain forward, towards the plus-end of the MT, to the next binding site.

3.4 Methods

3.4.1 Single-molecule experiments

Four single-cysteine homodimeric kinesin constructs were prepared, starting from a cystein-less (cys converted to ala), 560 amino acids long, ubiquitous human kinesin construct [82]. Cysteins were introduced on positions 324, 43, 215 and 149 (Entelechon, Regensburg, Germany), verified by sequencing. Kinesins were expressed, purified and labelled with a five-fold excess of both Alexa555 and Alexa647 (Invitrogen, Carlsbad, CA) as described before [82]. The experimental setup and assay [82] was modified to simultaneously detect donor and acceptor fluorescence. After passing through a 550DCLP dichroic mirror (Chroma, Rockingham, VT) the fluorescence was split in two channels by a second dichroic mirror, 645DCXR (Chroma), and filtered by emission filters HQ575/50 or HQ675/50 (Chroma). Instead of 4 mM dithiothreitol, we used 5 mM TROLOX (Sigma-Aldrich, St. Louis, MO) in the sample mix and no taxol was added. An ATP regeneration system was used at all ATP concentrations [69, 82].

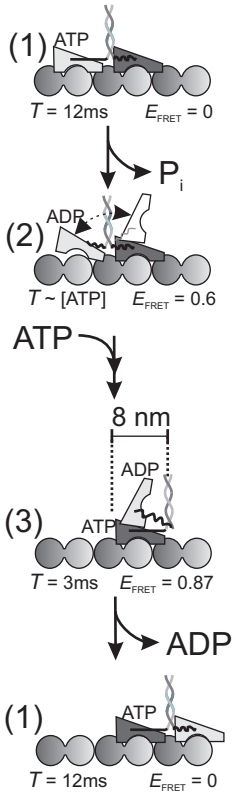

Figure 3.5 – Chemomechanical interpretation of the three-state model. In the no-FRET state (1), both motor domains are tightly MT-bound and 8 nm apart. ATP is hydrolyzed and phosphate released from the trailing motor domain, leading to the "ATP-waiting state" (2), with intermediate FRET efficiency, one motor domain tightly bound and the other tethered. Subsequent binding of ATP to the forward motor domain causes docking of its neck linker, moving kinesin's tail 8 nm forward, leading to a high-FRET intermediate state (3). In this state, only one motor domain is MT-bound and the other one is close, such that FRET can occur. After this intermediate state, the unbound motor domain (light grey), moves forward to the next binding site on the MT releasing ADP. Lifetimes (T) and FRET efficiencies (E_{FRET}) of the T324C construct are indicated.

3.4.2 Data analysis

Fluorescence intensity time traces (with 10 ms time bins) of single kinesins passing through the confocal spot were fitted with a Gaussian to obtain the amplitude, width and offset. The data was restricted to ∼100 ms background signal on both sides of the event for fitting and further analysis. The fitted offset (dark counts and background fluorescence) was used for background correction and the amplitudes of the donor and acceptor channels were used to select events that had both labels present. Also

events in which the signal vanished due to bleaching or detachment were included in the analysis, only when they traversed more than half the confocal volume. For these, the same criteria were applied, except that the fluorescence intensities after detachment or photobleaching were not taken into account. Background-corrected fluorescence intensity traces of the donor, x_i, and the acceptor, x_j, were binned at Δt = 0.1 ms and were cross- ($i \neq j$) and autocorrelated ($i=j$) using:

$$G_{ij}(n\Delta) = \sum_{k=0}^{2N-2} x_i(k\Delta t) x_j(n\Delta t + k\Delta t) \tag{3.1}$$

Where N denotes the total number of time bins of an event. The cross- and autocorrelations obtained using Equation 3.1 are not normalized and decay to zero for large time lags. Correlations obtained in this way were fitted with:

$$G(\tau) = N\left(1+\frac{\tau}{T_T}\right)^{-1} \exp\left(-\frac{\tau^2}{\alpha T_{step}^2}\right)\left(1+A\exp\left(-\frac{\tau}{T_{FRET}}\right)\right) \tag{3.2}$$

where T_{FRET} is the decay constant and A the relative amplitude of the decay due to FRET, N is the amplitude of the correlation, α is a factor that describes the width of our confocal volume (we fixed to $\alpha = 760$ ($= 4 * \sigma_{spot}$)), T_{step} is the average step time. The term involving T_T is an empirical term added to correct for distortions from the ideal Gaussian shape of time traces, due to photo bleaching, landing, detachment and the stochastic nature of stepping. All correlation curves were normalized by dividing the correlation values by the amplitude N. Note that we have switched to a continuous lag time variable τ here.

3.4.3 The autocorrelation of a stochastic two-state model

The theoretical description of the autocorrelation of a model where the donor fluorescence intensity cycles between a state without FRET (NF) and a state with FRET (F) is given by the following equations (adopted from Torres et al. [75]):

$$A = \frac{k_{NF} k_F E_F^2}{\left(k_F + k_{NF}\left(1-E_F\right)\right)} \tag{3.3}$$

$$T_{FRET} = \frac{1}{\left(k_{NF} + k_F\right)} \tag{3.4}$$

$$T_{step} = \frac{1}{k_F} + \frac{1}{k_{NF}} = \frac{1}{k_{step}} \tag{3.5}$$

where k_{NF} and k_F are the rates out of the No-FRET and FRET state respectively, E_F is the FRET efficiency of the FRET state, k_{step} is the step rate and T_{step} is the average step time of the passing motor. Here, the FRET efficiency of the No-FRET state, E_{NF}, is set to 0. In our experiments, we expected a state with both motor domains MT-bound and 8 nm apart. We calculated that for such a state a FRET efficiency of less than 0.05

is expected (assuming a Förster distance of 5.1 nm for the FRET pair Alexa Fluor 555 and 647 (Molecular Probes)). Furthermore, we set the sum of the lifetimes of both states equal to the average step time (Equation 3.5).

3.4.4 Fitting of the two-state model to the experimental autocorrelations

The average fit parameters of several autocorrelations, each from the fluorescence signal of a single kinesin, were converted into rates and FRET efficiencies using Equations 3.3, 3.4 and 3.5, yielding two sets of solutions, from which different time-averaged relative intensities were calculated. One of the sets was selected on basis of the experimental time-averaged intensities, which were obtained by dviding the average donor amplitude of donor-acceptor labelled events by the average donor amplitude of events due to kinesins labelled with one donor only.

3.4.5 Monte Carlo simulations of the ATP-dependence of the FRET signals using a cyclic three-state model

We assumed a cyclic, three-state model without backward reactions. In order to limit the number of free parameters we fixed the dwell times and intensities of two of the states to those obtained with the two-state model at 2 mM ATP concentrations. We allowed the lifetime of the third state to vary with ATP concentration (such that its lifetime was negligible at 2 mM ATP), and only left the FRET efficiency of this 'ATP-waiting' state as a free parameter. The lifetime of the ATP-waiting state, $T_{\mathrm{ATP-waiting}}$ was obtained from the following derivative of the Michaelis-Menten equation:

$$T_{ATP-waiting} = \frac{1}{k_{cat}} \left(\frac{K_M}{[ATP]} \right) \tag{3.6}$$

where k_{cat} is the motor's maximal stepping rate, K_{M} the concentration at which the motor moves with half the velocity and $[ATP]$ is the ATP concentration. The Michaelis-Menten constant ($K_{\mathrm{M}} = 19 \pm 8$ μM) was obtained from a fit to the combined average velocities of both constructs.

Using this model, we generated donor intensity time traces with simulation software written in LabVIEW (National Instruments), based on the Monte-Carlo approach. Typically, 15,000 cycles through the model were generated. Traces were generated for 20 ATP concentrations and different FRET efficiencies of the ATP-waiting state. From the simulated time traces, autocorrelations were calculated, which were fitted with an exponential function, yielding an amplitude and decay time.

3.5 Acknowledgements

This work was supported by a *VIDI* fellowship from the Research council for Earth and Life Sciences (ALW) and is part of the research programme of the 'Stichting voor

Fundamenteel Onderzoek der Materie (FOM)', which is financially supported by the 'Nederlandse Organisatie voor Wetenschappelijk Onderzoek (NWO)'.

3.6 Supplementary material

3.6.1 Intensity traces and apparent FRET for S43C and S149C

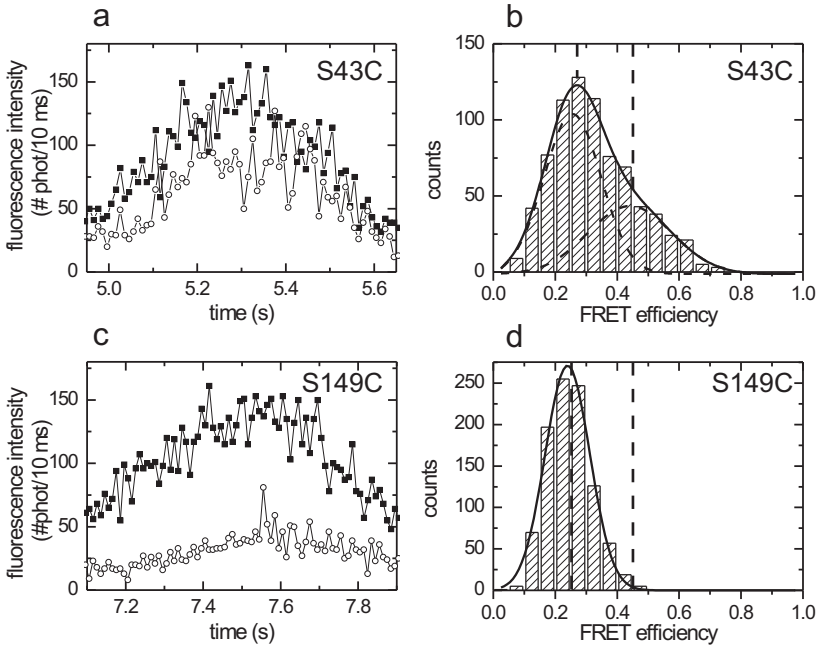

Figure 3.6 – Fluorescence intensity time traces and histograms of the apparent FRET efficiencies indicate that S43C shows FRET and S149C does not. a. Intensity time trace (number of photons per 10 ms bin) of an S43C kinesin with a donor and acceptor. Large intensity fluctuations (∼30 %) can be discerned that appear anti-correlated in donor (solid squares) and acceptor (open circels) traces. **b.** Histogram of the apparent FRET efficiency ($I_a/(I_a + I_d)$) of 8 events of the S43C construct, showing a peak at a FRET efficiency of 0.256 ± 0.012 and a second peak at 0.45 ± 0.09 (as obtained by fitting two Gaussians). The histogram was obtained from the central 200 ms of intensity time traces (2-ms binned). **c.** Intensity time trace of a single S149C donor-acceptor labelled kinesin. In this trace, the intensity fluctuations are substantially smaller than in **a**, in both donor (solid squares) and acceptor channel (open circles). **d.** Histogram of the apparent FRET efficiency of 6 events of S149C. This histogram shows only a single peak with a value of 0.240 ± 0.002 (from fitted Gaussian), corresponding to the low-FRET peak in **b**.

3.6.2 S43C time trace of acceptor photo bleaching

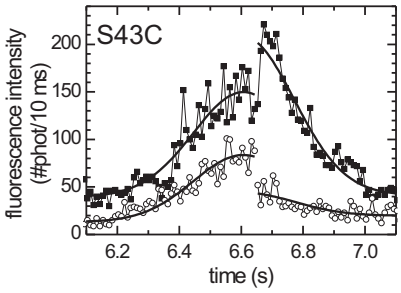

Figure 3.7 – S43C fluorescence intensity time trace of event where the acceptor photo bleached. After acceptor photo bleaching (at ∼6.65 s), the donor intensity increases by a factor of 1.52 ± 0.1. ATP concentration: 2 mM.

3.6.3 Auto- and crosscorrelations for S43C and S149C

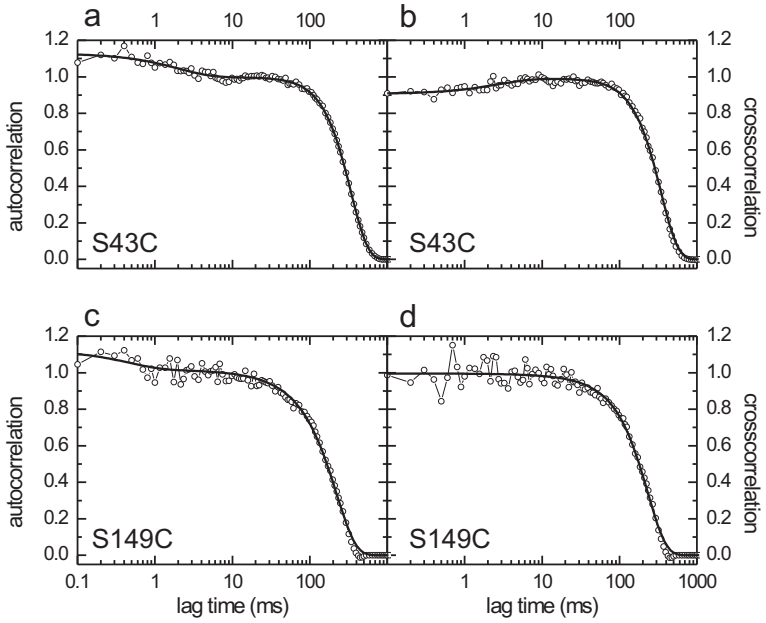

Figure 3.8 – Autocorrelation and cross-correlation of fluorescence intensity time traces of single, donor-acceptor-labelled kinesins show millisecond intensity fluctuations due to FRET for S43C and not for S149C. a. Autocorrelation of the fluorescence intensity time trace of Figure 3.6a (S43C). Shown is a fit (red curve) to the data with Equation 3.2, consisting of a Gaussian (transit through confocal spot) and an exponential (FRET) component. The decay of the correlation due to FRET has an amplitude of 0.13 ± 0.01 and a decay time of 1.9 ± 0.2 ms. **b.** Cross-correlation of donor and acceptor intensity time traces of the same S43C event as in **a**. The FRET-related exponential decay has an amplitude of -0.090 ± 0.007 and a decay time of 3.8 ± 0.7 ms. **c.** Autocorrelation of the fluorescence intensity time trace of a full S149C event. Only a small decay of the autocorrelation on the ∼ms timescale can be discerned (with amplitude 0.10 ± 0.03 and decay time is 0.46 ± 0.19 ms). **d.** Cross-correlation of donor and acceptor intensity time traces of the same S149C event as in **c**. No decay of the correlation is observed on the ∼ms timescale, indicating that the decay observed in **c** is not due to changes in FRET, but most probably due to photo-physical effects, such as blinking of the dye.

3.6.4 Intensity traces of T324C and S43C at 50 μM ATP

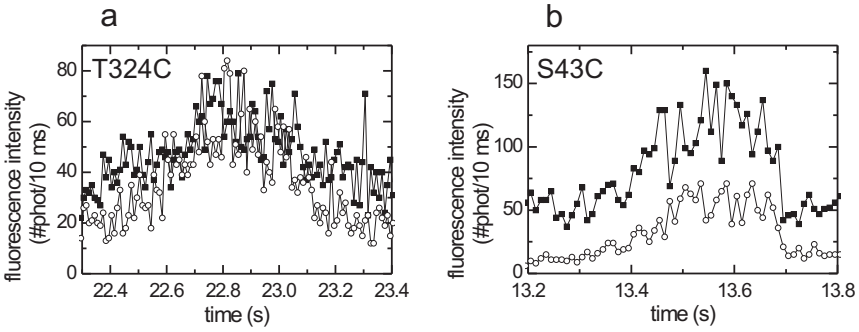

Figure 3.9 – Donor (solid squares) and acceptor (open circles) fluorescence intensity time traces of T324C (a) and S43C (b) at 50 μM ATP. Traces are background corrected and time binned over 10 ms.

3.6.5 Apparent FRET efficiency at low ATP

	T324C (N = 11, 7, 5)	S43C(N = 15, 6, 4)
[ATP](μM)	apparent FRET efficiency	apparent FRET efficiency
2000	0.43 ± 0.04	0.32 ± 0.03
50	0.50 ± 0.04	0.38 ± 0.02
20	0.63 ± 0.04	0.38 ± 0.06

Table 3.1 – Apparent FRET efficiency (background corrected) of the T324C and S43C constructs at three different ATP concentrations shows that the energy transfer increases with decreasing ATP concentration.

3.6.6 Auto- and cross-correlations at low ATP concentrations

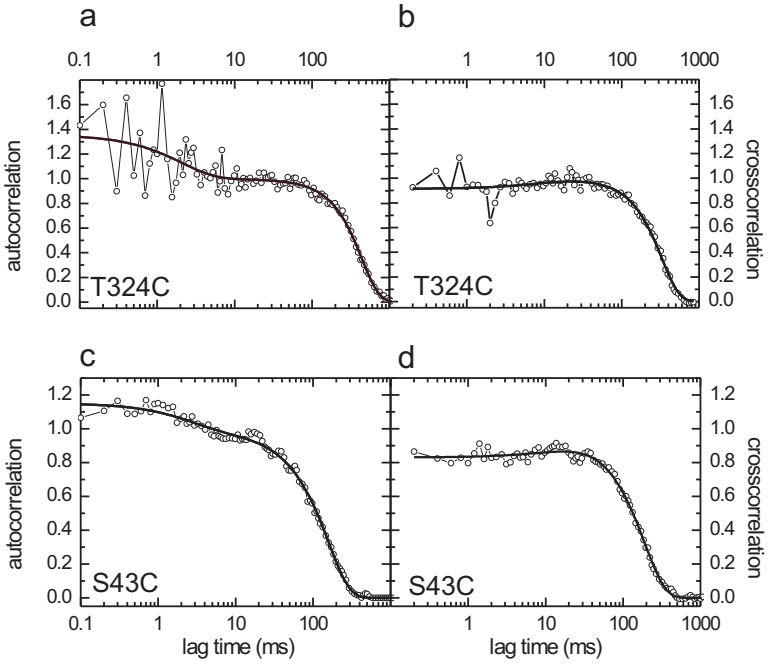

Figure 3.10 – Autocorrelation and cross-correlation of the intensity time traces of single T324C and S43C constructs confirm that the FRET parameters alter at lower ATP concentrations. a. Fluorescence intensity autocorrelation of a single T324C event. Fit (solid black line, with Equation 3.2) yields an amplitude of 0.35 ± 0.06 and a decay time of 2.1 ± 0.8 ms for the autocorrelation decay due to FRET. **b.** Cross-correlation of the donor and acceptor intensity of a single T324C event (same as in **a**). Fit yields an amplitude of -0.09 ± 0.03 and a decay time of 10 ± 9 ms. **c.** Fluorescence intensity autocorrelation of a single S43C event. Fit yields an amplitude of 0.15 ± 0.02 and a decay time of 2.6 ± 0.6 ms. **d.** Cross-correlation of the donor and acceptor intensity of a single S43C event (same as in **c**). Fit yields an amplitude of -0.17 ± 0.07 and a decay time of 20 ± 12 ms.

3.6.7 Results of two-state model at low ATP

	T324C (N = 11, 7, 5)			S43C (N = 15, 6, 4)		
[ATP] (μM)	t_{NOFRET} (ms)	t_{FRET} (ms)	E_{FRET}	t_{NOFRET} (ms)	t_{FRET} (ms)	E_{FRET}
2000	2.9 ± 0.3	12 ± 2	0.87 ± 0.1	3.8 ± 0.5	7.9 ± 0.7	0.72 ± 0.01
50	3.9 ± 1.1	18 ± 2	1.0 ± 0.1	3.0 ± 0.6	10.1 ± 1.2	0.69 ± 0.06
20	9 ± 3	24 ± 5	0.99 ± 0.08	6.3 ± 0.9	16 ± 4	0.79 ± 0.09

Table 3.2 – Results of the two-state-model calculations (Equations 3.3, 3.4 and 3.5) to the fit values obtained from donor-intensity autocorrelations of T324C and S43C events at different ATP concentrations. Values are averages ± standard error of the mean of *N* events. The lifetimes of both states are ATP dependent.

3.6.8 Monte-Carlo simulations of FRET autocorrelation decay parameters

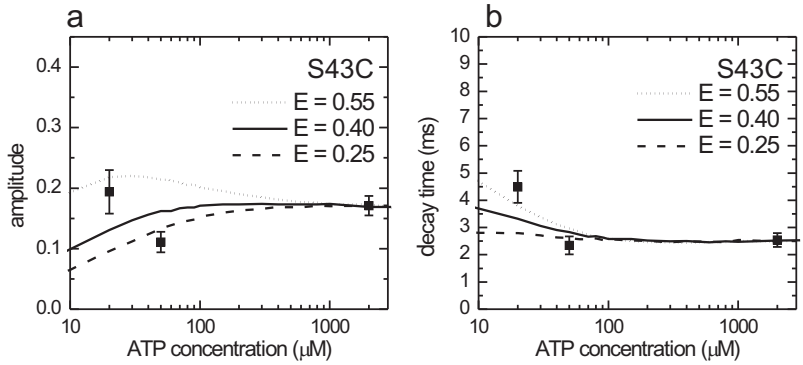

Figure 3.11 – Monte-Carlo simulations of FRET autocorrelation decay parameters (amplitude (a) and decay time (b) for the S43C construct. Symbols represent parameters obtained from fitting the experimental autocorrelation curves (mean ± s.e.m.). Simulations are shown for three different values of the FRET efficiency of the ATP-waiting state. A value of 0.40 for this parameter describes the data best. The simulation procedure is described in the Methods.

3.6.9 Molecular model of relative positions of both motor domains

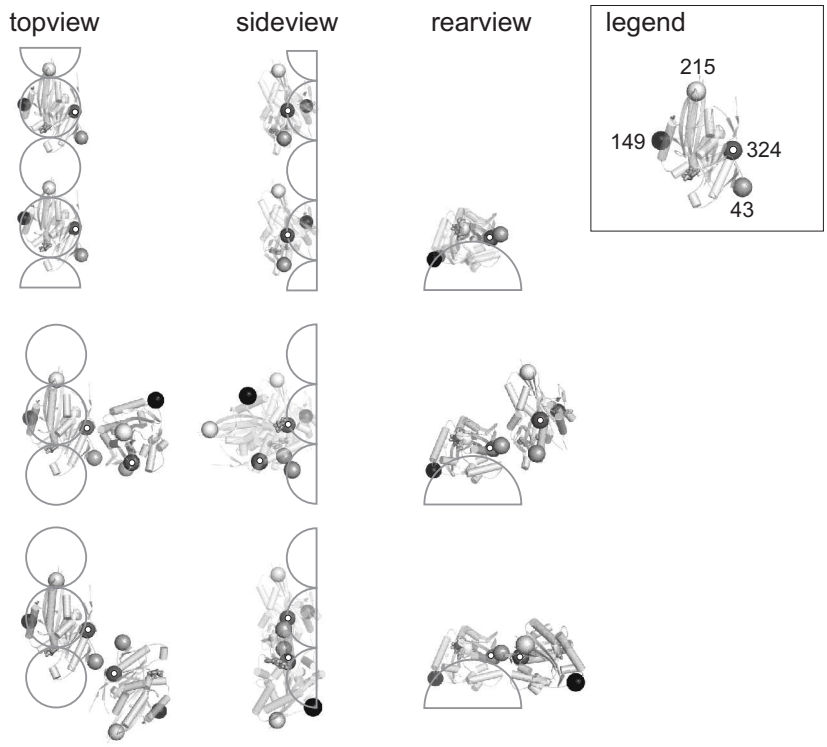

Figure 3.12 – Molecular model of the relative positions of both motor domains in the state in which both are MT-bound (top three images) and two potential configurations of the high-FRET intermediate state (bottom six images). These states correspond to (1) and (3) in Figure 3.4 respectively. Labelling sites are indicated with spheres (Grey is 43, Dark grey is 149, light grey is 215 and dark grey with a white dot is 324). Open circles represent tubulin monomers forming a protofilament. Three helices in the motor domain are coloured for clarity. The two potential intermediate configurations were obtained by applying the following restrictions: (i) 215-215 and 149-149 distance > 6 nm. (ii) 324-324 and 43-43 distance < 4 nm. The first possible configuration (row 2) has a tilted motor domain pointing away from the microtubule. Both neck linkers are in close proximity. The second possibility (row 3) has the unbound motor domain in the same plane as the MT-bound domain, however it is rotated almost 180 degrees. Models based on PDB entry 3KIN.

3.6.10 Estimate of the limits on deriving relative distances

From the FRET efficiencies we obtained, donor-acceptor distances can only be estimated, since the relative orientations and orientational freedom of the fluorophores is not known. To obtain an estimate of the distances, we assumed that the fluorophores are free to rotate. Under these conditions, distances can be calculated using Förster's relation [23]:

$$R = R_0 \sqrt[6]{\frac{1 - E_{FRET}}{E_{FRET}}} \tag{3.7}$$

where R is the distance between donor and acceptor and R_0 is the Förster distance (5.1 nm for FRET between Alexa Fluor 555 and Alexa Fluor 647, Molecular Probes). Using this equation, we find that the donor-acceptor distance is ∼3.7 nm for a transfer efficiency of 0.88 (T324C) and ∼4.5 nm for a transfer efficiency of 0.69 (S43C).

Chapter 4

Fluorescent-ATP turnover by individual, moving Kinesin-1 motors

Abstract — Kinesin-1 motor proteins move along microtubules in repetitive steps of 8 nm at the expense of ATP. To determine nucleotide dwell times during these processive runs, we are using here a FRET method at the single-molecule level that detects nucleotide binding to kinesin motor heads. We show that the fluorescent ATP analogue used produces processive motility with kinetic parameters altered less than two and a half-fold compared to normal ATP. Using our confocal fluorescence kinesin motility assay, we obtain fluorescence intensity time traces that are analyzed using autocorrelation techniques, yielding a time resolution of about a millisecond for the intensity fluctuations due to fluorescent nucleotide binding and release. To compare these experimental autocorrelation curves to kinetic models, we use Monte-Carlo simulations. We find that the experimental data can only be described satisfactory on the basis of models assuming an alternating site mechanism, thus supporting the view that kinesin's two motor domains hydrolyze ATP and step in a sequential way.

This paper has been published: *Sander Verbrugge*, Bettina Lechner, Günther Woehlke, Erwin J.G. Peterman, Biophysical Journal, 97(1):173-182, 2009

4.1 Introduction

Kinesin-1 (formerly conventional kinesin) is a molecular motor that moves along microtubules at the expense of ATP. Its mechanism has been studied extensively, and many of its features are well understood [87]. However, kinetic and laser trapping experiments suggest an incredibly fast rate from the pre-step to the post-step position in 8 nm distance of more than 1000-2000 s^{-1}, which is hard to reconcile with kinetic and structural models [14,18]. Several studies suggest that kinesin can adopt a conformation in which it 'waits' for a fresh ATP molecule that triggers the subsequent, extremely fast step. In this 'ATP waiting state', the tightly microtubule-bound head is nucleotide-free, the other one contains ADP. Kinesin's conformation in this ATP waiting state is still controversial but several structural and kinetic studies are consistent with the view that the ADP-containing, weakly microtubule-bound motor head lags behind the firmly attached, nucleotide-free head [5,29,33,34,47,67,91]. Alternatively, it has been suggested that the ADP-containing head may wait in a 'parked' position close to the tightly bound head and without contact to the microtubule [2]. To approach this problem and to understand the entrance into and the exit from the waiting state (regardless of what its structure is), accurate knowledge about the nucleotide binding times and rates is crucial. This issue has been addressed extensively in kinetic studies, which elucidated the microtubule-dependent ATPase cycle of Kinesin-1 and gave rise to the so-called alternating site catalysis model (for seminal early studies cf. [27,31,45]). It turned out, however, that the interpretation of these 'classical' experiments is not easy because the observed signals result from convoluted events of two inter-dependent kinesin heads. The two heads of kinesin undergo the same kinetic cycle but are shifted in phase. Moreover, it is not clear whether the experimental entry point into the kinetic cycle always reflected the kinetics during processive movement. For some purposes, for example, ADP release experiments were initiated by mixing free kinesin with microtubules. Under these conditions, one head binds to microtubules and looses ADP, but it is not clear whether this initial microtubule-binding event is fully equivalent to microtubule binding during processive movement.

To circumvent these problems we are using here a microscopy assay that allows the observation of nucleotide turnover by single kinesin motors moving processively along microtubules. To detect nucleotide binding to kinesin, we use Förster Resonance Energy Transfer (FRET) between motor head and nucleotide (Figure 4.1). To obtain the time resolution required (millisecond) we use the kinesin motility assay based on single-motor confocal fluorescence microscopy, we recently developed [82]. Our approach reveals key features of kinesin's chemomechanical cycle.

4.2 Materials and Methods

4.2.1 Construction, purification and labelling of Kinesin-1

The Kinesin-1 used in this study was a 391 amino acids long version of human ubiquitous kinesin (KIF5B) with a reduced number of cysteine residues [74]. Its gene

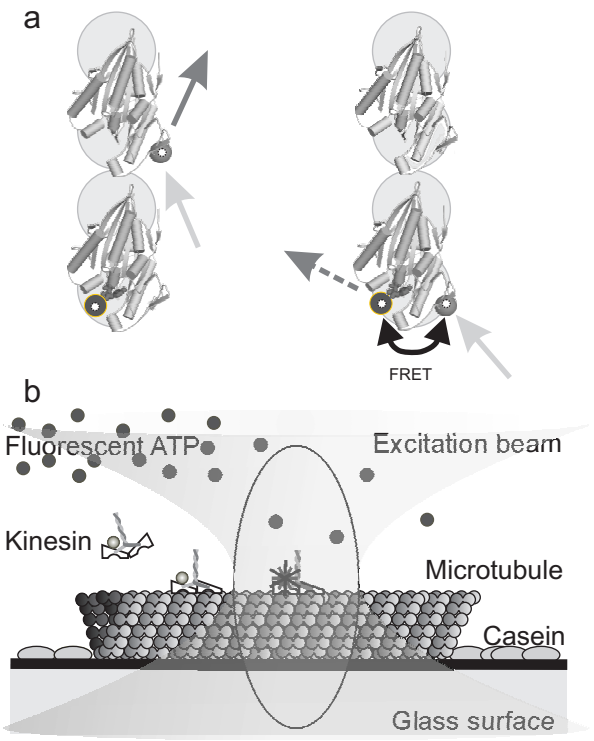

Figure 4.1 – Schematic representation of the experimental setup. **a.** Molecular model of FRET between S43C-labelled kinesin and fluorescent nucleotide. Two microtubule-bound motor domains (PDB: 2KIN [59]), one of them Alexa Fluor 555-labelled (spheres with white dots), are depicted from the top (+ end upwards). The acceptor-labelled nucleotide (dark grey spheres with white dots) is bound to the rearward head. Negligible FRET efficiencies are expected in the situation shown in the left, where fluorescent nucleotide is bound to the leading head. The close proximity of S43C to the nucleotide binding pocket gives rise to efficient FRET when Alexa Fluor 555-label and fluorescent ATP are at the same motor domain (right). **b.** Schematic representation of the single-motor FRET assay based on confocal fluorescence microscopy. A microtubule is attached to a glass surface using charge interactions. The surface is blocked for non-specific interactions with casein. The confocal spot of a fluorescence microscope is positioned on the microtubule. Alexa Fluor 555 labelled kinesins walk through the excitation spot and either emit or transfer the excitation to Alexa Fluor 647-labelled ATP bound to the motor. The fluorescence of both Alexa Fluor 555 and 647 is collected and detected.

was cloned into a bacterial pET17 expression vector by PCR. Residue S43 was chosen as a labelling target on the basis of the crystal structure (PDB accession code 1BG2

and 3KIN). This residue is solvent-exposed and does not appear to be functionally important. The distances from the Cα atom of residue 43 to the 2'OH of ADP in 3KIN is approximately 25 - 30 Å (intra-head distances in head A and B). The codon for S43 was replaced with a cysteine codon using the QuikChange protocol (Stratagene Inc., La Jolla, CA). Protein was expressed in *E. coli* BL21(RIL) and purified by phosphocellulose and Q-sepharose chromatography in 25 mM Pipes·NaOH, pH 7.2, 2 mM $MgCl_2$ and 1 mM EGTA. Kinesin was eluted in the same buffer with increasing NaCl concentrations.

The protein was labelled with Alexa Fluor 555 maleimide (Invitrogen, Carlsbad, CA). To this end, protein was incubated on ice with a 4-fold stoichiometric excess of dye for 45 min. The reaction was stopped with 2 mM DTT, and excess dye was removed by microtubule affinity. For this, kinesin was incubated with an excess of microtubules and 1 mM AMP-PNP (adenosine5[2032?]-(β,γ-imido)triphosphate) for 30 minutes at room temperature, followed by 10 min of centrifugation at 80,000 rpm over a 40% (w/v) sucrose cushion in a Beckman Optima TLA 100 rotor. The pellet was thoroughly washed and suspended in buffer containing 1 mM ATP. For fluorimetric FRET assays, the release was induced by 1 mM Alexa Fluor 647 ATP (Alexa Fluor647 2'-(or-3')-O-(N-2-aminoethyl)urethane), hexa(triethylammonium)) (A22362, Invitrogen, Carlsbad, CA). To wash out excess fluorescent ATP, the solution was successively concentrated and diluted three times in an Amicon Ultra4 centrifuge bottle. The labelling stoichiometry was assessed by comparing the absorption at 280 nm and the wavelength of maximal dye absorption. The stoichiometry was comparable in different preparation with approximately 1 fluorophore per kinesin dimer.

Bulk fluorescence spectra were measured in an Aminco Bowman AB1 spectrophotometer in PEM80 buffer (80 mM Pipes·KOH, pH 6.8, 5 mM $MgCl_2$, 0.5 mM EGTA, 20 μM taxol).

4.2.2 Sample preparation for confocal fluorescence assays

Microtubule seeds were polymerized by mixing 7.5 μM unlabelled tubulin, 2.5 μM TMR-labelled tubulin and 0.2 mM GMPCPP (Guanosine-5'[(α,β)-methyleno]triphosphate (Jena bioscience, Jena, Germany)) for 15' at 36 °C. Afterwards they were stabilized with PEM80 buffer (80 mM Pipes·KOH pH 6.8, 1 mM EGTA, 2 mM $MgCl_2$) containing 10 μM taxol. Microtubules were diluted and injected into the sample chamber and incubated for 10 minutes. Casein (sodium salt, from bovine milk, Sigma-Aldrich) at 0.4 mg/ml in PEM80 was flushed into the chamber and allowed to incubate for 10 min. The chamber was rinsed with 10 μl PEM12 buffer (identical to PEM80 but with 12 mM Pipes·KOH). After these steps the mix with kinesin motors was flushed into the chamber and the sample was sealed with vacuum grease. The mix consisted of PEM12 buffer containing kinesin, 2 mM $MgCl_2$, 5 mM TROLOX (Sigma-Aldrich, St. Louis, MO), an oxygen scavenger system (20 μg/ml glucose-oxidase, 35 μg/ml catalase and 25 mM glucose) [54, 82], an ATP regeneration system (10 mM phosphocreatine and 50 μg/ml creatine kinase) and fluorescent ATP and/or regular ATP (disodium salt, Sigma, A-2383). Use of DTT instead of TROLOX did not result in good motility.

Sample chambers were prepared as described before [82]. Cover slips and slides

were cleaned by incubating for 10 min in a plasma cleaner (Harrick Plasma, Ithaca, NY, USA).

4.2.3 Confocal fluorescence microscope

The experimental setup used to measure donor fluorescence alone was exactly as described before [82]. For simultaneous donor and acceptor measurements the detection path was altered. The emitted fluorescence first passed a 550DCLP dichroic long-pass mirror, and was then split into donor and acceptor channels by a second dichroic mirror 645DCXR. Finally, the emission beams passed band-pass filters before detection (filters HQ575/50 or HQ675/50; all dichroic mirrors and filters from Chroma, Rockingham, VT). Two separate avalanche photo diodes (SPQM-AQR-14, PerkinElmer, Vaudreuil, Quebec, Canada) were used to count single photons in the donor and acceptor channel. Photon arrival times were detected with 12.5 ns time-resolution using a counter board (6602, National Instruments, Austin, TX) and stored on a computer using custom-built LabVIEW software (LabVIEW 7.1, National Instruments).

4.2.4 Calculation and analysis of the intensity autocorrelation

To detect single-molecule motility events, photon arrival times in the donor channel were binned in 20-ms time slices and analyzed visually. Only traces with a Gaussian shape, an amplitude corresponding to one donor fluorophore, and a width corresponding to the expected velocity were used for autocorrelation. The intensity autocorrelation, G, was calculated from the discrete intensity time traces ($x(k\Delta t)$), Δt=1 ms) using the equation (discrete form of [46]):

$$G(n\Delta t) = \sum_{k=0}^{2N-2} x(k\Delta t)\, x(n\Delta t + k\Delta t) \tag{4.1}$$

where N denotes the total number of bins that describe the signal. Equation 4.1 describes an autocorrelation that is not normalized and decays to zero for large time lags (from now on $n\Delta t$ is approximated as being continuous time lag, τ). The correlations obtained by Equation 4.1 were fitted with:

$$G(\tau) = \left(1 + \frac{\tau}{T_{\mathrm{T}}}\right)^{-1} \exp\left(-\frac{\tau^2}{\alpha T_{\mathrm{step}}^2}\right)\left(1 + A\exp\left(-\frac{\tau}{T_{\mathrm{FRET}}}\right)\right) \tag{4.2}$$

which contains two contributions. The last term describes the intensity fluctuations due to FRET (with decay time T_{FRET} and amplitude A) [75]. The first two terms, describe the transit through the confocal spot, consisting of a Gaussian term (with α a factor describing the width of our confocal volume and T_{step} the average step time) and a term containing the apparent diffusional contribution due to the stochastic nature of stepping (described by T_{T}) [82].

4.2.5 Monte Carlo modelling of the autocorrelations

To understand which chemomechanical models, kinetics and fluorescence intensities may underlie the observed autocorrelation curves, we performed Monte Carlo simulations. The simulations and their analyses were performed using LabVIEW. First, we chose a kinetic scheme that could describe our data, consisting of the interconversion rates between the states and the fluorescence intensities of all the states. Initially, a circular 4-state model without back reactions was used. From such a kinetic scheme, we randomly generated a series of dwell times in the states. On basis of this and the intensities of the different states, we calculated intensity time traces that were subsequently transformed by autocorrelation and fitted with a single exponential.

4.3 Results

4.3.1 Fluorescent ATP binds, hydrolyzes and produces movement

To measure the kinetic characteristics of ATP turnover during processive motility, we considered a FRET-based assay to detect motor-bound nucleotide (Figure 4.1). To assess the feasibility of this approach, we characterized the binding of fluorescent ATP (ATP-Alexa Fluor 647, acceptor) to labelled kinesin (hKinS43C-Alexa Fluor 555, donor) in bulk fluorescence spectroscopy (Figure 4.2). Alexa Fluor 555-labelled kinesin that was purified in the presence of ATP-Alexa Fluor 647 and therefore did not contain regular ATP was incubated with microtubules and additional fluorescent ATP. The fluorescence intensity was higher in the spectral range of acceptor emission (around 670 nm) than in that of the donor (560 nm). After chasing the fluorescent nucleotide with a large excess of regular, unlabelled ATP, the acceptor intensity decreased substantially, while the donor intensity increased (Figure 4.2a, open circles). These observations show that ATP-Alexa Fluor 647, or its hydrolysis product ADP-Alexa Fluor 647, binds to the motor domain of labelled Kinesin-1 and causes FRET.

To determine whether the fluorescent ATP analogue is able to drive motility we measured FRET signals at the single-molecule level using the confocal fluorescence kinesin motility assay we recently developed [82]. In this approach, the focus of the excitation laser is positioned on a microtubule (Figure 4.1b). Photons emitted by individual, labelled fluorescent kinesin motors moving along the microtubule are collected, separated into two spectral channels and counted by an APD. For further analysis, photon arrival times are recorded and binned in appropriate time slots. Time traces generated on the basis of these data typically show a Gaussian intensity profile, from which the motor's velocity (proportional to the width of the Gaussian curve) and the labelling stoichiometry (proportional to the amplitude) can be determined (Figure 4.2, 4.3 and [82]). Using the Alexa Fluor 555-labelled kinesin mutants described above in the presence of 5 μM regular and 0.5 μM fluorescent ATP, we observed time traces with this characteristic shape. The acceptor intensity was roughly constant in time and rather high, due to direct excitation of acceptor molecules free in solution. Once in a while, the donor intensity showed short dips accompanied by concurrent short jumps in acceptor intensity (Figure 4.2b). These events show clear characteris-

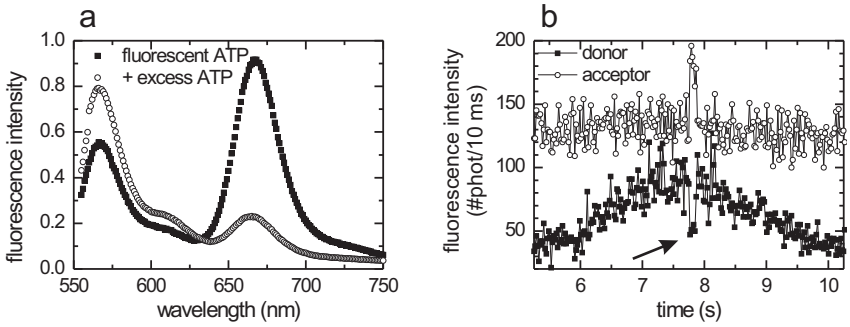

Figure 4.2 – Properties of the fluorescent kinesin-ATP complex. a. Emission spectra of Alexa Fluor 647-ATP: black squares show the emission spectrum of Alexa Fluor 647-ATP bound to Alexa Fluor 555-labelled kinesin (∼20 nM kinesin with an approximately equimolar amount of fluorescent ATP (cf. Methods); $\lambda_{\text{excitation}} = 535$ nm). The open circles represent the same sample after addition of 1 mM regular ATP. The drop of the acceptor emission (∼670 nm) and the rise of the donor emission (∼560 nm) after the ATP-chase indicate resonance transfer between Alexa Fluor 647-ATP and Alexa Fluor 555-labelled kinesin. **b.** Simultaneously collected fluorescence intensity time trace of both donor (black squares) and acceptor channel (open circles) of a donor-labelled kinesin moving through a confocal spot in the presence of 5 μM regular ATP and 0.5 μM fluorescent ATP. A dip in the donor signal (black arrow) is accompanied by a peak in the acceptor intensity, indicating that in this short time interval a fluorescent ATP was bound to the labelled motor domain.

tics of FRET and can be attributed to binding of acceptor-labelled ATP to the motor.

To test whether fluorescent ATP does not only bind to the motor, but is also able to fuel processive movement, we measured the motility of single Kinesin-1 motors in the presence of fluorescent ATP only. At 40 μM fluorescent ATP, we obtained Gaussian-shaped intensity time traces, with a width of 0.80 ± 0.12 s (average ± s.e.m., N=8, Figure 4.3a. This indicates that Kinesin-1 moved processively with a velocity of 126 ± 19 nm/s under these conditions. Since the kinesin used for these experiments was purified in the presence of fluorescent ATP, it can be ruled out that trace amounts of unlabelled ATP caused movement. To determine how the kinetics of Kinesin-1 motility were altered by the substrate fluorescent ATP, we measured the motor's velocity at different fluorescent ATP concentrations and fitted the data with the Michaelis-Menten equation (Figure 4.3b). Data could be obtained only in a limited range of concentrations: below ∼10 μM the number of events was very low, above 40 μM the background fluorescence due to directly excited fluorescent ATP was too high to discern single-motor events. A weighted fit of the data set yielded a maximum velocity, v_{max} of 247 ± 99 nm/s and a Michaelis constant, K_{m} of 32 ± 22 μM. For comparison, when normal ATP was used, v_{max} was 575 ± 9 nm/s and K_{m} 13.4 ± 0.6 μM (Figure 4.3c). These results show that Alexa Fluor 647 ATP can fuel Kinesin-1's pro-

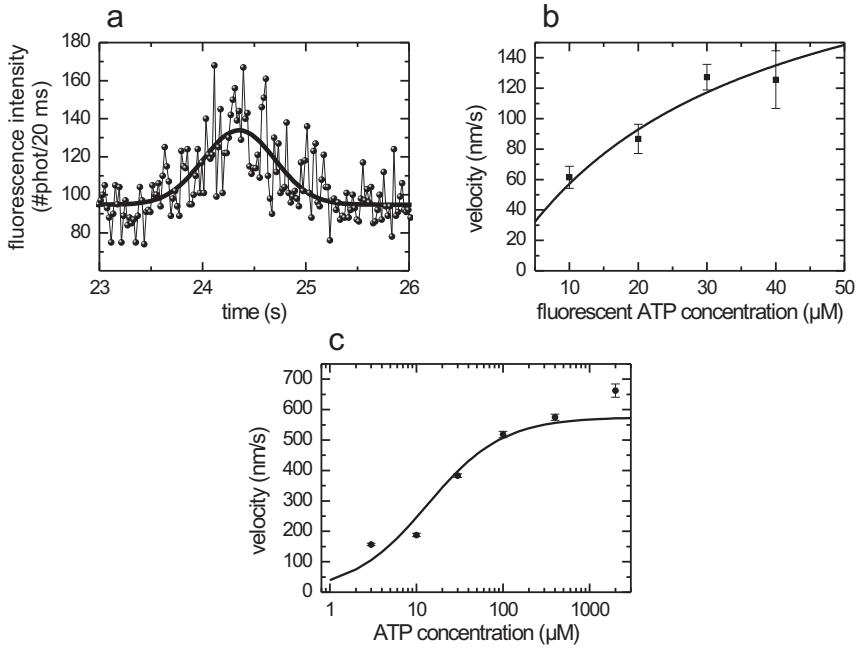

Figure 4.3 – ATP and fluorescent ATP dependence of kinesin's velocity. a Donor fluorescence intensity trace of single-labelled kinesin in the presence of 40 μM fluorescent ATP. Solid black line represents a Gaussian fit with a width of 700 ± 70 ms (v = 170 nm/s). The relatively high background signal is due to acceptor fluorescence excited at the donor exitation wavelength. **(b) and (c).** Average velocities (± standard error of the mean) of kinesin at different concentrations of fluorescent ATP (**b**) or ATP (**c**), as determined from time traces such as shown in **a**. Lines represent weighted Michaelis-Menten fits to the data.

cessive motion, that it is a suitable substrate analogue, but that it alters the motor's kinetic parameters.

4.3.2 The kinetics of fluorescent nucleotide turnover measured on single motors

Next, we set out to determine the kinetics of nucleotide binding and release during processive Kinesin-1 movement. To this end we further analyzed fluorescence time traces obtained from single motors in the presence of fluorescent ATP using the confocal fluorescence assay described previously [82]. Although under the conditions of these experiments (10-40 μM fluorescent ATP) the background intensity caused by direct excitation of fluorescent ATP in solution was too high to discern signals of ATP bound to motors in the acceptor channel, the donor fluorescence intensity of

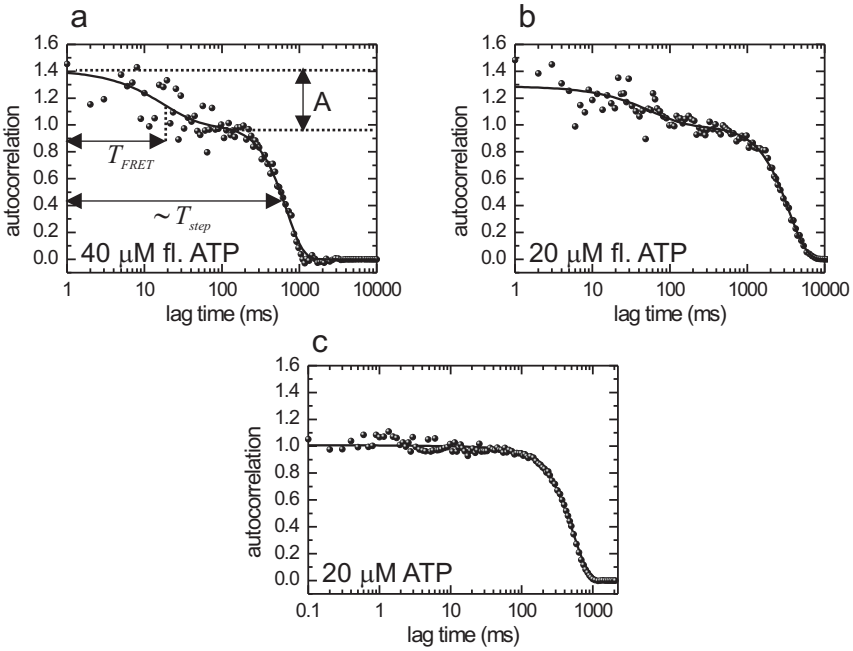

Figure 4.4 – **a.** Autocorrelation of the intensity signal represented in Figure 4.3a (40 μM fluorescent ATP). The slower (time scale ∼1 s), Gaussian decay of the autocorrelation reflects the transit time of the kinesin through the confocal spot, its width is proportional to the velocity and stepping rate. An additional decay of the autocorrelation is observed on a time scale of ∼10 ms. It is due to intensity changes caused by repetitive binding and release of fluorescent ATP. The black curve is a fit of Equation 4.2, with $A = 0.4$ and $T_{\mathrm{FRET}} = 18 \pm 5$ ms. **b.** Autocorrelation of the fluorescence intensity of a kinesin in the presence of 20 μM fluorescent ATP. The slower rate occurs at a longer time scale, reflecting the lower velocity at this lower fluorescent ATP concentration. In addition, the decay time of the fast FRET component has increased. The solid black curve represents a fit of Equation 4.2, with $A = 0.29$ and $T_{\mathrm{FRET}} = 57$ ms. **c.** Intensity autocorrelation of the fluorescence intensity from a single kinesin motor in the presence of regular ATP only. In contrast to (**a**) and (**b**), no decay of the autocorrelation can be discerned on a ∼10 ms time scale, and the slower decay is much faster (∼400 ms).

labelled motors could be reliably determined (Figure 4.3a). Because of the nature of resonance transfer, changes in the donor intensity alone are enough to determine the FRET-properties of the nucleotide-bound state, if other sources of intensity fluctuations can be excluded (see below). The fluorescence intensity time traces (Figure 4.3a) do not show clear dips that can unambiguously be attributed to the binding and release of single fluorescent ATP or ADP (as in Figure 4.2b). This is to be expected since binding and release of fluorescent nucleotides are taking place continuously on

a timescale of tens of ms, leading to the observed large and apparently random intensity fluctuations (compare the amplitude of the fluctuations in Figure 4.3a to that in Figure 4.2b). To determine the timescale of these fluctuations, we analyzed the donor fluorescence intensity time traces of individual motors by autocorrelation, an approach similar to fluorescence correlation spectroscopy [46]. The autocorrelation of intensity time traces spanned almost four orders of magnitude in time (from 1 millisecond to 6 seconds), and revealed two phases (Figure 4.4a, b). The slower phase corresponds to the time it takes a motor to pass the confocal spot [82]. The faster phase (at a time scale of tens of milliseconds) reflects donor intensity fluctuations due to FRET caused by the binding and release of acceptor-labelled nucleotide. In support of this interpretation, a fast component of ∼10 ms was absent when no fluorescent ATP was present (Figure 4.4c). To obtain quantitative information on the intensity fluctuations, we fitted the autocorrelations using Equation 4.2, yielding values for the amplitude (A) and decay time (T_{FRET}) of the FRET component. At 40 μM fluorescent ATP, we derived a $T_{\mathrm{FRET}}$of 18 ± 5 ms, at 20 μM ATP 57 ms. We generally observed increasing decay times with lowered ATP concentrations (Figure 4.5b).

In order to understand this increase and its implications for kinesin's chemomechanical cycle, the experimental autocorrelations need to be compared to autocorrelations calculated from kinetic models. To determine the type of model required to describe our data, one has to carefully consider the experimental setup. (i) The S43C kinesin construct that we used was labelled only at one of its two motor domains. Hence, the symmetry between both motor domains was broken, requiring inspection of a double-cycle for modelling. (ii) Furthermore, the fluorescence donor on the motor domain's residue S43C was very close to the nucleotide (2.5-3 nm; cf. PDB entries 2KIN, 2BG1 or 1MKJ), making it very likely that FRET between the Alexa Fluor 555 donor dye and the Alexa Fluor 647-ATP (or ADP) acceptor dye bound to the same motor head was very efficient. (iii) In addition, donor quenching could also occur due to inter-head FRET, because resonance energy transfer is efficient below distances of approximately 5 nm, and structural models predict distances in that range during the ATP waiting state. (iv) Finally, our experiments were performed at fluorescent ATP concentrations close to $K_{m,ATP}$, implying that more than one kinetic step was rate-limiting (at least one ATP-dependent and one ATP-independent transition). Together, these considerations suggest that the minimal scheme describing our FRET data has to comprise at least four states, with potentially different FRET efficiencies and consequently intensities (head A ATP-bound, head B ATP-bound, head A in ATP waiting state, head B in ATP waiting state; Figure 4.5a). We devised a model in which these four states were connected in a unidirectional cyclic scheme, with rate constants that were equal between the two halves of the scheme, each representing a single 8 nm step. The two rates of a single 8 nm step were chosen such that they obeyed Michaelis-Menten kinetics. We assumed that the lifetime of one of the states (T_2) was independent of ATP concentration and set it to d/v_{max} (with d the step size, 8 nm). We furthermore assumed that the other lifetime reflects the effective time of ATP binding and set it equal to $\frac{K_M d}{v_{max}[ATP]}$. The only parameters that were varied are the relative intensities of the 4 states. We supposed that the dominating factor in the intensity is FRET within a single motor domain between donor and acceptor-labelled nucleotide

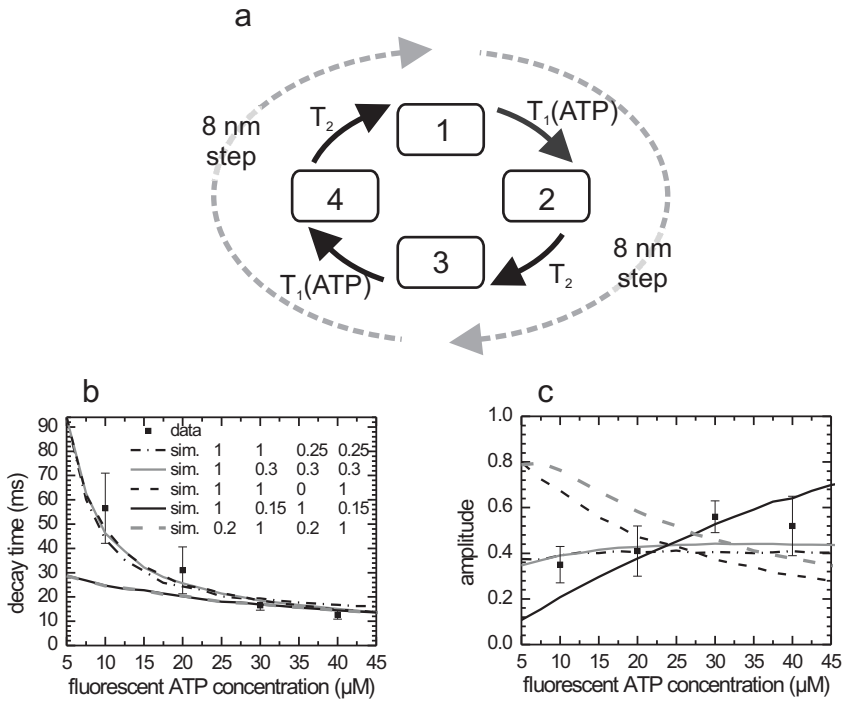

Figure 4.5 – Experimental and simulated decay times and amplitudes of the autocorrelations of donor intensity time traces at different fluorescent ATP concentrations. a. Schematic representation of the four-state model used for the simulations. Each state has its own intensity, due to differences in FRET efficiency. One full cycle consists of two 8 nm steps and two nucleotide turnovers. Both steps / turnovers are built up of the same transitions, characterized by lifetimes T_1 and T_2. Only T_1 depends on the concentration of fluorescent ATP. **b.** Average (± standard error of the mean) decay times obtained from exponential fits to the experimental (solid squares with error bars) and simulated autocorrelations of the donor fluorescence intensity (black and grey lines). For all simulations the v_{max} and K_m values obtained from the fit of Figure 4.3b were used to determine T_1 and T_2. Shown are simulations calculated according to the 4-state model shown in panel **a**, with intensities for the respective states as indicated. **c.** Average (± standard error of the mean) amplitude obtained from exponential fits to the experimental (solid squares with error bars) and simulated autocorrelations of the donor fluorescence intensity (black and grey lines).

and limited the number of free parameters by only considering in total two different intensities for all the states. To compare this model with our data, we constructed intensity time traces using Monte Carlo simulations and different realizations of the model. Next, we calculated the autocorrelation of these traces and fitted them with a single exponential decay. The resulting amplitudes and decay times were compared

to those obtained from the experimental autocorrelation traces, Figure 4.5b and c. The low intensity values of each simulation were optimized for best comparison with the experimental amplitudes (changing these intensities did not influence the decay times). Good descriptions of the data with this 4-state model could only be obtained when just one of the ATP-dependent states had a lower intensity as a result of FRET with fluorescent nucleotide, in addition to one or both of the ATP-independent states. In these cases, we found that a FRET efficiency of 0.25 ± 0.05 is required, consistent with the small distance between donor and acceptor when fluorescent nulceotide is bound to the labelled motor domain. Noteworthy, simulations using intensities that were identical for both halves of the cycle did not correspond well to the data. Such simulations could correspond to single-site catalysis (only one of the motor domains, the labelled one, is turning over ATP) or independent site catalysis (both motor domains hydrolyze ATP independent of each other and only the labelled one shows fluctuations in fluorescence intensity). Our data, which directly probes binding and release of nucleotides to an individual motor domain, thus are inconsistent with kinetic models based on single-site or independent site catalysis. A kinetic scheme with both motor domains hydrolyzing ATP in sequence, can describe the data well.

To further test whether the models proposed describe kinesin's properties appropriately, we performed similar FRET experiments using donor-labelled kinesin and acceptor-labelled ATP (20 μM) in the presence of varying amounts of normal ATP (0, 5, 10, 20, and 30 μM). We recorded donor intensity time traces, calculated their autocorrelations, and fitted the autocorrelations. The decay times and amplitudes obtained in this way are represented in Figure 4.6 (note that at 30 μM ATP, the fluorescent ATP concentration was 30 μM, instead of 20 μM used for the other data points). The decay times appear to decrease slightly with increasing ATP concentration, while a drop of the amplitude is more pronounced. To understand which kinetic cycles can cause such signals, we again used Monte Carlo simulations. For the case of mixtures of fluorescent and normal ATP, we expanded the 4-state model used above by eight additional states and twelve additional transitions (Figure 4.6a). This increase in complexity arises because each ATP-dependent step can either lead to a nucleotide-bound state, or an Alexa Fluor 647 nucleotide-bound state. In our model, we used the Michaelis-Menten parameters to assign a transition probability from nucleotide-free binding site to either ATP or Alexa Fluor-ATP bound states. The intensities of the states were taken to be the same as in the 4-state model for the corresponding states. The new states with normal nucleotide bound were set to an intensity of 1, since FRET cannot occur. The autocorrelations of the simulated time traces were fitted with a single exponential decay and compared to experimental data (Figure 4.6b and c). Presented are two simulations corresponding to the ones that described the fluorescent ATP data best (Figure 4.5b and c), in addition to the model that could represent independent or single-site catalysis. As for the 4-state model, the independent or single-site models poorly described the data, in particular the decrease of the autocorrelation amplitude at increasing ATP concentrations. This aspect of the data was described better by both other models, in particular the one where only one fluorescent ATP-dependent state and one fluorescent ATP-independent state showed FRET. Interestingly, in all of the simulations we tried using this model (also when changing the Michaelis-Menten parameters within reasonable limits) we ob-

served an increase of decay times with ATP concentration, saturating at roughly half the step time. None yielded the slight decrease of the decay time at higher ATP concentrations that we experimentally observed, which might suggest that the implicit assumption made in the modelling that the kinetic rates of transitions on one motor domain are independent of the nature of the substrate bound to the other one is not absolutely correct. The decrease might be explained by v_{max} of fluorescent ATP being higher when ATP binds to the other motor domain than fluorescent ATP. Despite these minor deviations from the simple stochastic models used, our experimental results can only be explained well using a model that assumes alternating site catalysis, at least under limiting ATP-conditions.

4.4 Discussion

Here, we have investigated Kinesin-1's kinetic cycle, in particular the so-called alternating site catalysis, by means of single-molecule fluorescence techniques on a time scale of milliseconds. So far, the ATP turnover has not been resolved to such a high resolution in single-molecule assays [47]. Furthermore, our approach allows, for the first time, measurement of nucleotide binding rates in the course of processive kinesin runs. To this end, we used FRET between donor-labelled kinesin and acceptor-labelled ATP, which allowed for the detection of single-nucleotide binding events. Our experiments show that Kinesin-1 moves processively at the expense of Alexa Fluor 647 ATP with a kinetic cycle that appears qualitatively unaltered compared to that of the natural substrate.

We analyzed the single-molecule donor fluorescence intensity time traces obtained from single kinesins walking through the confocal spot with a temporal resolution not achieved previously. This method is technically challenging due to the limited number of photons that can be collected during one run, and the resulting limited statistics. Consequently, some of the kinetic parameters that can be deduced from these data in theory are not available in practice. For example, the rate of detected photons was too low and as a consequence the shot noise too high to allow direct discrimination of transitions between states of high (fluorescent nucleotide bound to the labelled motor domain) and low FRET (no fluorescent nucleotide bound) in the single-motor fluorescence traces. We therefore transformed the primary data by autocorrelation, allowing the analysis of intensity fluctuations over almost four orders of magnitude in time (ms – 10 s). Autocorrelation curves, however, average out part of the direct information on the underlying transition rates, intensities and FRET efficiencies [35]. To find out what kinetic models can underlie the observed autocorrelations, different probable models need to be solved, transformed into intensity autocorrelations and compared to the experimental data. We chose to perform Monte Carlo simulations, to fit both experimental and simulated autocorrelations with single-exponential decays, and to compare the resulting amplitudes and decay times. Using this analysis, we could well describe our data using models consisting of 4 states. We tried more complex models and in some cases these models gave matching curve fits, but our data did not provide experimental basis for more complex models and the additional free parameters associated.

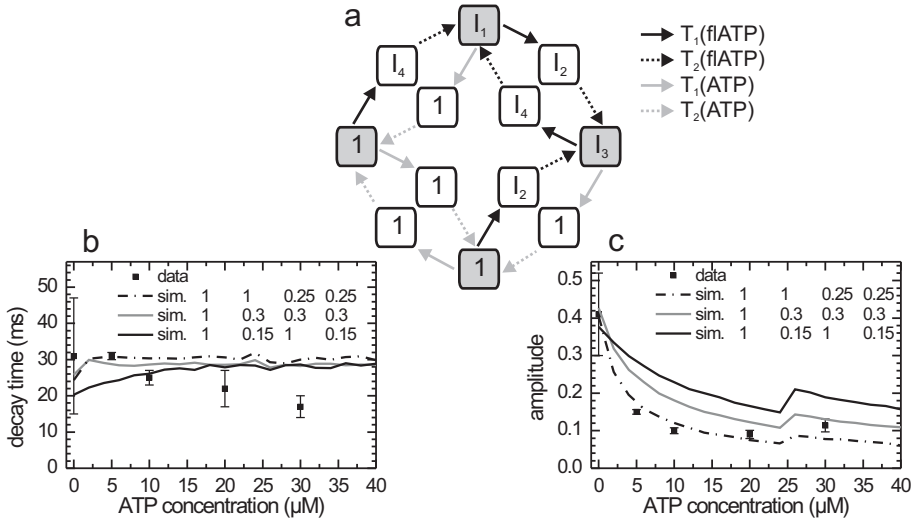

Figure 4.6 – Experimental and simulated decay times and amplitudes of the autocorrelations of donor intensity time traces obtained with mixtures of fluorescent and normal ATP. a. Schematic representation of the twelve-state model used for the simulations. The model is an extension of the one presented in Figure 4.5 and it incorporates all the possible conformations and transitions of a single-labelled construct with two types of substrate. The intensities of the states corresponding to those in the four-state model are indicated, the additional states have normal nucleotide bound and consequently intensity 1. Four transition rates are considered, as indicated. T_1 for fluorescent ATP depends on the fluorescent ATP concentration, T_1 for ATP on the ATP concentration and are calculated using the respective Michaelis-Menten parameters. Both T_2 are independent of the nucleotide concentrations and are obtained from v_{max} of the respective nucleotide. The four states on the corners (shaded gray) represent ATP waiting states and are the ATP waiting states and act as branching points, where a fluorescent or normal ATP can bind. **b.** Average (± s.e.m) decay times obtained from exponential fits to the experimental (solid squares with error bars) and simulated autocorrelations of the donor fluorescence intensity (grey and black lines). For the simulations, a 12-state model was used, corresponding to the model used in Figure 4.5a, with additional branching to states with normal nucleotide bound. The three simulations shown correspond to those with the same labelling and colour in Figure 4.5 (the intensities of other states, with ATP bound, were set to 1). **c.** Average (± s.e.m.) amplitudes obtained from exponential fits to the experimental (solid squares with error bars) and simulated autocorrelations of the donor fluorescence intensity (grey and black lines). The discontinuity at 25 μM ATP is caused by the abrupt increase of the fluorescent ATP concentration from 20 to 30 μM, for better comparison with the data.

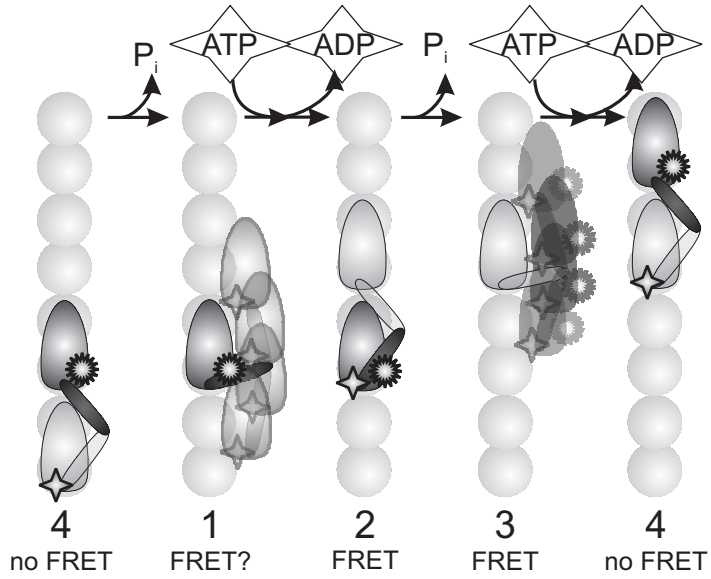

Figure 4.7 – Structural model of the proposed 4-state model of two sequential kinesin steps. The reaction sequence shown is consistent with the kinetic model that fitted the autocorrelation curves best. It includes two ATP concentration-dependent transitions, leading to high FRET in one case and low FRET efficiency in the other case. We depicted the state in which a motor domain waits for ATP to bind as a tethered state. Our data and modelling do not provide conclusive evidence whether this state, in the case of fluorescent nucleotide bound to the unlabeled head, shows FRET or not. The donor label attached to one of the motor domains is depicted as a 16-pointed star, the acceptor labelled nucleotide as a 4-pointed star.

We have been able to test several models that differ substantially in the connection between nucleotide turnovers in both motor domains. What we observed is that models that are based on only one motor domain hydrolysing ATP or both independently, poorly describe the fluorescent ATP concentration dependence of the experimental fluorescence intensity autocorrelations (Figure 4.5 and 4.6). In the two models that describe the data satisfactory, ATP turnover takes place sequentially in each of the two motor domains. A chemomechanical scheme consistent with these two kinetic models is represented in Figure 4.7. In the first state, both motor domains are bound to subsequent binding sites on the microtubule. Fluorescent ATP is bound to the trailing, unlabeled motor domain. In this configuration, donor and acceptor are more than 8 nm apart, thus the FRET efficiency is expected to be less than 6% (assuming a Förster radius of 5.1 nm for this dye pair (Invitrogen/Molecular Probes) and fast rotation of the probes). The lifetime of this state is independent of the fluorescent ATP concentration and in our model determined by the maximal turnover rate, at saturating substrate concentrations. In the next state the fluorescent ATP on the un-

labeled motor domain is hydrolyzed and this motor domain could release from the microtubule into a tethered state [2, 47]. In this state, donor and acceptor could be close enough for FRET to occur as in the "1 0.3 0.3 0.3" model (grey line in Figure 4.5b and c), however it is more likely that FRET in this state is low or zero, since the "1 1 0.25 0.25" model (black dotted line) describes the fluorescent ATP data as well (Figure 4.5b and c), but is better in describing the mixture data (Figure 4.6b and c). This state lives as long as fluorescent nucleotide binds to the labelled head, a lifetime that depends on the concentration of nucleotide. After fluorescent ATP binding the motor is in a state equivalent to the first, with both motor domains microtubule bound. Now, however, the labelled motor domain has fluorescent nucleotide bound and is trailing. Since the nucleotide binding pocket is very close to the 43 residue to which the donor label is attached, efficient FRET can be expected, as observed. This state lives as long as the first state, independent of the fluorescent ATP concentration. In the final, fourth state (equivalent to the second one), the fluorescent ATP has been hydrolyzed, but the product (fluorescent) ADP is still bound and close to the donor, such that efficient FRET can take place, as observed. After binding of fluorescent ATP (with a concentration-dependent rate), the motor is back in state 1 and a new cycle commences. In the minimal model presented here, important nuances are left out. For example, it is well established that the chemomechanical cycle of Kinesin-1 consists of at least two ATP-independent kinetic events [9] and it would be very likely that nucleotide binding to one motor domain and release from the other are two different processes. These important aspects could in principle be taken into account by considering more complex models. We noticed, however, that the autocorrelations hardly changed when we added an additional ATP-independent state, with or without FRET (data not shown; compare [9]). Furthermore, as indicated above, our data did not provide a solid basis to determine the additional parameters required for such models.

Apart from these conclusions on the general mechanism, we observed that the size of key kinetic parameters of Kinesin-1 was clearly affected by the use of Alexa Fluor-ATP. Both the maximum velocity and the Michaelis constant were reduced to $\sim$40% of normal, and it is likely that both substrate binding and catalysis were affected. Given the additional size of the labelled nucleotide (the weight is about four times that of ATP), it can be imagined that its binding properties are altered compared to its natural counterpart because of steric effects or additional charged and hydrophobic interactions. This could alter the kinetics of initial nucleotide binding and the fast conformational change that disables ATP release after binding of regular ATP [19, 61], as well as decrease the stabilization of the transition state of γ-phosphate bond breaking.

To conclude, we have shown that Alexa Fluor 647 ATP is a valid substrate for Kinesin-1. We have determined the kinetics of binding and release of individual motor domains in walking kinesin, using a FRET-based assay, with a donor fluorophore on one of kinesin's motor domain and Alexa Fluor 647 ATP as acceptor. By comparing the donor fluorescence intensity autocorrelations with curves obtained from stochastic models, we find that they are only consistent with models in which each motor domain hydrolyzes ATP in turn [31], consistent with current models for kinesin's hand-over-hand mechanism [4, 39, 92].

4.5 Acknowledgments

This research was supported by a *VIDI* fellowship from the Research council for Earth and Life Sciences, *ALW* (EP), by the Netherlands Foundation for Fundamental Research on Matter, *FOM* (EP, SV), the *Deutsche Forschungsgemeinschaft* (GW), the *Elite Network of Bavaria*, the national graduate program *Protein Dynamics in Health and Disease* (GW, BE) and a travel grant from Laserlab Europe, funded by the *Transnational Access To Research Infrastructures Programme* of the European Commission.

Chapter 5

Novel ways to determine Kinesin-1's run length and randomness, using total internal reflection fluorescence microscopy

Abstract — The molecular motor protein Kinesin-1 drives intracellular transport of vesicles, by binding to microtubules and making hundreds of consecutive 8 nm steps along them. Three important parameters define the motility of such a linear motor: velocity, run length and the randomness (a measure of the stochasticity of stepping). We have used total internal reflection fluorescence microscopy to measure these parameters under conditions without external load acting on the motor. In a first approach, we tracked the motility of single motor proteins at different ATP concentrations and determined both velocity and, for the first time using single-molecule fluorescence assays, randomness. We found that the rate of Kinesin-1 is limited by two exponentially distributed processes at high ATP concentrations, but that a third, ATP-dependent process becomes the sole rate-limiting process at low ATP concentrations. In a second approach, we measured the concentration profile of moving Kinesin-1 along a microtubule. This allowed us to determine the average run length without the need to observe single-molecules and to correct for photobleaching. At saturating ATP concentration, we measured a run length of 1220 ± 50 nm. This value did not significantly change when lowering the ATP concentration down to 5 μM.

This paper has been submitted. *Sander Verbrugge*, Siet van den Wildenberg and Erwin J.G. Peterman

5.1 Introduction

Kinesin-1 is a motor protein that drives intracellular transport of vesicles and organelles in many eukaryotic organisms [79]. To fulfill this task, kinesin steps along microtubules (MTs), which are part of the cytoskeleton, with a step size of 8 nm [63, 71]. Each step is driven by the hydrolysis of one ATP-molecule into ADP [63]. Both Kinesin-1's velocity and ATPase rate are dependent on the ATP concentration and follow Michaelis-Menten kinetics [36]. Kinesin-1 has two identical motor domains that transiently bind to the MT and contain the active site for ATP-hydrolysis. These two motor domains are kept out of phase and thus work together such that it can make hundreds of consecutive steps along the MT (a property called processivity [15])

Over the last years, the technical approaches that allow for the resolution of single steps have tremendously increased our insight in Kinesin-1's mechanism. Optical trapping experiments have taught us that Kinesin-1's center of mass makes 8 nm steps at an average step time of about 10 ms (at saturating ATP concentration) [71], that one ATP molecule is hydrolyzed per step [63] and that Kinesin-1 slows down when a load is applied and stalls at a counteracting force of about 5 pN [15, 71]. Single steps have also been discerned in wide-field optical microscopy experiments. Traveling-wave tracking [13] has allowed for determination of step sizes and rates with microsecond time resolution and sub-nanometer spatial-resolution without external load [12]. In wide-field fluorescence microscopy also a localization accuracy of several nanometers has been achieved by fitting the point-spread function [43, 62, 90]. This approach has been applied to Kinesin-1 with a fluorescent label attached to only one of the motor domains, directly demonstrating that each individual motor domain makes steps of 16 nm [92], confirming that the motor domains move in a hand-over-hand fashion [4, 39].

Although these techniques have provided fundamental insight in Kinesin-1's stepping mechanism, many key properties of motor motility do not require the resolution of single steps and can thus be determined with less complex and more widely available instrumentation. This is important in light of the many other motor proteins with motility properties different than Kinesin-1 that have been or will be isolated and studied, such as Eg5 and dynein [37, 55]. We see in particular three parameters as important for defining a motor protein's motile properties: the run length, the velocity and the so-called randomness [63] and all three as a function of ATP concentration.

1. The run length is the average distance a motor protein travels along its track before it releases and describes how processive a motor protein is. The run length is in most cases measured using wide-field single-molecule fluorescence microscopy on labeled motors. For Kinesin-1, typical values on the order of a micrometer (depending on the exact conditions) have been obtained, indicating that it makes more than one hundred of 8 nm steps before it releases from the MT [66, 72]. Single-molecule fluorescence measurements of the run length are complicated by photo bleaching of the fluorophores, which requires measurements at different excitation intensities and subsequent (non-linear) extrapolation to zero intensity. Here, we demonstrate another way of determin-

ing the run length using TIRF microscopy that does not require the observation of single motors and can thus be performed under illumination conditions at which photo bleaching is negligible. In our approach, we measure the fluorescence of many motors walking along a MT and derive the run length from the motor-concentration profile on the minus end of the MT.

2. The velocity of a motor protein is another key motility parameter. The two most widely applied approaches to measure the velocity of a kinesin are surface-gliding assays and single-motor walking assays, detected with single-molecule fluorescence. The former approach is a multimotor assay, in which the motors are stuck to a surface and the motility of the MT track driven by these stuck motors is measured using fluorescence or other microscopy methods [36]. In the latter, single-molecule approach, the MTs are stuck to the surface and the motion of single motors is followed. Although it requires more advanced instrumentation, we have a preference for the latter method since it allows for monitoring of the multimeric state of the motor proteins, it is less prone to undesired interactions with the surface, and can resolve potential heterogeneous behavior. By performing the measurements at different ATP-concentrations the Michaelis-Menten parameters can be obtained. These parameters describe the intrinsic catalytic rates and the affinity of the active site for ATP. Typically, for Kinesin-1 a maximal velocity around 900 nm s^{-1} and a K_m (the substrate concentration at which half the velocity is reached) around 30 μM has been determined [88].

3. The randomness of motility (r) of a motor protein can be obtained from time-displacement trajectories ($x(t)$) of individual motors using Equation 5.1 [71], once the step size, s, is known.

$$r = \lim_{t\to\infty} \frac{\left\langle \left\langle x(t)^2 \right\rangle - \langle x(t)\rangle^2 \right\rangle}{s\,\langle x(t)\rangle} = \frac{1}{sv} \frac{d\left\langle \left\langle x(t)^2 \right\rangle - \langle x(t)\rangle^2 \right\rangle}{dt} \tag{5.1}$$

With v the velocity of the motor. The randomness is a measure of the stochasticity of the time between steps. If the motor were to be a perfect clock (*i.e.* the duration between steps would be constant), there would be no variance in the displacement and consequently the randomness would be zero. If, on the other hand, the stepping would be determined by a single exponentially-distributed, rate-limiting process, the randomness would be one. In the case of two sequentially occurring exponentially-distributed processes with (on average) equal duration, the randomness would be one half. For Kinesin-1, the randomness has been measured using traveling-wave tracking [13] and optical tweezers [63, 69, 83]. In the most elaborate studies using optical tweezers, at different ATP concentrations and a load of 1.05 pN [83], it was found that the randomness is about one half at saturating ATP, decreases with ATP-concentration to one third (around K_m) and then increases to one at even lower ATP-concentrations. This behavior was explained by Kinesin-1's mechanism consisting of two rate-limiting, ATP-concentration independent exponential processes and one ATP-dependent process. At lower ATP-concentrations

ATP-binding takes longer and longer, first leading to a decrease of the randomness (three processes become rate limiting) and subsequently, at concentrations below K_m, to an increase to one (only ATP-binding is rate limiting). Here, we show that the randomness of kinesin motility can also be measured using single-molecule fluorescence microscopy, which has the advantage of less complicated and more widely available instrumentation and of measuring without applying a load to the motor.

5.2 Materials and methods

5.2.1 Experimental setup

Assays were performed at 21 °C using an epi-illuminated wide-field fluorescence microscope [80]. Excitation light was coupled into a TIRF-objective (Nikon TIRF Plan Apo 100x/1.45 oil) with a polychromatic dichroic mirror (Chroma Z488RDC/532/-633RPC) that allowed for combined excitation with a 635nm (Power Technology Inc., IQ1C10(LD1338)G3H5) and a 532 nm (Coherent, Compass 215M-20) laser. To induce TIRF the excitation beam was coupled off-axis into the objective creating an evanescent wave in the sample. Fluorescence was collected with the objective and filtered using HQ610/75M or a HQ700/75M band-pass filter (Chroma). The two spectral bands were imaged sequentially on a CCD camera (Roper Scientific, MicroMax 512FTB).

5.2.2 Microtubule preparation

Tubulin was purified from pig brain and labeled with Cy5 [37]; biotinylated tubulin was purchased (027T333-A, Cytoskeleton). To polymerize MTs, tubulin was incubated in PEM 80 (80 mM H_2PIPES, 1 mM EGTA, 2 mM $MgCl_2$, pH 6.8, adjusted with NaOH) with GMPCPP (200 μM, Jena Bioscience) at 37 °C for 20 minutes. Subsequently, the MTs were stabilized with 10 μM Taxol and stored at room temperature.

5.2.3 Kinesin concentration profile assay

To determine the motor concentration profile along a MT, a chamber was prepared by attaching plasma-cleaned dimethyl-dichlororsilane-treated slides to cover slips using double-stick tape. The chambers were incubated for 5 minutes with BSA-biotin at 0.1 mg ml^{-1} (Sigma, A2289) in PEM80, washed with buffer and incubated for 5 minutes with streptavidin at 0.1 mg ml^{-1} (Biochemika, 8587). The surface was blocked by incubating with 0.2 % (w/v) Pluronic F108 (BASF) for five minutes. Next, the chamber was incubated with biotinylated Cy5-labeled MTs for 5 minutes. After rinsing with buffer, the chambers were flushed with Alexa555-labeled human kinesin at a concentration of roughly 20 nM (truncated human Kinesin of 391 amino acids with a single surface-exposed cysteine at amino acid position 217 (hKin391-T217C), kind gift from Günter Woehlke) in motility buffer containing PEM80 with

4 mM DTT, 25 mM glucose, 20 μg ml^{-1} glucose oxidase, 35 μg ml^{-1} catalase, ATP and an ATP-regeneration system was added as previously described [82].The exposure time during the measurements of the motor density on the MT was 1 second and the excitation power was 9 μW (more than ten times lower than the power required for single-molecule imaging). To obtain an intensity profile of many kinesin motors on a single MT over one hundred frames were averaged. Stacks of images were acquired using Winview (Roper Scientific) and analyzed with routines written in Labview 8.2 (National Instruments).

5.2.4 Velocity and randomness assay

In the experiments to determine velocity and randomness different assay conditions were used. Cover slips were cleaned by plasma cleaning for 20 min. A positively charged surface was created by amino-silanization with DETA (3-[2-(2-aminoethylamino)ethyl-amino]propyl-trimethoxysilane, Aldrich). Sample chambers were first incubated with Cy5 labeled MTs followed by 5 minutes incubation with 0.2 mg ml^{-1} casein. Next, the chambers were flushed with Alexa555-labeled kinesin at a concentration below 1 nM in the motility buffer. In these experiments a trunctated (at amino acid 560) human kinesin construct containing only a single native cysteine residue at position 421 (hKin560-421C) was used [82]. At 4 μM ATP an ATP-regeneration system was added.

5.2.5 Calculation of velocity and randomness

From stacks of images traces were extracted using kymographs as described elsewhere [37]. A trace was defined as the discretely sampled trajectory of a single motor between appearance and disappearance of a fluorescent spot on a MT. The x-y-coordinates of a moving spot were determined by fitting a 2D-Gaussian to the observed fluorescence intensity profile in each frame [62]. Only traces with a minimal length of three time points were used. In the rare events that a motor stalled, traces were discarded or only the beginning segment was used. The mean displacement ($MD(\tau)$) was calculated from the traces for all independent (non-overlapping) time lags (τ) in all trajectories at a given ATP concentration. The error was estimated by calculating the standard error of the mean. The motor velocity, at each ATP concentration, was determined from a weighted linear fit to $MD(\tau)$ ($MD(\tau) = v\tau$). Next, the variance of the MD ($var(\tau)$) was calculated for each time lag τ with $var(\tau) = \left\langle x^2(\tau) \right\rangle - \langle x(\tau) \rangle^2$. The error was estimated by calculating the standard error of the mean. The variance of the mean displacement at a certain time lag has a time-dependent contribution due to the randomness of stepping [70] and a time-independent offset due to the localization uncertainty of fluorescent spots [42]. The offset was approximately constant in all experiments (560 ± 230 nm^2), implying a localization uncertainty of ∼24 nm. The randomness (Equation 5.1), was determined by a weighted linear fit to the variance at the first 5 time lags (corresponding to a traveled distance of about 100 nm, about a third of the average length of runs observed in these experiments [60]) for every ATP concentration.

5.2.6 Modeling the randomness

The ATP-concentration dependence of the randomness was modeled with three distinct models [63]. All three consist of one ATP-concentration-dependent process (that dominates at low ATP concentrations). The duration of this process (T_{ATP}) is calculated using $T_{ATP} = \frac{K_m}{k_{cat}[ATP]}$, with $k_{cat} = \frac{v_{max}}{s}$ and K_m the Michaelis-Menten parameters determined in the velocity experiments. The three models differ by having in addition 1, 2 or 3 exponential processes with the same duration ($\frac{T_n}{nk_{cat}}$ (n representing the number of additional ATP-independent processes). The randomness is then calculated using $r = \left(\frac{T_{ATP}}{T_{tot}}\right)^2 + \sum_{i=1}^{n}\left(\frac{T_i}{T_{tot}}\right)^2$, with $T_{tot} = T_{ATP} + \sum_{i=1}^{n} T_i = \frac{K_M}{k_{cat}[ATP]} + \frac{1}{k_{cat}}$ the total stepping time. It should be noted that the models do not contain fitting parameters.

5.3 Results

5.3.1 Determination of kinesin's velocity and randomness using TIRF microscopy

In order to explore whether it is possible to determine the randomness of Kinesin-1's motility at zero load using TIRF microscopy, we tracked single, fluorescently labeled kinesin motors binding to and moving unidirectionally along MTs (Figure 5.1a). The illumination conditions were optimized for signal-to-noise and an average displacement of at most 20 nm was allowed within the integration time of one frame. From stacks of images obtained in this way (Figure 5.1b) time trajectories of individual kinesin motors (position as function of time) were extracted (Figure 5.1c). For each ATP concentration we obtained typically ninety trajectories (except at 4 μM ATP where 44 were obtained). From these trajectories, we calculated the mean displacement and the variance of the mean displacement over time for each ATP concentration (Figure 5.2a and b) and found that both increase linearly with time. The velocities were determined from the slopes of mean displacement time traces, yielding for example (Figure 5.2a) a velocity of 64 ± 3 nm s^{-1} at an ATP concentration of 10 μM. The average velocities obtained at different ATP concentrations can be fit well with the Michaelis-Menten model, yielding an apparent Michaelis-Menten constant (K_m) of 42 ± 6 μM and a maximum velocity at an infinite ATP concentration (v_{max}) of 925 ± 33 nm s^{-1} (Figure 5.2c), in agreement with literature values [17,17,49]. From the velocity, the variance of the mean displacement, and a step size of 8 nm, we determined the randomness of motility for each ATP concentration using Equation 5.1 (Figure 5.2d). The values we obtained using TIRF microscopy at zero load are similar to those obtained with an optical tweezers force clamp at a load of 1.05 pN [83]. We determined that the randomness at 2 mM ATP (almost saturating) is 0.46 ± 0.1 indicating that at saturating ATP two exponential processes are rate limiting (Figure 5.2d). At ATP concentrations near K_m the randomness decreases slightly, suggest-

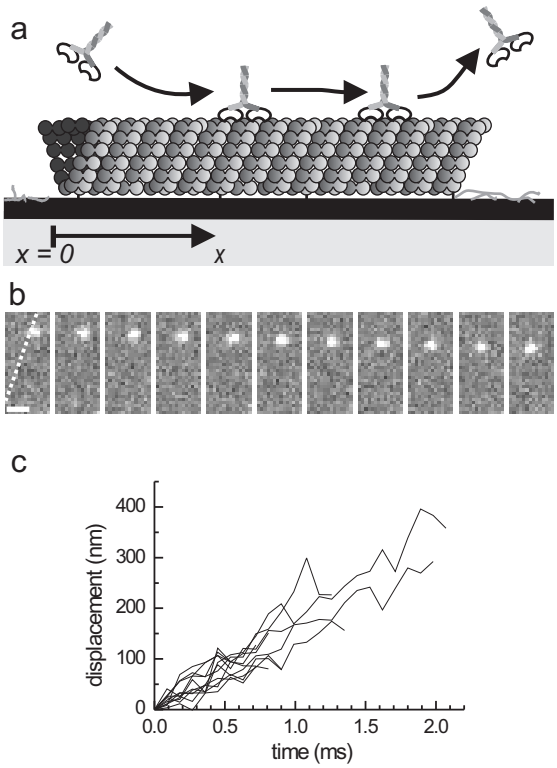

Figure 5.1 – **a.** Schematic representation of experimental assay. Labeled (Cy5) MTs are fixed to the surface Labeled (Alexa-555) Kinesin-1 and ATP are present. The surface is blocked to prevent non-specific kinesin binding to the glass surface. MTs and motors are visualized using TIRF microscopy. **b.** Several frames from a time-laps recording showing an individual Alexa-555-labeled Kinesin-1 (hKin560-421C) moving along a MT at 10 μM ATP (exposure time 150 ms, frames displayed are 450 ms apart). The MT position is indicated in the first frame by the red dashed line, black scale bar: 1 μm. **c.** Eleven representative single-molecule trajectories of Kinesin-1 at 10 μM ATP, obtained from stacks of images like in **b**.

ing that an additional, third process becomes rate limiting. At concentrations below K_m, the randomness increases and becomes close to one (0.9 ± 0.4 at 4 μM ATP), indicating that at very low ATP concentrations a single exponential process is rate limiting, namely the binding of ATP. For comparison, we also plotted three curves that represent simple models with one ATP-dependent exponential process, representing ATP binding and with one, two, or three ATP-independent rate limiting exponential processes. The ATP-dependence of the randomness as obtained with TIRF microscopy is best explained by a model in which the kinetics of Kinesin stepping are governed by two ATP-independent Poissonian processes (that have the same rate and are both

rate limiting at saturating ATP concentrations) and a third ATP-dependent one (that becomes rate limiting at low ATP concentrations).

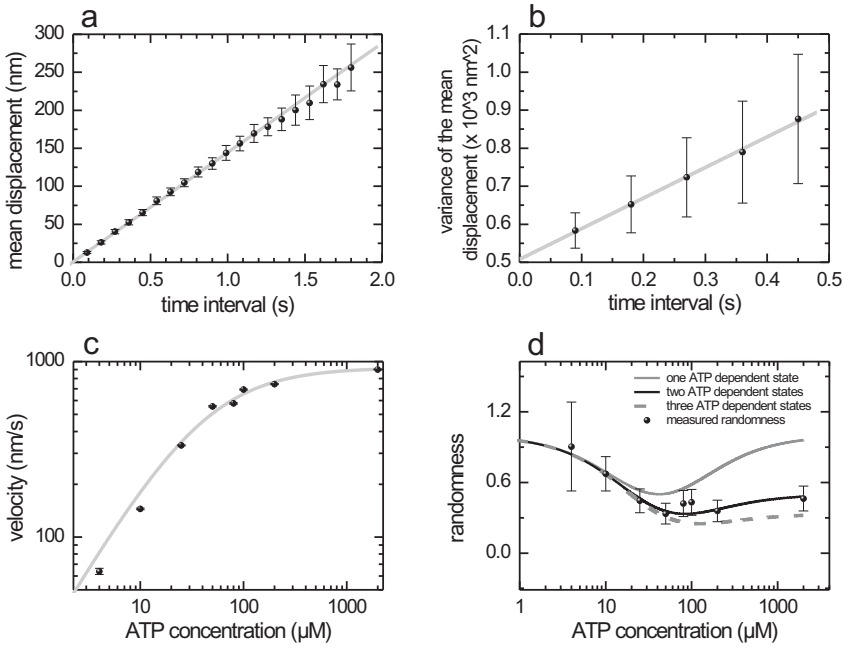

Figure 5.2 – a. Mean displacement, at 10 μM ATP, calculated for all independent intervals in the trajectories of all runs measured. Error bars represent standard error of the mean. Grey line is a weighted fit: $MD = v\tau$ (with $v = 64 \pm 3$ nm s^{-1}). **b.** Variance of the mean displacements depicted in Figure 5.2a. Error bars represent standard error of the mean. Red line is a weighted fit to $varMD = C\ \tau\ +\ offset$ (*offset* reflects the localization uncertainty of 24 nm, the slope $C = 800 \pm 44$ nm^2 s^{-1}). **c.** The average velocity for Kinesin-1 at different ATP concentrations as calculated from a weighted fit of the mean displacement and plotted as a function of the ATP concentration. Data is fitted with the Michaelis-Menten model $v = \dfrac{v_{\mathrm{M}}[ATP]}{[ATP] + K_{\mathrm{M}}}$ yielding $K_{\mathrm{M}} = 42 \pm 6$ μM and $v_{\max} =$ nm s^{-1}. **d.** Randomness as a function of ATP concentration, calculated from a weighted fit of the time trace of the variance (Figure 5.2b), an 8 nm step size and the average velocity (Equation 5.1). The three curves are models of the ATP dependence of the randomness assuming 1, 2, or 3 ATP-independent exponential processes (grey solid, black solid, grey dashed curve respectively). The randomness is best described by a model with 2 ATP-independent exponential processes.

5.3.2 Kinesin's concentration profile along a MT reveals the average run length

Next, we set out to determine the run length of our Kinesin-1 construct. The kinesin motility traces we used above are not well suited for this purpose since photo bleaching severely limited the observed length of the runs. We performed single-molecule measurements with longer integration times and lower excitation intensity and determined a run length of 950 ± 100 nm after correction for photo bleaching (at 2 mM ATP, data not shown). To steer clear of the necessity to correct for photo bleaching we developed another approach to determine the run length. We noticed that at kinesin concentrations too high for clearly resolving single motors, the motor concentration profile on one end of the MT was clearly different from that on the other end. Our hypothesis was that this was caused by the motors' finite run length. In Figure 5.3a a TIRF microscopy image (integration time about three minutes) is shown of a Kinesin-1 coated MT. In this experiment the Alexa-555-labeled hKin391–T217C concentration was 25 times higher than with the single-molecule measurements and the ATP concentration was saturating (2 mM). Due to the long integration time, the motility of individual kinesins is smeared out. The intensity profile of this image (Figure 5.3a), is clearly asymmetric: the intensity increases steeply, within about 350 nm on the right end of the MT, while it increases far more gradual, apparently exponentially saturating, on the left end of the MT. Similar, asymmetric intensity profiles were measured for all the other MTs in the sample. If, on the other hand, the non-hydrolysable analogue AMPPNP was used instead of ATP, the intensity profiles became more symmetric and the intensity rise at both ends of the MT was sharp, within 350 nm (Figure 5.3b). This observation indicates that the gradual, exponentially saturating increase in kinesin concentration on one end of the MT is the consequence of moving kinesin motors.

To quantitatively understand this intensity profile, we modeled the concentration profile of kinesins binding to a MT from solution and walking unidirectionally along it. Assuming equilibrium between MT-bound kinesins and kinesin in solution (i.e. the average number of kinesins detaching equals the average number of kinesin attaching to a MT) and assuming that the kinesin binding sites on the MT do not saturate, a steady-state differential equation can be written down as follows:

$$v\frac{dn(x)}{dx} = kn_0 - k'n(x) - k'_{\text{bleach}}n(x) \tag{5.2}$$

Where v is kinesin's velocity, n_0 its concentration in solution, k the attachment rate, k' the detachment rate of MT-bound motors, k'_{bleach} the rate of photo bleaching, and $n(x)$ the kinesin concentration on the MT as a function of the position x. The minus end of the MT is the $x=0$ position (Figure 5.1a). Here we assume a homogenous field of illumination, such that the rate of photo bleaching is position independent. To solve this differential equation, we set the kinesin concentration on the minus-end of the MT to zero and find:

$$n(x) = \frac{l_{\text{app}}kn_0}{v}\left(1 - \exp\left(-\frac{x}{l_{\text{app}}}\right)\right) \tag{5.3}$$

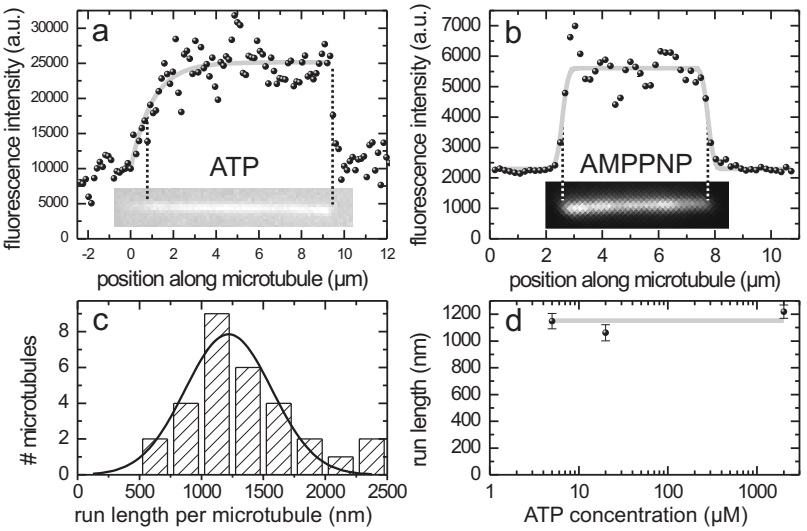

Figure 5.3 – **a.** Time-integrated intensity profile of a MT with moving Alexa-555 labeled Kinesin-1 (hKin391-T217C). The corresponding integrated image of the MT is shown below the profile. The profile was determined summing over the width of the image of the microtubule (three pixels). This profile was constructed by integrating 200 frames with one second exposure time each. The grey line represents a fit of Equation 5.3 ($y = A(1\text{-}\exp(-x/l)$) to the data points with the same position range as the fit curve. Fit parameters are $A = 15.1{*}10^3 \pm 1.3{*}10^3$ and $l = 1020 \pm 140$ nm. **b.** Time-integrated intensity profile of a MT decorated with AMPPNP fixed kinesins. The MT is shown below the profile and was illuminated with a threefold higher intensity than the MT in **a**. Each point in the profile is calculated in the same manner as described in **a**, the z-scale has the same relative scale, the integration was 1 second and 30 frames were summed. The grey line represents a fit of a convolution of a block function with a Gaussian with a fixed width, $A(erf(2(x\text{-}x_{c1})/FWHM) + erf(2(x\text{-}x_{c2})/FWHM)) + I_o$, (erf being the error function, and x_{c1} and x_{c2} are the locations of the MT ends). Fit values are $A = 3310$, $x_{c1} = 2576$ nm, $x_{c2} = 7759$ nm and $I_0 = 2298$. The *FWHM* was set to 350 nm. **c.** Distribution of run lengths obtained from individual MTs decorated with moving Kinesin-1 at an ATP concentration of 2 mM. The black line represents a Gaussian fit with a center position at 1220 ± 50 nm. **d**. Average run length of Kinesin-1 at different ATP concentrations. Averages and their s.e.m. are determined from the Gaussian fit on the distribution of average run lengths of single MT's (2 mM: 30 MTs; 20 μM: 26 MTs; 5 μM: 18 MTs). The grey line, to guide the eye, represents the average of the three values 1140 ± 40 nm.

Where l_{app} is the apparent run length, defined as follows (with l the real run length):

$$l_{app} = \frac{v}{k' + k'_{bleach}} = \frac{l}{1 + \frac{k'_{bleach}}{k'}} \tag{5.4}$$

Fitting Equation 5.3 to the intensity profile shown in Figure 5.3a yields an apparent run length of 1020 ± 140 nm (fit value ± uncertainty). The apparent run lengths obtained from fitting the intensity profiles of 30 MTs observed under the same conditions form a Gaussian distribution, with an average of 1220 ± 50 nm (s.e.m.) (Figure 5.3c). This apparent run length could in principle deviate from the real one for two reasons. First, as described by Equation 5.4, the apparent run length could be an underestimate if the rate of detachment is not substantially larger than the rate of photo bleaching. We determined that under our experimental conditions the rate of photo bleaching is less than 0.001 s^{-1}, by measuring the rate of single fluorophore bleaching on MT-bound kinesins in the presence of 1 mM AMPPNP (data not shown). The average detachment rate of the motor was more than an order of magnitude larger, 0.05 s^{-1} (v/l, at the lowest velocity measured: $v = 60$ nm/s at 5 μM ATP, see below), indicating that photo bleaching did not affect our determination of the run length, within the measurement uncertainty. A second source of error could be the limited resolution of imaging. The point-spread function of our microscope can be well approximated by a Gaussian with a FWHM of 310 ± 10 nm, obtained from the width observed of kinesin-coated MTs in the presence of AMPPNP (note that a MT has a width that is negligible compared to the optical resolution). Convolution of a step function with this Gaussian results in a steep increase in fluorescence intensity that follows an error function, similar to what we observed on both MT ends in the presence of AMPPNP and on the MT plus-end in the presence of ATP (Figure 5.3a and b), indicating that on these edges there is an abrupt drop in kinesin concentration to zero (beyond the length of the MT). The gradual, exponentially saturating intensity increase on the MT minus-end (in the presence of ATP) is hardly affected by convolution with the point-spread function: an exponential saturation curve due to a run length of 1000 nm will be observed as 1040 nm, an overestimate of 4 %, well within our experimental error. Taken together, we determined a run length of 1220 ± 50 nm from the kinesin concentration profile on the MT minus end, using illumination intensities at which photo bleaching is negligible. This value is in good agreement with values reported before for similar Kinesin-1 constructs at saturating ATP concentrations [17, 66, 72].

5.3.3 The run length of kinesin at low ATP concentrations

Next, we set out to measure the run length of our Kinesin-1 construct at lower ATP concentrations. At low ATP concentrations kinesin spends an appreciable amount of its total cycle time in an ATP waiting state, an amount that increases with decreasing ATP concentration. If the ATP waiting state is a weakly bound state with a relatively high probability for detachment, one would expect the run length to be ATP concentration dependent. If, on the other hand, the ATP waiting state were to be a strongly

bound state, with a low probability of detachment (compared to the other states in the cycle) the run length would not be affected by the concentration of ATP. Experimental determinations of the ATP-dependence of the run length have yielded conflicting results [64, 88], but have been used for modeling of Kinesin-1 motility [21, 64]. When we apply the intensity profile approach to samples with a low ATP concentration, we observe that the run length is independent of ATP concentration (Figure 5.3d), confirming the results of an earlier report [88]. Our results are consistent with models with an ATP-waiting state that is tightly MT bound and has a very low off rate [76].

5.4 Conclusions

TIRF microscopy is a well-established technique to measure the motility of single, fluorescently labeled motor proteins such as kinesin under different conditions (ATP concentration and ionic strength) *in vitro*. In particular, it has been widely applied to determine the motor's velocity and run length [77, 77, 88] and it has been used to measure the step sizes of individual motor domains [92]. Here we have shown that TIRF microscopy can also be used to measure the randomness of the motility. The randomness is a parameter that provides information on the stochastic nature of the underlying motility process, in particular the number of rate limiting, exponential processes that underlie motility.

Furthermore, we demonstrated a novel way of determining the run length of kinesin from the intensity profile of many fluorescent kinesins walking along a MT. We observed that on the MT minus end the intensity increase follows exponential saturation, with an exponential constant equal to the run length. Run lengths have before been determined from single-molecule tracking measurements using optical tweezers [71] or fluorescence microscopy [77]. The former approach can only be performed under load, the latter suffers from complications due to photo bleaching. Our approach has the key advantages that it provides data averaged over many motors obtained in a single measurement and that it hardly suffers from photo bleaching.

We have shown here that TIRF microscopy, which is far less complex than other methods such as optical tweezers and is available in many labs, can be used to reliably determine the key motility parameters run length, velocity and randomness, all three as a function of ATP concentration. An additional advantage of TIRF microscopy is that using this method no load is applied to the motors. We envision that the approaches presented here can be applied by many labs to various other motor proteins from the kinesin super family and beyond that still remain to be characterized.

5.5 Acknowledgements

We thank Bettina Ebbing and Günter Woehlke for their generous gift of the hKin391-T217C labeled construct, Marcel Janson, Gijsje Koenderink and Marina Soares e Silva for purifying tubulin. This research was supported by a *VIDI* fellowship from the Research council for Earth and Life Sciences (ALW). This work is part of the research programme of the 'Stichting voor Fundamenteel Onderzoek der Materie (FOM)', which

is financially supported by the 'Nederlandse Organisatie voor Wetenschappelijk Onderzoek (NWO)'.

Bibliography

[1] Bruce Alberts, Alexander Johnson, Julian Lewis, Martin Raff, Keith Roberts, and Peter Walter. *Molecular Biology of THE CELL*. Garland Science, 5 edition, 2008.

[2] M. C. Alonso, D. R. Drummond, S. Kain, J. Hoeng, L. Amos, and R. A. Cross. An ATP gate controls tubulin binding by the tethered head of kinesin-1. *Science*, 316(5821):120–123, 2007.

[3] L. A. Amos and A. Klug. Arrangement of Subunits in Flagellar Microtubules. *Journal of Cell Science*, 14(3):523–549, 1974.

[4] C. L. Asbury, A. N. Fehr, and S. M. Block. Kinesin moves by an asymmetric hand-over-hand mechanism. *Science*, 302(5653):2130–2134, 2003.

[5] A. B. Asenjo, N. Krohn, and H. Sosa. Configuration of the two kinesin motor domains during ATP hydrolysis. *Nature Structural Biology*, 10(10):836–842, 2003.

[6] A. B. Asenjo, Y. Weinberg, and H. Sosa. Nucleotide binding and hydrolysis induces a disorder-order transition in the kinesin neck-linker region. *Nature Structural & Molecular Biology*, 13(7):648–654, 2006.

[7] A. Ashkin, J. M. Dziedzic, J. E. Bjorkholm, and S. Chu. Observation of a Single-Beam Gradient Force Optical Trap for Dielectric Particles. *Optics Letters*, 11(5):288–290, 1986.

[8] S. M. Block. Kinesin motor mechanics: Binding, stepping, tracking, gating, and limping. *Biophysical Journal*, 92(9):2986–2995, 2007.

[9] S. M. Block, C. L. Asbury, J. W. Shaevitz, and M. J. Lang. Probing the kinesin reaction cycle with a 2D optical force clamp. *Proc Natl Acad Sci U S A*, 100(5):2351–6, 2003.

[10] S. M. Block, L. S. B. Goldstein, and B. J. Schnapp. Bead Movement by Single Kinesin Molecules Studied with Optical Tweezers. *Nature*, 348(6299):348–352, 1990.

[11] T. P. Burghardt and D. Axelrod. Total Internal Reflection-Fluorescence Photobleaching Recovery Study of Serum-Albumin Adsorption Dynamics. *Biophysical Journal*, 33(3):455–467, 1981.

[12] L. Busoni, A. Dupont, C. Symonds, J. Prost, and G. Cappello. Short time investigation of the neurospora kinesin step. *Journal Of Physics-Condensed Matter*, 18(33):S1957–S1966, 2006.

[13] G. Cappello, M. Badoual, A. Ott, J. Prost, and L. Busoni. Kinesin motion in the absence of external forces characterized by interference total internal reflection microscopy. *Physical Review E*, 68(2), 2003.

[14] N. J. Carter and R. A. Cross. Mechanics of the kinesin step. *Nature*, 435(7040):308–312, 2005.

[15] N. J. Carter and R. A. Cross. Kinesin's moonwalk. *Current Opinion In Cell Biology*, 18(1):61–67, 2006.

[16] R. B. Case, D. W. Pierce, N. HomBooher, C. L. Hart, and R. D. Vale. The directional preference of kinesin motors is specified by an element outside of the motor catalytic domain. *Cell*, 90(5):959–966, 1997.

[17] D. L. Coy, M. Wagenbach, and J. Howard. Kinesin takes one 8-nm step for each ATP that it hydrolyzes. *Journal Of Biological Chemistry*, 274(6):3667–3671, 1999.

[18] Imtc Crevel, M. Nyitrai, M. C. Alonso, S. Weiss, M. A. Geeves, and R. A. Cross. What kinesin does at roadblocks: the coordination mechanism for molecular walking. *Embo Journal*, 23(1):23–32, 2004.

[19] R. A. Cross. The kinetic mechanism of kinesin. *Trends in Biochemical Sciences*, 29(6):301–309, 2004.

[20] C. Eggeling, J. Widengren, R. Rigler, and C. A. M. Seidel. Photobleaching of fluorescent dyes under conditions used for single-molecule detection: Evidence of two-step photolysis. *Analytical Chemistry*, 70(13):2651–2659, 1998.

[21] M. E. Fisher and A. B. Kolomeisky. Simple mechanochemistry describes the dynamics of kinesin molecules. *Proceedings Of The National Academy Of Sciences Of The United States Of America*, 98(14):7748–7753, 2001.

[22] L. Fleury, J. M. Segura, G. Zumofen, B. Hecht, and U. P. Wild. Nonclassical photon statistics in single-molecule fluorescence at room temperature. *Physical Review Letters*, 84(6):1148–1151, 2000.

[23] T. Förster. *Zwischenmolekulare Energiewanderung Und Fluoreszenz. *Annalen Der Physik*, 2(1-2):55–75, 1948.

[24] T. Funatsu, Y. Harada, M. Tokunaga, K. Saito, and T. Yanagida. Imaging Of Single Fluorescent Molecules And Individual Atp Turnovers By Single Myosin Molecules In Aqueous-Solution. *Nature*, 374(6522):555–559, 1995.

[25] J. Gelles, B. J. Schnapp, and M. P. Sheetz. Tracking Kinesin-Driven Movements with Nanometre-Scale Precision. *Nature*, 331(6155):450–453, 1988.

[26] A. Gennerich and R. Vale. Walking the walk: How kinesin and dynein coordinate their steps. *Current Opinion In Cell Biology*, 21:59–67, 2009.

[27] S. P. Gilbert and K. A. Johnson. Pre-Steady-State Kinetics of the Microtubule-Center-Dot-Kinesin Atpase. *Biochemistry*, 33(7):1951–1960, 1994.

[28] M. Gosch, H. Blom, J. Holm, T. Heino, and R. Rigler. Hydrodynamic flow profiling in microchannel structures by single molecule fluorescence correlation spectroscopy. *Analytical Chemistry*, 72(14):3260–3265, 2000.

[29] N. R. Guydosh and S. M. Block. Backsteps induced by nucleotide analogs suggest the front head of kinesin is gated by strain. *Proceedings Of The National Academy Of Sciences Of The United States Of America*, 103(21):8054–8059, 2006.

[30] T. Ha, T. Enderle, D. F. Ogletree, D. S. Chemla, P. R. Selvin, and S. Weiss. Probing the interaction between two single molecules: Fluorescence resonance energy transfer between a single donor and a single acceptor. *Proceedings Of The National Academy Of Sciences Of The United States Of America*, 93(13):6264–6268, 1996.

[31] D. D. Hackney. Evidence for Alternating Head Catalysis by Kinesin During Microtubule-Stimulated Atp Hydrolysis. *Proceedings of the National Academy of Sciences of the United States of America*, 91(15):6865–6869, 1994.

[32] D. D. Hackney. Pathway of ADP-stimulated ADP release and dissociation of tethered kinesin from microtubules. Implications for the extent of processivity. *Biochemistry*, 41(13):4437–4446, 2002.

[33] D. D. Hackney. The tethered motor domain of a kinesin-microtubule complex catalyzes reversible synthesis of bound ATP. *Proceedings of the National Academy of Sciences of the United States of America*, 102(51):18338–18343, 2005.

[34] D. D. Hackney. Processive motor movement. *Science*, 316(5821):58–59, 2007.

[35] E. Haustein and P. Schwille. Ultrasensitive investigations of biological systems by fluorescence correlation spectroscopy. *Methods*, 29(2):153–166, 2003.

[36] J. Howard, A. J. Hudspeth, and R. D. Vale. Movement Of Microtubules By Single Kinesin Molecules. *Nature*, 342(6246):154–158, 1989.

[37] L. C. Kapitein, E. J. G. Peterman, B. H. Kwok, J. H. Kim, T. M. Kapoor, and C. F. Schmidt. The bipolar mitotic kinesin Eg5 moves on both microtubules that it crosslinks. *Nature*, 435(7038):114–118, 2005.

[38] Lukas Kapitein. *Dynamics of active and passive microtubule-crosslinking proteins*. PhD thesis, 2007.

[39] K. Kaseda, H. Higuchi, and K. Hirose. Alternate fast and slow stepping of a heterodimeric kinesin molecule. *Nature Cell Biology*, 5(12):1079–1082, 2003.

[40] R. H. Kohler, P. Schwille, W. W. Webb, and M. R. Hanson. Active protein transport through plastid tubules: velocity quantified by fluorescence correlation spectroscopy. *Journal Of Cell Science*, 113(22):3921–3930, 2000.

[41] F. Kozielski, S. Sack, A. Marx, M. Thormahlen, E. Schonbrunn, V. Biou, A. Thompson, E. M. Mandelkow, and E. Mandelkow. Phe crystal structure of dimeric kinesin and implications for microtubule-dependent motility. *Cell*, 91(7):985–994, 1997.

[42] B. H. Kwok, L. C. Kapitein, J. H. Kim, E. J. G. Peterman, C. F. Schmidt, and T. M. Kapoor. Allosteric inhibition of kinesin-5 modulates its processive directional motility. *Nature Chemical Biology*, 2(9):480–485, 2006.

[43] D. R. Larson, R. Thompson, and W. W. Webb. Precise nanometer localization analysis for individual fluorescent probes. *Biophysical Journal*, 82(1):45A–45A, 2002.

[44] S. Leibler and D. A. Huse. Porters Versus Rowers - A Unified Stochastic-Model Of Motor Proteins. *Journal Of Cell Biology*, 121(6):1357–1368, 1993.

[45] Y. Z. Ma and E. W. Taylor. Interacting head mechanism of microtubule-kinesin ATPase. *Journal of Biological Chemistry*, 272(2):724–730, 1997.

[46] D. Magde, W. W. Webb, and E. Elson. Thermodynamic Fluctuations In A Reacting System - Measurement By Fluorescence Correlation Spectroscopy. *Physical Review Letters*, 29(11):705–&, 1972.

[47] T. Mori, R. D. Vale, and M. Tomishige. How kinesin waits between steps. *Nature*, 450(7170):750–U15, 2007.

[48] K. C. Neuman and S. M. Block. Optical trapping. *Review Of Scientific Instruments*, 75(9):2787–2809, 2004.

[49] M. Nishiyama, H. Higuchi, and T. Yanagida. Chemomechanical coupling of the forward and backward steps of single kinesin molecules. *Nature Cell Biology*, 4(10):790–797, 2002.

[50] N. Opitz, P. J. Rothwell, B. Oeke, and P. S. Schwille. Single molecule FCS-based oxygen sensor (O-2-FCSensor): a new intrinsically calibrated oxygen sensor utilizing fluorescence correlation spectroscopy (FCS) with single fluorescent molecule detection sensitivity. *Sensors and Actuators B-Chemical*, 96(1-2):460–467, 2003.

[51] E. J. G. Peterman, H. Sosa, L. S. B. Goldstein, and W. E. Moerner. Polarized fluorescence microscopy of individual and many kinesin motors bound to axonemal microtubules. *Biophysical Journal*, 81(5):2851–2863, 2001.

[52] E. J. G. Peterman, H. Sosa, and W. E. Moerner. Single-molecule fluorescence spectroscopy and microscopy of biomolecular motors. *Annual Review Of Physical Chemistry*, 55:79–96, 2004.

[53] H. Qian and E. L. Elson. Single-molecule enzymology: stochastic Michaelis-Menten kinetics. *Biophysical Chemistry*, 101:565–576, 2002.

[54] I. Rasnik, S. A. McKinney, and T. Ha. Nonblinking and long-lasting single-molecule fluorescence imaging. *Nat Methods*, 3(11):891–3, 2006.

[55] S. L. Reck-Peterson, A. Yildiz, A. P. Carter, A. Gennerich, N. Zhang, and R. D. Vale. Single-molecule analysis of dynein processivity and stepping behavior. *Cell*, 126(2):335–348, 2006.

[56] S. Rice, A. W. Lin, D. Safer, C. L. Hart, N. Naber, B. O. Carragher, S. M. Cain, E. Pechatnikova, E. M. Wilson-Kubalek, M. Whittaker, E. Pate, R. Cooke, E. W. Taylor, R. A. Milligan, and R. D. Vale. A structural change in the kinesin motor protein that drives motility. *Nature*, 402(6763):778–784, 1999.

[57] R. Rigler, U. Mets, J. Widengren, and P. Kask. Fluorescence Correlation Spectroscopy with High Count Rate and Low-Background - Analysis of Translational Diffusion. *European Biophysics Journal with Biophysics Letters*, 22(3):169–175, 1993.

[58] S. S. Rosenfeld, P. M. Fordyce, G. M. Jefferson, P. H. King, and S. M. Block. Stepping and stretching - How kinesin uses internal strain to walk processively. *Journal Of Biological Chemistry*, 278(20):18550–18556, 2003.

[59] S. Sack, J. Muller, A. Marx, M. Thormahlen, E. M. Mandelkow, S. T. Brady, and E. Mandelkow. X-ray structure of motor and neck domains from rat brain kinesin. *Biochemistry*, 36(51):16155–16165, 1997.

[60] M. J. Saxton. Single-particle tracking: The distribution of diffusion coefficients. *Biophysical Journal*, 72(4):1744–1753, 1997.

[61] V. R. Schief and O. Howard. Conformational changes during kinesin motility. *Current Opinion in Cell Biology*, 13(1):19–28, 2001.

[62] T. Schmidt, G. J. Schutz, W. Baumgartner, H. J. Gruber, and H. Schindler. Imaging of single molecule diffusion. *Proceedings Of The National Academy Of Sciences Of The United States Of America*, 93(7):2926–2929, 1996.

[63] M. J. Schnitzer and S. M. Block. Kinesin hydrolyses one ATP per 8-nm step. *Nature*, 388(6640):386–390, 1997.

[64] M. J. Schnitzer, K. Visscher, and S. M. Block. Force production by single kinesin motors. *Nature Cell Biology*, 2(10):718–723, 2000.

[65] P. Schwille. Fluorescence correlation spectroscopy and its potential for intracellular applications. *Cell Biochemistry and Biophysics*, 34(3):383–408, 2001.

[66] A. Seitz and T. Surrey. Processive movement of single kinesins on crowded microtubules visualized using quantum dots. *Embo Journal*, 25(2):267–277, 2006.

[67] G. Skiniotis, T. Surrey, S. Altmann, H. Gross, Y. H. Song, E. Mandelkow, and A. Hoenger. Nucleotide-induced conformations in the neck region of dimeric kinesin. *Embo Journal*, 22(7):1518–1528, 2003.

[68] H. Sosa, E. J. G. Peterman, W. E. Moerner, and L. S. B. Goldstein. ADP-induced rocking of the kinesin motor domain revealed by single-molecule fluorescence polarization microscopy. *Nature Structural Biology*, 8(6):540–544, 2001.

[69] K. Svoboda and S. M. Block. Force And Velocity Measured For Single Kinesin Molecules. *Cell*, 77(5):773–784, 1994.

[70] K. Svoboda, P. P. Mitra, and S. M. Block. Fluctuation Analysis of Motor Protein Movement and Single Enzyme-Kinetics. *Proceedings of the National Academy of Sciences of the United States of America*, 91(25):11782–11786, 1994.

[71] K. Svoboda, C. F. Schmidt, B. J. Schnapp, and S. M. Block. Direct Observation Of Kinesin Stepping By Optical Trapping Interferometry. *Nature*, 365(6448):721–727, 1993.

[72] K. S. Thorn, J. A. Ubersax, and R. D. Vale. Engineering the processive run length of the kinesin motor. *Journal Of Cell Biology*, 151(5):1093–1100, 2000.

[73] M. Tomishige, N. Stuurman, and R. Vale. Single-molecule observations of neck linker conformational changes in the kinesin motor protein. *Nature Structural & Molecular Biology*, 13(10):887–894, 2006.

[74] M. Tomishige and R. D. Vale. Controlling kinesin by reversible disulfide cross-linking: Identifying the motility-producing conformational change. *Journal of Cell Biology*, 151(5):1081–1092, 2000.

[75] T. Torres and M. Levitus. Measuring conformational dynamics: A new FCS-FRET approach. *Journal of Physical Chemistry B*, 111(25):7392–7400, 2007.

[76] S. Uemura, K. Kawaguchi, J. Yajima, M. Edamatsu, Y. Y. Toyoshima, and S. Ishiwata. Kinesin-microtubule binding depends on both nucleotide state and loading direction. *Proceedings Of The National Academy Of Sciences Of The United States Of America*, 99(9):5977–5981, 2002.

[77] R. D. Vale, T. Funatsu, D. W. Pierce, L. Romberg, Y. Harada, and T. Yanagida. Direct observation of single kinesin molecules moving along microtubules. *Nature*, 380(6573):451–453, 1996.

[78] R. D. Vale and R. A. Milligan. The way things move: Looking under the hood of molecular motor proteins. *Science*, 288(5463):88–95, 2000.

[79] R. D. Vale, T. S. Reese, and M. P. Sheetz. Identification Of A Novel Force-Generating Protein, Kinesin, Involved In Microtubule-Based Motility. *Cell*, 42(1):39–50, 1985.

[80] M. A. van Dijk, L. C. Kapitein, J. van Mameren, C. F. Schmidt, and E. J. G. Peterman. Combining optical trapping and single-molecule fluorescence spectroscopy: Enhanced photobleaching of fluorophores. *Journal of Physical Chemistry B*, 108(20):6479–6484, 2004.

[81] J. Van Mameren Schotvanger. Integrating Single-Molecule Visualization and DNA Micromanipulation. 2008.

[82] S. Verbrugge, L. C. Kapitein, and E. J. G. Peterman. Kinesin moving through the spotlight: Single-motor fluorescence microscopy with submillisecond time resolution. *Biophysical Journal*, 92(7):2536–2545, 2007.

[83] K. Visscher, M. J. Schnitzer, and S. M. Block. Single kinesin molecules studied with a molecular force clamp. *Nature*, 400(6740):184–189, 1999.

[84] M. Wahl, I. Gregor, M. Patting, and J. Enderlein. Fast calculation of fluorescence correlation data with asynchronous time-correlated single-photon counting. *Optics Express*, 11(26):3583–3591, 2003.

[85] C. M. Waterman-Storer, A. Desai, J. C. Bulinski, and E. D. Salmon. Fluorescent speckle microscopy, a method to visualize the dynamics of protein assemblies in living cells. *Current Biology*, 8(22):1227–1230, 1998.

[86] J. Widengren, U. Mets, and R. Rigler. Fluorescence Correlation Spectroscopy Of Triplet-States In Solution - A Theoretical And Experimental-Study. *Journal Of Physical Chemistry*, 99(36):13368–13379, 1995.

[87] G. Woehlke and M. Schliwa. Walking on two heads: The many talents of kinesin. *Nature Reviews Molecular Cell Biology*, 1(1):50–58, 2000.

[88] J. Yajima, M. C. Alonso, R. A. Cross, and Y. Y. Toyoshima. Direct long-term observation of kinesin processivity at low load. *Current Biology*, 12(4):301–306, 2002.

[89] J. T. Yang, W. M. Saxton, R. J. Stewart, E. C. Raff, and L. S. B. Goldstein. Evidence That the Head of Kinesin Is Sufficient for Force Generation and Motility Invitro. *Science*, 249(4964):42–47, 1990.

[90] A. Yildiz, J. N. Forkey, S. A. McKinney, T. Ha, Y. E. Goldman, and P. R. Selvin. Myosin V walks hand-over-hand: Single fluorophore imaging with 1.5-nm localization. *Science*, 300(5628):2061–2065, 2003.

[91] A. Yildiz, M. Tomishige, A. Gennerich, and R. D. Vale. Intramolecular strain coordinates kinesin stepping behavior along microtubules. *Cell*, 134(6):1030–1041, 2008.

[92] A. Yildiz, M. Tomishige, R. D. Vale, and P. R. Selvin. Kinesin walks hand-over-hand. *Science*, 303(5658):676–678, 2004.

[93] Ch Zander, J. Enderlein, and Richard A. Keller. *Single molecule detection in solution : methods and applications*. Wiley-VCH, Berlin, 2002.

Samenvatting

In deze samenvatting probeer ik de inhoud van dit proefschrift, *Nieuwe manieren om het mechanisme van Kinesine te ontrafelen*, weer te geven op een manier die voor iedereen begrijpelijk is. Om dit te bereiken begin ik met een korte inleiding over het biologische functie van kinesine en de belangrijkste eigenschappen van dit fascinerende eiwit. Een eiwit dat zowel u als ik op dit moment in groten getale in ons lichaam hebben rondwandelen. Om deze samenvatting niet te veelomvattend te maken verwijs ik naar figuren die in de de rest van het proefschrift staan. Uiteraard wens ik u veel leesplezier!

Kinesine speelt een essentiële rol in intracellulair transport

De cel is de bouwsteen van het leven. Levensvormen die bestaan uit heel veel cellen, zoals mensen, dieren en planten, bevatten soms hele lange cellen. Een goed voorbeeld is de zenuwcel in het menselijk lichaam die van het onderste stuk van de ruggengraat tot en met het puntje van de teen loopt. Deze enkele cel heeft een specifieke plek waar nieuwe eiwitten worden geproduceerd. Deze 'verse eiwitten' moeten door de hele cel heen getransporteerd worden om de cel levend te houden. Het is dus van levensbelang dat elke cel in staat is om eiwitten (maar ook andere bouwstoffen en losstaande onderdelen van de cel) te transporteren naar elke plek in de cel. Om het transport goed te regelen zijn er in de cel motoreiwitten (zorgen voor actief transport) en eiwitfilamenten (fungeren als spoorbanen door de cel), zie voor een schematische weergave van een cel Figuur 1.1. De filamenten zijn er niet alleen voor transport, maar geven de cel ook zijn stevigheid, omdat ze lang en sterk zijn. Er zijn drie verschillende filamenten waarvan ik er hier één wil bespreken; de microtubel, omdat dit het filament is waar kinesine op loopt. Microtubels zijn holle buizen die opgebouwd zijn uit bouwstenen van 8 nm groot (1 nanometer is 1 miljardste meter) maar tientallen micrometers (1 micrometer is 1 miljoenste meter) lang kunnen worden. Door hun specifieke bouw hebben ze directionaliteit en om de transportrichting te simplificeren liggen ze met hun plus-richting in de richting van de periferie van de cel. Kinesine is

een motoreiwit dat over de microtubels in de richting van het plus-einde loopt en dus loopt kinesine altijd de goede kant op om bouwstoffen van het centrum naar de periferie te transporteren. Dit proefschrift gaat over kinesine, een specifiek motoreiwit dat op mictorubuli kan binden, terwijl het zijn lading vasthoudt aan zijn andere uiteinde, en vervolgens vele stappen kan lopen, zie Figuur 1.2 voor een schematische weergave van kinesine. In de komende paragrafen zal ik de belangrijkste eigenschappen van kinesine behandelen. Het gaat om zijn processiviteit, stapgrootte, stapsnelheid en de manier van lopen. Daarna zal ik kort elk hoofdstuk van dit proefschrift toelichten.

De belangrijkste eigenschappen van kinesine

Kinesine is een motoreiwit van ongeveer 80 nm lang, met twee domeinen die aan een microtubel kunnen binden en ATP (brandstofmolecuul dat in de cel voorkomt) kunnen verbranden, deze domeinen heten motordomeinen. Verder heeft kinesine een staart die aan de ene kant de twee domeinen met elkaar verbind en aan de ander kant een speciaal stuk heeft waar de lading, die in de cel vervoerd moet worden, kan binden (Figuur 1.2). In dit proefschrift werken we met speciale verkorte kinesines die geen lading meer kunnen vervoeren, maar wel op dezelfde manier 'bewegen' over de microtubel. Een van de belangrijkste eigenschappen van kinesine is dat hij honderden stapjes over een microtubel kan maken als hij er op geland is. Deze eigenschap, processiviteit genaamd, is van groot belang voor de functie die het eiwit in de cel heeft, bovendien laat het ook meteen zien dat kinesine via een goed gereguleerde interactie kan zorgen dat er altijd tenminste één motordomein gebonden is aan de microtubel. Het stapmechanisme gaat op de volgende manier; voordat een stap plaatsvindt zitten de twee motordomeinen achter elkaar gebonden aan de microtubel, 8 nanometer uit elkaar. Bij elke stap die het eiwit maakt verplaatst het achterste motordomein 16 nm naar voren en passeert daarbij het andere motordomein. De staart van het eiwit is na de stap 8 nm verplaatst. Voor één stap is het nodig om één ATP molecuul te verbranden, en dat maakt het tot een zeer efficiente motor. De tijdsduur van een stap is ongeveer 10 milliseconde en dus kan hij 100 stappen per seconde maken, mits er voldoende brandstofmoleculen aanwezig zijn. Laten we voor de grap even uitrekenen hoe lang kinesine over het afleggen van 1 meter doet. Honderd 8-nm stapjes per seconde zorgt voor ongeveer een micrometer verplaatsing per seconde. Dus legt hij in 1 miljoen seconden een meter af. Dat is ongeveer 20.000 minuten, 330 uur en dus 14 dagen! Om 1 meter af te leggen! Het klinkt erg langzaam, maar het is al vele malen sneller dan wachten op diffusie van de belangrijke bouwstoffen van de celkern naar het uiteinde van de cel (afhankelijke van de berekening kom je dan al snel op jaren terecht).

Hoge tijdsresolutie metingen op individuele motordomeinen

Uit de vorige paragraaf blijkt wel dat er veel van het stapmechanisme van kinesine bekend is. Echter zijn er nog steeds vragen onopgelost. Het blijkt dat veel interessante vragen die nog over blijven, betrekking hebben op de positie en orientatie van de individuele motordomeinen en op de toestand van het brandstofmolecuul dat vastzit aan het motordomein. Bovendien is het ook interessant als we de individuele motordomeinen en de chemische toestand van het brandstofmolecuul kunnen volgen - om op die manier inzicht te kunnen krijgen in de exacte methode hoe kinesine in staat is om meer dan honderd stapjes achter elkaar te maken zonder los te laten van de microtubel. In dit proefschrift zijn we dan ook op zoek gegaan naar een methode die ons in staat stelt om individuele motordomeinen te kunnen volgen met een tijdsresolutie die hoger is dan de tijd van een stap van kinesine (10 milliseconden). De techniek die dit mogelijk maakt is confocale fluorescentie microscopie.

Confocale fluorescentie microscopie

Fluorescentie is een natuurkundige eigenschap van een molecuul (fluorofoor genaamd), waarbij licht van een bepaalde golflengte (in ons geval laserlicht) geabsorbeerd wordt en vervolgens uit wordt gezonden in licht met een langere golflengte. Door het verschil in golflengten kan het fluorescentielicht gesplitst worden van het laserlicht, met behulp van een spectraal filter (Figuur 1.5) waardoor een enkele fluorofoor afgebeeld kan worden op een zeer gevoelige camera of op andere lichtdetectoren. Fluoroforen kunnen vastgemaakt worden op specifieke plekken van alle eiwitten, zo ook aan kinesine. Onderzoek aan kinesine met behulp van fluorescentie wordt nu al meer dan tien jaar gedaan, maar tot nu toe werd er altijd gebruik gemaakt van camera's om het fluorescentielicht af te beelden. Helaas hebben deze zeer gevoelige camera's een tijdsresolutie die het niet mogelijk maakt om de individuele motordomeinen te zien verplaatsen tijdens een stap (duurt 10 milliseconden, dus een tussenfase in de stap is nog korter dan dat). Met behulp van confocale microscopie kan de tijdsresolutie verhoogd worden tot onder een milliseconde.

Bij confocal microscopie (zie Figuur 1.6b voor een schematische weergave van een confocale opstelling) wordt een laser gefocusseerd tot het kleinst mogelijke punt, de confocale spot (met ruwweg de breedte van half de golflengte van het laserlicht en dus ongeveer 250 nanometer). Vervolgens wordt het fluorescentie licht opgevangen en afgebeeld op een gevoelige puntdetector die het licht van individuele fotonen kan detecteren. Elke keer als een lichtdeeltje gedetecteerd is, wordt de aankomsttijd gemeten en opgeslagen op de computer met behulp van zelfgeschreven software. De aanpak die in dit proefschrift is toegepast werkt als volgt. De confocale spot wordt op

een microtubel geplaatst en dan is het wachten...
wachten...
wachten...
totdat er een kinesine molecuul met een fluorofoor eraan vast door de spot heen loopt. Als dit gebeurt vangen we al het fluorescentielicht van het fluorofoor op en slaan de aankomsttijden van de individuele lichtdeeltjes op. Deze aankomsttijden kunnen achteraf geanalyseerd worden om te kunnen herleiden wat er gebeurde toen het kinesine langsliep. In hoofdstuk 2, 3 en 4 van dit proefschrift staat beschreven welke nieuwe observaties er zijn gedaan met deze opstelling, in hoofdstuk 5 staat beschreven hoe drie essentiële eigenschappen van kinesine gemeten kunnen worden met een opstelling die zeer veel laboratoria in de wereld tot hun beschikking hebben.

Hoofdstuk 2. Technische aspecten van metingen aan kinesine met een confocale opstelling

Dit hoofdstuk behandelt de eigenschappen van het signaal van een kinesine motor met een fluorofoor aan de staart die door een confocale spot heen loopt. Aangezien in de staart niets gebeurt dat betrekking heeft op het stapmechanisme, staat hier niets nieuws in over kinesine. Echter omdat confocale microscopie voor het eerst is toegepast op deze manier, hebben we hier bewezen dat we de snelheid van individuele motoren kunnen herkennen (Figuur 2.4). Tevens kan het aantal fluoroforen dat aan het kinesine vastzit vastgesteld worden en als laatste behandelen we een analyse methode die het mogelijk maakt om met sub-milliseconde tijdsresolutie kinesine te bestuderen (Figuur 2.6).

Hoofdstuk 3. Kinesine heeft een tussentoestand tijdens een enkele stap

Lange tijd is het onderzoek naar kinesine erop gericht geweest om te achterhalen of de twee motordomeinen tijdens een stap voornamelijk vastzitten aan de microtubel of dat een van de twee motordomeinen het grootste gedeelte van de tijd los is van de microtubel. In dit hoofdstuk laten we zien dat de relatieve afstand tussen twee motordomeinen met milliseconde tijdsresolutie is gevolgd terwijl kinesine op volle snelheid liep. Hierbij is gebruik gemaakt van kinesine dat aan elk motordomein een fluorofoor met verschillende eigenschappen had (Figuur 3.1). Deze twee verschillende fluoroforen dragen energie aan elkaar over als ze dicht bij elkaar in de buurt komen en dan zend de tweede fluorofoor licht uit met een nog grotere golflengte dan het eerste fluorofoor. Door het fluorescentielicht dat van de confocale spot afkomt in verschillende golflengtes op te splitsen is het mogelijk om te bepalen hoeveel energie

er is overgedragen tussen de twee fluoroforen. Die energie is om te rekenen naar de afstand tussen de motordomeinen. Na het testen van vier verschillende constructen die allemaal op een andere plek op het motordomein de fluoroforen hadden zitten, is het gelukt om te bepalen dat één motordomein vastzit aan de microtubel en dat het andere motordomein drie milliseconden lang los is van de microtubel en zich dan in een speciale configuratie in de buurt van het vastzittende motordomein bevindt (Figuur 3.5).

Hoofdstuk 4. Fluorescent-ATP is gedurende een gehele stap aan kinesine gebonden

Het maken van een stap verbuikt één ATP molecuul, echter is nooit direct en nauwkeurig gemeten hoe lang een enkel ATP molecuul aan een motordomein gebonden zit. Met behulp van gelabeld ATP, dat energie kan opnemen van de fluorofoor die aan de motor zit (zie beschrijving van hoofdstuk 3 hierboven), hebben we het binden en loslaten van enkele ATP-moleculen aan enkele motoreiwitten onderzocht (Figuur 4.1). Het blijkt dat een enkel ATP-molecuul gedurende een hele stap vastzit. Dit is mogelijk doordat de twee motordomeinen allebei een bindingsplek hebben voor een ATP-molecuul en de binding wordt elke keer afgewisseld tussen de twee domeinen (Figuur 4.7). De grootste moeilijkheid van deze metingen was de enorme hoeveelheid achtergrondsignaal afkomstig van de duizenden gelabelde ATP-moleculen die zich in de confocal spot bevinden. Hierdoor wordt het detecteren van het signaal dat interessant was (de binding van één ATP) ernstig bemoeilijkt. De resultaten van dit hoofdstuk laten zien dat de twee motordomeinen om de beurt een ATP molecuul binden en verbranden.

Hoofdstuk 5. Nieuwe methoden om meerdere belangrijke aspecten van het stapmechanisme van kinesin te achterhalen

In dit hoofdstuk wordt geen gebruik gemaakt van de confocal meetmethode, maar wordt het fluorescentie licht van een groot gebied afgebeeld op een gevoelige camera. We hebben ons gericht op het ontwikkelen van twee meetmethoden die gebruik maken van een opstellling die voor veel onderzoeksgroepen over de gehele wereld beschikbaar is. Met de eerste meetmethode kan op een innovatieve wijze de gemiddelde afgelegde afstand bepaald worden en met een tweede methode is het mogelijk om het aantal snelheidslimiterende processen van een enkele stap te bepalen. De gemiddelde afgelegde afstand van een kinesine molecuul wordt tot nu toe altijd gemeten door de afgelegde afstand van veel individuele kinesines afzonderlijk te meten en daarna het gemiddelde te bepalen. Deze methode kost veel tijd en vereist speciale

software. De hier gepresenteerde methode meet de gemiddelde afgelegde afstand door het meten van het concentratieprofiel van veel motoren die tegelijk op de microtubel lopen. Doordat er op elk stuk van de microtubel evenveel motoren landen en ze na de landing een afstand afleggen in de plus-richting van de microtubel, zullen er op het begin (min-einde) minder motoren zitten dan aan het einde van de microtubel (plus-einde)(Figuur 5.3). Door dit concentratieverschil van motoren nauwkeurig te meten is het mogelijk om de gemiddelde afgelegde afstand te bepalen. Wij hebben gevonden dat kinesine ongeveer 1200 nm aflegt, onafhankelijk van de ATP concentratie waarbij het kinesine voortbeweegt. De tweede methode die we in dit hoofdstuk behandelen meet nauwkeurig de positie van een enkel kinesine in de tijd en daardoor ontstaat een traject van posities. Door deze trajecten grondig te analyzeren is het mogelijk om te bepalen uit hoeveel snelheidslimiterende processen een enkele stap bestaat (denk bijvoorbeeld aan het binden, verbranden en loslaten van een ATP molecuul of het maken van de stapbeweging als voorbeelden van een snelheidslimiterend proces). Onze metingen bevestigen dat kinesine bij hoge ATP concentraties met twee snelheidslimiterende processen stapt en bij lage ATP concentraties stapt het met een enkel limiterend process. Het snelheidslimiterende proces bij lage ATP concentraties is natuurlijk het wachten totdat ATP bind aan het motoreiwit. De beide methoden verifiëren eigenschappen van kinesine die al bekend waren, maar beiden met een opstelling die voor heel veel onderzoeksgroepen in de wereld makkelijk te gebruiken is.

Dankwoord

Een doctoraal proefschrift over een natuurkundig onderwerp is voor veel mensen geen genot om te lezen. De materie staat te ver van de dagelijkse wereld, de taal bevat te veel onbekende begrippen, de wiskunde lijkt in de verste verte niet op de wiskunde van de middelbare school en waarschijnlijk zijn er nog wel meer dingen die niet leuk, interessant of nuttig zijn. De leukste stukken van het proefschrift voor de meeste lezers zijn dan ook de Samenvatting, die ik u ook van harte kan aanbevelen, en het dankwoord. In het dankwoord worden mensen bedankt die vaak weinig met de inhoud van het boekje te maken hebben en dat is volgens mij een van de redenen waarom juist dit hoofdstuk leesbaar is voor iedereen. Geen Fysica, geen wiskunde, gewoon een warme, behaaglijke stortvloed aan bedankjes. Laat ik maar snel beginnen, want er zijn mensen die hun naam hier terug willen zien...

Let's start with the colleaugues. They helped me in the lab, in the office, drank beers in the bar in Lunteren/Veldhoven and they helped me obtain and shape the content of this thesis. Zdenek, koeienmaagsoep has never tasted as good as it tasted when you prepared it. It is actually a good metaphor for our scientific work as well. It takes a long time to prepare, it seems easy to do but is actually tricky to do it well and once it is finished you need to look carefully for the tasty parts. I think there were actually colleaugues that didn't find any in the koeienmaagsoep, but I'm glad that we were able to manage and get some cool scientific work done. Bettina, thanks for purifying proteins, travelling to Amsterdam to slave away in the lab and many thanks for the positive atmosphere the good ideas and the constant drive to go on. Except for the slaving away in the lab part, the same goes for your former supervisor Günther. Many thanks for enabling Bettina to come to Amsterdam, for sharing your vast knowledge of Biochemistry, Kinesin and many other things. Many thanks for inviting us to Munich and showing us the sights. It was great. Nu verder met de Nederlandse collega's aan wie ik dank verschuldigd ben. Iris en Els, in hun pogingen om een fysicus biochemie te leren of in ieder geval een poging te doen. Bram en Hayko voor het doen van een project bij me. Het was leerzamer, vele malen leuker en

wellicht zelfs succesvoller voor me om jullie het project te laten doen dan het ooit was geweest als ik het zelf had gedaan. De directe VU collega's voor hun eindeloze energie en passie voor het onderzoek, de gezelligheid, de koffie en koekjes. Deze groep kan ik niet zo terloops noemen en daarom een specificatie van de groep: Joost *acknowledged LabVIEW koning* van Mameren, Jeroen *de alleskunner* van der Zon, Maarten *No problem* Noom, Lukas *het onbegrepen genie* Kapitein, Iwan *het verschrikkelijke* Schaap, Bram *it is all in the details* van den Broek, Gijs *Q traps and soup* Wuite, Siet *GO!* van den Wildenberg, Steph *the emotional scientist* Calmat, Peter *the Pirate* Gross, Niels *Tethered Particle Master* Laurens, Andrea *Berlusconi is the man* Candelli, Remus *Love my Pet architectural proteins!* Thei Dame, Wouter *Kill the virus* Roos, Daisuke *Yes, Yes, I see* Mizuno, Chase *filaments forever* Broedersz, Christoph *the professor* Schmidt, Moumita *Let's go to the movies* Das, Catherine *French PostDoc* Tardin, Stefan *the fridge* Lakaemper, Mikhail *vraagje* Korneev, Maryam *G prime...* Atakhorrami, Gijsje *...G double prime* Koenderink, Irena *quiet but very talented* Ivanovska, Marcel *the voice* Janson en Karen *de doorzetter* Vermeulen. Naturally Enrico 'Fredde' Conti deserves a place in this list as well, rest in peace my dear colleague. Verder wil ik alle studenten die in de groep hebben meegelopen danken voor de gezelligheid en het enthousiasme voor het onderzoek. In het bijzonder wil ik natuurlijk graag Erwin bedanken. Door je enthousiasme, je inzichten in de mogelijkheden van het onderzoek en het verrichten van belangrijke stukken werk op de momenten dat ik zelf vast zat heb je me iedere keer weer gemotiveerd genoeg gehouden om mijn proefschrift af te ronden. Daarvoor veel dank. Praten over bergketens, fietsen, bier, muziek, politiek, literatuur, wetenschap en vele andere dingen zijn me altijd een genoegen geweest en zal ik niet snel vergeten. Uiteraard wil ik ook Fred bedanken dat hij mijn promotor wil zijn en omdat hij meerdere malen heeft laten zien dat theorie niet moeilijk is als het goed uitgelegd wordt.

Op de VU waren uiteraard nog meer mensen die ik wil memoreren. De studenten van MENS die me altijd wisten te vinden als ze een borrel organiseerden of als er iemand geïnterviewd moest worden. Mijn dansleraressen Linda en Darinka en hun vriendinnen Esmé en Sanne. Melanie, die begon als busmaatje maar per se in Amsterdam wilde wonen. Gelukkig hadden ze pannenkoeken bij de medische faculteit, zodat ik je toch nog regelmatig zag.

Graag wil ik ook mijn mede afstudeerders van MB aan de TUDelft bedanken. De conferenties waren onvergetelijk, de discussies waren heerlijk scherp en de overtuiging dat Delftenaren slimmer zijn dan de rest van de wereld voelde elke keer weer als een warm bad. In het bijzonder wil ik toch even noemen: Koentjuh, Tijn, Ralph en (als niet Delftenaar of medestudent) John...dank, ook voor de gesprekken over werk na de promotie.

Denkend over deeltjes die je niet kan zien, die stappen maken op holle buizen waar niets doorheen kan, of die geen stappen maken als het kleinste detail in het protocol niet klopt, zorgt ervoor dat ontspanning heel belangrijk is. Bij de handbal kon dat altijd perfect. Nooit over wetenschap praten, altijd over belangrijke levenszaken. Heren dank voor de de biertjes, Formule 1 kijken, de toernooien, de etentjes en natuurlijk de wekelijkse derde helft. Ontspannend was het ook bij vrienden en familie. Rick en Yara, Huib en Lisette, Chiel en Margot, Ruben en Kristina, Bas en Twiggy, Judith, Berend en Marieke, dank voor de mooie avonden met wijn en bier, met zin en onzin, gezelligheid en mooie verhalen, bij ons en bij jullie. Gerard en Tuong Anh, vroeger bekend als Harry en Vicky, dank voor de twee fantastische vakanties en de gezellig avonden in de lage landen.

Zoals altijd worden de belangrijkste mensen voor het laatst bewaard. Waarom dat is weet ik niet, want waarschijnlijk zijn de meeste lezers al afgehaakt. Degene die dit nog lezen moeten weten dat mijn dank uitgaat naar Tijn, Shanna, Thor en Njörd, Marianne, Jos en Joice. Ook veel dank aan Hans en Maria voor de mogelijkheid om aan mijn proefschrift te werken op de zolderkamer, het verbouwen van ons huis en alle steun.

Als laatste rest mij nog de liefste, mooiste en belangrijkste vrouw in mijn leven en ons prachtige lieve kind. Marjan en Jesse, jullie maken elke dag mooier, elke ervaring intenser en veranderen de kleine dagelijkse dingen in de mooiste gebeurtenissen. Ik hou van jullie tot de maan.....